# MODELING AND SIGNAL PROCESSING FOR IDENTIFICATION OF OCEAN SUBSURFACE FEATURES FROM ACOUSTIC REFLECTIONS



FERIAL M. EL-HAWARY

CANADIAN THESES ON MICROFICHE

I.S.B.N.

THESES CANADIENNES SUR MICROFICHE

National Library of Canada
Collections Development Branch

Canadian Theses on
Micrgfiche Service

Ottawa, Canada
K1A 0N4

Bibliothèque nationale du Canada
Direction du développement des collections

Service des thèses canadiennes
sur microfiche

## NOTICE

The quality of this microfiche is heavily dependent upon the quality of the original thesis submitted for microfilming. Every effort has been made to ensure the highest quality of reproduction possible.

If pages are missing, contact the university which granted the degree.

Some pages may have indistinct print especially if the original pages were typed with a poor typewriter ribbon or if the university sent us a poor photocopy.

Previously copyrighted materials (journal articles, published tests, etc.) are not filmed.

Reproduction in full or in part of this film is governed by the Canadian Copyright Act, R.S.C. 1970, c. C-30. Please read the authorization forms which accompany this thesis.

THIS DISSERTATION
HAS BEEN MICROFILMED
EXACTLY AS RECEIVED.

## AVIS

La qualité de cette microfiche dépend grandement de la qualité de la thèse soumise au microfilmage. Nous avons tout fait pour assurer une qualité supérieure de reproduction.

S'il manque des pages, veuillez communiquer avec l'université qui a conféré le grade.

La qualité d'impression de certaines pages peut laisser à désirer, surtout si les pages originales ont été dactylographiées à l'aide d'un ruban usé ou si l'université nous a fait parvenir une photocopie de mauvaise qualité.

Les documents qui font déjà l'objet d'un droit d'auteur (articles de revue, examens publiés, etc.) ne sont pas microfilmés.

La reproduction, même partielle, de ce microfilm est soumise à la Loi canadienne sur le droit d'auteur, SRC 1970, c. C-30. Veuillez prendre connaissance des formules d'autorisation qui accompagnent cette thèse.

LA THÈSE A ÉTÉ
MICROFILMÉE TELLE QUE
NOUS L'AVONS REÇUE

NL-339 (r. 82/08)

Canada

# MODELLING AND SIGNAL PROCESSING FOR IDENTIFICATION OF OCEAN SUBSURFACE FEATURES FROM ACOUSTIC REFLECTIONS

by

© Ferial M. El-Hawary, B.Sc.E.E., M.Sc.E.E.

A Thesis submitted in partial fulfillment
of the requirement for the degree of
Doctor of Philosophy

Faculty of Engineering and Applied Science
Memorial University of Newfoundland

May 1981

St. John's Newfoundland

## ABSTRACT

This thesis is concerned with aspects of modeling and signal processing for identifying features of the ocean subsurface layered media on the basis of acoustic reflection data. Techniques from communications and signal analysis are combined with estimation and system theory to develop procedures to estimate the properties and characteristics of underwater sediments and layered strata.

Models of the response of the subsurface to acoustic or seismic source signals are reviewed and classified. A layer indexed reflection model that accounts for higher order reflections in a systematic manner is detailed. This provides the basis for the estimation task.

Reflection data are generated and acquired using a towed-body system, the so-called "fish", which contains the acoustic source and sensors. The motions of the deep towed system introduce inaccuracies in the reflection data. The fish dynamics exhibit a degree of regularity which is utilized in the design of a Kalman-based filter for estimating the heave effects. The estimates are then used to remove the heave component from the reflection data.

The problem of estimating amplitude and delay parameters associated with replicas of the source signal

primary and multiple reflections imbedded in the return signal is investigated. Three proposed estimation procedures are given. The first adopts a sequential algorithm where the delay parameters are estimated first followed by those of the corresponding amplitudes. A second approach developed in this thesis involves the simultaneous evaluation of all the parameters of interest. The third procedure is based on a balance property inherent in the source signal waveforms.

The proposed procedures are evaluated utilizing simulated return records to provide a basis for comparing the effectiveness of each. The application of the procedures to actual field data obtained in a sea-trial in outer Placentia Bay, off the coast of Newfoundland is given.

ACKNOWLEDGEMENT

This research was conducted under the guidance and supervision of Dr. W. J. Vetter. I wish to thank him for his continued advice and encouragement. I am also grateful to my thesis committee, the late Dr. David Dunsiger and Dr. Adam Zeilinski, for their cooperation and many stimulating discussions.

I am also grateful to members of the Memorial University of Newfoundland Ocean Engineering Group under the leadership of Dr. G. R. Peters for the continuing interest, and accommodation of the diverse needs of this project, particularly during collecting the sea-bed data in the cruise of 1978, results of which have been used during the course of work reported in this thesis. Having had the comptutation and other laboratory and physical facilities of the Faculty of Engineering at my disposal for conducting this investigation, has greatly eased the task.

I also wish to acknowledge the financial support during the course of this work received through the Natural Science and Engineering Research Council of Canada, teaching assistantship in the Faculty of Engineering and Applied Science, and from the School of Graduate Studies at Memorial University of Newfoundland.

For skillful and expedient typing I am grateful to Mrs. M. Ewing.

Last but not least, I wish to acknowledge the continual encouragement received from my husband, Dr. M. E. El-Hawary, and the understanding and great compromises by all my family, husband, sons Bobby and Rany, and daughter Elizabeth, during the period of this work.

TABLE OF CONTENTS

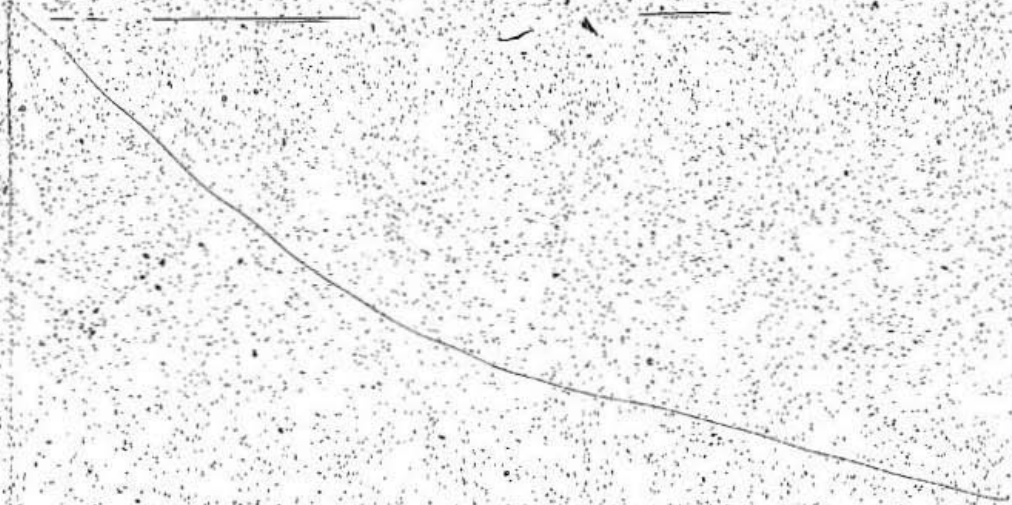

## LIST OF TABLES

## LIST OF FIGURES

## LIST OF SYMBOLS

| | |
|---|---|
| $A_k(x)$ | Auxilfary variable |
| $A^{(N)}(z)$ | Characteristic polynomial of order N |
| $a_i$ | Amplitude parameters (scale factor) |
| $C_i$ | Amplitude of ith harmonic |
| c | Sound propagation velocity |
| D | Down-going component of pressure waves |
| d | Layer thickness |
| E[x] | Expected value of x |
| $E_m$ | The energy of the signal m(t) |
| $E^{(N)}(z)$ | Reflection polynomial of order N |
| f | Frequency |
| g(t) | Part of the random signal $\tilde{m}(t)$ |
| $G_m(f)$ | Power spectral density function of signal m(t) |
| H(f) | Linear system transfer function in the frequency domain |
| $\underline{H}$ | Coefficient matrix |
| h(t) | Impulse response of linear system |
| $\underline{K}(k+1,k)$ | Kalman filter gain matrix |

| | |
|---|---|
| $K$ | Bulk modulus or incompressibility |
| $\|M(f)\|$ | Continuous amplitude spectrum |
| $M(f)$ | Fourier spectrum of the source signal $m(t)$ |
| $m(t)$ | Source signal (input) |
| $m_p(t)$ | Periodic signal |
| $\tilde{m}(t)$ | Random process signal |
| $N$ | Number of layers |
| $\underline{P}(k+1/k)$ | Predictor covariance matrix |
| $p_t(t)$ | Transmitted pressure wave |
| $p_r(t)$ | Reflected pressure wave |
| $p_i(t)$ | Incident pressure wave |
| $\underline{Q}(k)$ | Error covariance matrix |
| $\frac{1}{Q}$ | Specific dissipation constant |
| $R$ | Pressure reflection coefficient |
| $R_n$ | Resistive component of acoustic impedance |
| $\underline{R}(k)$ | Error covariance matrix |
| $\tilde{r}(t)$ | Reflectivity function |
| $s$ | Laplace operator |
| $T_e$ | Equivalent duration of a signal |

| | |
|---|---|
| $\bar{T}$ | Pressure transmission coefficient |
| $T(s)$ | Transfer function of a linear system in the s-domain |
| $T$ | Time period |
| $t$ | Time, independent variable |
| $U$ | Up-going component of pressure waves |
| $u(t)$ | Particle velocity |
| $X_n$ | Reactive component of complex acoustic impedance |
| $x$ | Vertical distance (depth) |
| $x(t)$ | State variable. |
| $\tilde{x}(k/k)$ | Filtering error in the state variable |
| $v(t)$ | Noise signal |
| $W_e$ | Equivalent signal bandwidth |
| $W(t)$ | Disturbance (random process) |
| $Y(f)$ | Fourier transform of the output signal $y(t)$ |
| $y(t)$ | Received signal, (output) |
| $\tilde{y}(t)$ | Output signal (random) |
| $Z$ | Acoustic impedance |
| $Z(f)$ | Fourier transform of the record $z(t)$ |
| $Z_n$ | Acoustic impedance (frequency dependent) |

| | |
|---|---|
| $z$ | Z-transform in (chapter 4) |
| $z(t)$ | Time dependent fish heave |
| $< >$ | The time average |
| $\alpha$ | Attenuation coefficient |
| $\alpha(f)$ | The gain of the system |
| $\beta$ | Compressibility of sediments |
| $\beta(f)$ | The phase of the system |
| $\gamma_k$ | Auxiliary variable |
| $\gamma_i$ | Total travel time |
| $\delta(t)$ | Dirac delta function |
| $\Delta t$ | Time increment |
| $\theta_i$ | Angle of incident wave |
| $\theta_r$ | Angle of reflected wave |
| $\theta_T$ | Angle of transmitted wave |
| $\theta(f)$ | Continuous phase spectrum |
| $\mu$ | The shear (rigidity) modulus |
| $\mu$ | Marker multiplicity in (Chapter 3) |
| $\xi(f)$ | Particle displacement in frequency domain |
| $\xi(t)$ | Particle displacement in time domain |

| | |
|---|---|
| $\Pi(x)$ | Auxiliary variable |
| | $\Pi(x) = c^2 \frac{d\xi(x)}{dx}$ |
| $\rho$ | density |
| $\underline{\Phi}$ | Transition matrix |
| $\Phi$ | Serial correlation |
| $\Phi_{12}(\tau)$ | Cross-correlation function |
| $\Phi_m(\tau)$ | Autocorrelation function of m(t) |
| $\tau$ | Time delay |
| $\psi_m^2$ | Mean square value of signal m(t) |
| $\omega$ | Radian frequency |

# Chapter 1

# INTRODUCTION

## 1.1 Background

In this thesis, the problem of signal processing for identification of lossless layered media systems is considered. Such systems arise in a number of application areas such as optics where multiple reflections of light in layered lenses and thin film coatings are studied. The same phenomenon applies to electromagnetic problems involving wave propagation in multiple dielectrics, waveguides, and transmission lines. Attention is focused here on the specific application to the marine seismic reflection method involving acoustic wave propagation in water and the underlying sediments and rock formations. Emphasis is given to application to real data collected from the outer Placentia Bay region on the Newfoundland Grand Banks, collected during a scientific cruise conducted jointly by Memorial University's Ocean Engineering Group and the Bedford Institute of Oceanography on board the C.S.S. Hudson, cruise 78-012. Track chart and station locations are shown in Fig. I.1.1. Many parallels exist between this area of application and that in geophysical ground seismic exploration involving the seismic reflection method. Research, development, and advances in implementation in these areas are mainly motivated on account of

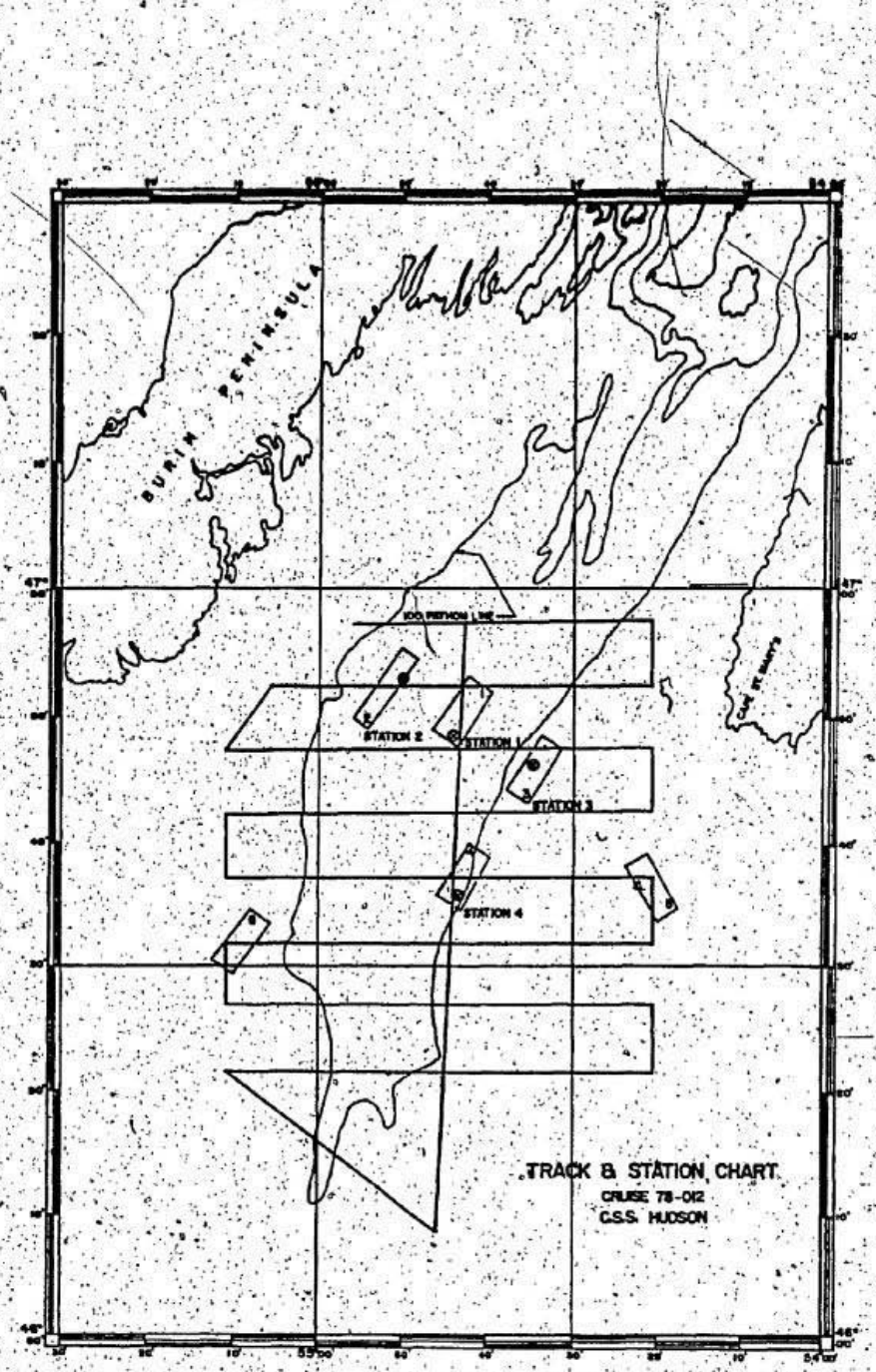


Figure 1.1.1 Track chart and station locations. Cruise 78-012, C.S.S. Hudson 1-6, intensive study areas; ⊗ , station locations.

their relevance to hydrocarbon and mineral exploration.

In the search for hydrocarbons, one needs to consider only a small portion of the earth's crust. Oil and gas accumulations are related to certain sedimentary rock formations which have been generated in the course of the geological/biological history of the earth. The rates of deposition have varied widely as have the times during which a particular form of deposition has taken place. This process results in a layered system within the sedimentary basin.

Seismic signals are the earth's response to excitations that arise either from natural phenomena such as earthquakes or from man-made acoustic sources used in geophysical exploration.

In the marine seismic method, the distance between the source and receivers are relatively small. The data are usually recorded on magnetic tape for further computer processing. The purpose of processing is to enhance the signals with respect to the noise, extract the significant information and display the data in such a form that a geological interpretation can be readily carried out. In petroleum prospecting the length of a seismic record seldom exceeds four or five seconds. The "interpretation" of these events consists in identifying them as to their nature (i.e, reflection, refraction, surface wave, etc.) and in determining the depth and

cause of their origin.

The earliest experiments with the seismic reflection method in oil exploration date back to 1921 when J. C. Karcher mapped a shallow reflecting bed in central Oklahoma. By the early 1930's, reflection became the most widely used of all geophysical techniques in exploration for hydrocarbons. The land-based seismic work activity has also been paralleled by similar activities in water covered areas. By the end of World War II, a limited number of seismic surveys were being undertaken in the open ocean. By the middle 1960's marine exploration efforts were extended to include almost all the shelf areas of the world. For example, exploration for oil is now being carried out off the coast of Newfoundland and Labrador, in the Beaufort Sea, the North Sea, the Gulf of Mexico, off-shore Alaska, off-shore Africa, and in the Mediterranean Sea.

Our main concern in this study is to extract information on ocean bottom and subbottom structure, i.e. on the spatial dimensions or extent of media components characterized essentially by their densities and sound propagation velocities; for sediment categories and formations which can be considered as layerwise homogeneous and isotropic. For rough media these assumptions are not applicable and different approaches are necessary. Such basic information enables an experienced geophysicist or a ma-

rine sedimentologist to identify diverse geological or sedimentary properties of the media. A major potential use of results of the present study is in the detection of the presence of hydrocarbon and mineral deposits under the sea bed. A second potential use is in identifying soil properties for possible locations of underwater foundations necessary for ocean structures and pipelines. Sources for construction materials may also be identified. The results are also potentially useful in connection with the detection of, and age determination for bottom scour due to iceberg grounding.

## 1.2 Scope of the thesis

The problem addressed in this thesis is the development of procedures to estimate the properties and characteristics of underwater sediments and layered strata. These properties can be related to amplitude and delay parameters associated with the return-acoustic signal which is the response of the medium to acoustic excitation signals. Some fundamental concepts from acoustic wave propagation are presented in Chapter 2. A description of acoustic source signal characteristics is given after a review of concepts from signal theory. Acoustic wave propagation theory is briefly discussed together with the phenomenon of wave reflection at the interface of two media. This last aspect is of fundamental importance since it provides the basis for identifying media structures and properties. Relevant marine sediment acoustic properties are discussed as well as noise considerations. Finally the chapter concludes with a discussion of the wave attenuation phenomenon.

Chapter 3 deals with modeling the response of the subsurface to acoustic or seismic source signals. These models lead to what are commonly known as synthetic seismograms in exploration geophysics. A review of nine models for earth's response is given in this chapter. In each case the underlying assumptions and the resulting

procedure for generating synthetic seismograms are discussed.

A major source of inaccuracy in data collected in underwater acoustic experiments is due to dynamics of the towed body. The effect of heaving motion should be filtered out from the data prior to further processing. In Chapter 4 a discussion of heave compensation is given. A proposed procedure for extracting the heave motion component from the collected data is detailed first. This is followed by a physically-based model for the heave motion. A state-space form of this model suitable for Kalman filtering application is then derived. Details of a procedure based on Kalman filtering to obtain refined estimates of the heave motion contribution in the actual data records are discussed.

Extracting information related to amplitude and delay parameters from sea bed response is the subject of Chapter 5. This is essentially a problem in parameter estimation. The discussion is initiated by an outline of a number of approaches to formulating the problem. Each of the formulations provides a basis for a proposed estimation procedure. Three proposed procedures are then outlined. The first adopts a sequential algorithm where estimates of the delay parameters are obtained followed by estimates of the amplitude parameters. The second approach involves the simultaneous evaluation of both

delay and amplitude parameters. This is essentially a matched filter approach, A third procedure utilizing an observed balance property of the source signal is also introduced. In each case computational results pertaining to simulated records as well as field data are given.

# Chapter 2

## SOME FUNDAMENTAL CONCEPTS FROM ACOUSTIC WAVE PROPAGATION

### 2.1 Introduction

The purpose of this Chapter is to introduce some useful definitions and concepts related to signals and underwater acoustic wave propagation. A discussion of concepts and terms from signal analysis is given. This is important since the interpretation of reflection data depends on a clear understanding of the signal details. This is followed by a description of acoustic signal characteristics and a review of modeling of sound propagation in homogeneous and isotropic media. A discussion of the reflection phenomenon at the interface between water and sea bed and its relation to media properties is then outlined.

The classification of the subbottom layers using reflection information demands a knowledge of the relations between the physical properties (such as density and velocity) and acoustic properties of marine sediments. A brief discussion of this is given in Section (2.5). The received signals are usually corrupted with noise. A summary of noise sources and properties is given in Section (2.6). The chapter concludes with a treatment of a possible approach to modeling of the attenuation effects in the marine environment.

## 2.2 Signal theory background

The intent of this section is to review some fundamental concepts and definitions from systems and signal theory which are pertinent to the work reported in this thesis. This review deals with signals and means for their specifications for both deterministic and random variations.

A system may be defined as a device or physical medium that produces an output signal or signals when subjected to an input signal or signals. In a linear system, the principle of superposition applies. As a result, the response of a linear system to a number of excitations (input signals) applied simultaneously is equal to the sum of the responses of the system when each excitation is applied individually.

In the time domain, a linear single input - single output system is described in terms of its impulse response which is defined as the response of the system to a unit impulse or delta function $\delta(t)$ applied as an input to the system. The impulse response is denoted by $h(t)$. The output signal due to an input signal $m(t)$ is given by the convolution integral.

$$y(t) = \int_{-\infty}^{\infty} m(\tau)\, h(t-\tau)\, d\tau \qquad (2.2.1)$$

For a system operating in real time to be physically realizable it must be causal. A causal system does not respond before the excitation is applied. For a linear time-invarient system to be causal the impulse response must vanish for negative time

$$h(t) = 0 \qquad t<0 \qquad , \quad (2.2.2)$$

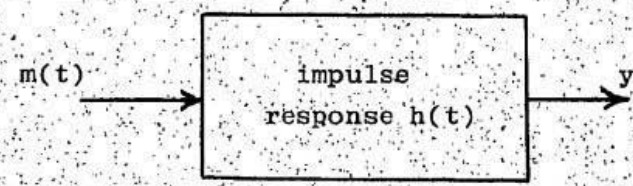


Linear system

Figure 2.2.1

The analysis of signals encountered in many engineering problems requires a procedure for signal representation. The resolution of signals into sinusoidal components has played a significant role in signal processing. This is essentially made possible through the use of the Fourier series expansion in the case of periodic signals that satisfy the Dirichlet conditions on the signal function $m_p(t)$. Periodic signals commonly encountered in engineering systems are usually single valued,

with at most a finite number of discontinuities, and a finite number of maxima and minima in the interval [o,T] defined by the period T. The foregoing three conditions and the absolute integrability condition

$$\int_{-T/2}^{T/2} |m_p(t)|\, dt < \infty \qquad (2.2.3)$$

constitute the Dirichlet conditions.

According to the complex exponential Fourier series expansion, a periodic signal contains all frequencies which are harmonically related to the fundamental frequency: $o, \pm f_o, \pm 2f_o, \pm 3f_o, \ldots$ where $f_o = \frac{1}{T}$. The frequency domain description of the signal consists of components at these discrete frequencies and is called the spectrum. Parseval's power theorem deals with the average signal normalized power defined by

$$P = \frac{1}{T} \int_{-T/2}^{T/2} |m_p(t)|^2\, dt \qquad (2.2.4)$$

In terms of the amplitudes of all harmonics $c_i$, the power is given by

$$P = \sum_{i=-\infty}^{\infty} |c_i|^2 \qquad (2.2.5)$$

Thus Parseval's theorem requires knowledge of the amplitude spectrum. The quantity $|c_i|^2$ is referred to as the discrete power spectrum of the periodic signal.

For non-periodic signals m(t), a limiting procedure results in the Fourier integral representation,

$$m(t) = \int_{-\infty}^{\infty} M(f) \exp.( j2\pi ft)\, df \qquad (2.2.5)$$

where

$$M(f) = \int_{-\infty}^{\infty} m(t) \exp.(-j2\pi ft)\, dt \qquad (2.2.7)$$

The function M(f) is a transformed version of m(t) and is referred to as the Fourier transform of m(t). The time function m(t) is referred to as the inverse Fourier transform of M(f). A Fourier transform pair is m(t) and M(f). For a signal to have a Fourier transform it is sufficient that it satisfies the Dirichlet conditions with $T \to \infty$. In particular we require

$$\int_{-\infty}^{\infty} |m(t)|^2\, dt < \infty \qquad (2.2.8)$$

A signal satisfying the above inequality is referred to as a finite-energy signal.

In a manner similar to that for periodic signals, we can state that the Fourier transform M(f) of the signal

specifies relative amplitudes of the various frequency components of the signal. In general, the Fourier transform is a complex function of frequency f.

$$M(f) = |M(f)| \exp.[j\theta(f)] \qquad (2.2.9)$$

Here $|M(f)|$ is the continuous amplitude spectrum of m(t) and $\theta(f)$ is the continuous phase spectrum of m(t).

The analog of Parseval's power theorem for the case of non-periodic signals is given by Rayleigh's energy theorem which specifies that the energy of the signal $E_m$ is given by

$$E_m = \int_{-\infty}^{\infty} |m(t)|^2 \, dt$$

$$= \int_{-\infty}^{\infty} |M(f)|^2 \, df \qquad (2.2.10)$$

The quantity $|M(f)|^2$ is referred to as the energy-density spectrum of the function m(t), since the total area under the $|M(f)|^2$ curve is the energy.

There is an important class of signals called the finite-power signals which are not absolutely integrable but for which the limit

$$\lim_{T\to\infty} \frac{1}{T} \int_{-T/2}^{T/2} m^2(t) \, dt \qquad (2.2.11)$$

exists. The Fourier transform for such signals is defined in a limiting sense provided that the delta functions are included.

There are two kinds of correlation which is a process closely related to that of convolution. The cross-correlation applies to two different signals $m_1(t)$ and $m_2(t)$ and provides a measure of similarity between one signal and a time-delayed version of the other. For finite energy signals we have

$$\phi_{12}(\tau) = \int_{-\infty}^{\infty} m_1(t)\, m_2(t-\tau)\, dt \qquad (2.2.12)$$

The cross-correlation function is a function of the time-delay parameter $\tau$. The Fourier transform of $\phi_{12}(\tau)$ is equal to $M_1(f)$ multiplied by $M_2(f)$. That is

$$\phi_{12}(\tau) = \int_{-\infty}^{\infty} M_1(f)\, M_2(f)\, \exp.(j2\pi f\tau)\, df \qquad (2.2.13)$$

The autocorrelation function of a finite energy signal $m(t)$ is defined by

$$\phi_m(\tau) = \int_{-\infty}^{\infty} m(t)\, m(t-\tau)\, dt \qquad (2.2.14)$$

This is a special case of cross-correlation and measures the similarity of the signal with itself when shifted by

the amount $\tau$. The signal energy is the value of the autocorrelation function at $\tau=0$

$$\phi_m(0) = \int_{-\infty}^{\infty} |m(t)|^2 \, dt \qquad (2.2.15)$$

The energy-density spectrum and the autocorrelation function are a Fourier transform pair.

For <u>periodic signals</u> (having an infinite energy) the cross-correlation $\phi_{12}(\tau)$ is defined as

$$\phi_{12}(\tau) = \frac{1}{T} \int_{-T/2}^{T/2} m_1(t) m_2(t-\tau) \, dt \qquad (2.2.16)$$

Similarly the autocorrelation function is defined by

$$\phi_m(\tau) = \frac{1}{T} \int_{-T/2}^{T/2} m(t) \, m(t-\tau) \, dt \qquad (2.2.17)$$

The autocorrelation function of a periodic function is also periodic and it thus provides us with a means for detecting a periodic signal in the presence of additive noise.

Describing a signal $m(t)$ in the time domain requires a specification of its <u>duration</u>. In the frequency domain we require to specify its <u>bandwidth</u>. There are many possible ways to define the bandwidth and duration. The choice of a particular set is a matter of convenience. A

convenient choice is to define the bandwidth of the signal m(t) as the highest frequency beyond which the amplitude spectrum $|M(f)|$ of the signal is less than say 1 percent of the maximum value $|M(o)|$. We may thus ignore the spectrum of the signal which lies outside the useful band, of frequencies thus defined. In a similar fashion the duration of m(t) may be defined as the interval within which m(t) is larger than 1 percent of its maximum value. A second definition of bandwidth is the <u>equivalent rectangular bandwidth</u> denoted by $W_e$. This matches the area under the energy-density spectrum $|M(f)|^2$ of the signal to the area of a rectangle with height equal to the maximum value of $|M(f)|^2$ and width $2W_e$. Thus

$$W_e = \frac{\int_{-\infty}^{\infty} |M(f)|^2 \, df}{2|M(o)|^2} \qquad (2.2.18)$$

The equivalent duration is

$$T_e = \frac{\left[\int_{-\infty}^{\infty} |m(t)| \, dt\right]^2}{\int_{-\infty}^{\infty} |m(t)|^2 \, dt} \qquad (2.2.19)$$

Using Rayleigh's energy theorem we can show that

$$T_e \, W_e \geq 0.5 \qquad (2.2.20)$$

For signals m(t) that are positive or negative real-

valued functions of time for all t, we have

$$T_e W_e = 0.5 \qquad (2.2.21)$$

Thus the bandwidth of the signal is inversely proportional to its duration. This holds true irrespective of the definitions used.

In the frequency domain the system transfer function H(f) is the Fourier transform of the impulse response function h(t). The input-output relation of the system in the frequency domain is

$$Y(f) = H(f)\, M(f) \qquad (2.2.22)$$

The bandwidth of the system specifies the constancy of $|H(f)|$ and is customarily defined as the frequency at which the amplitude response $|H(f)|$ is 0.707 times its maximum value. This is the 3-dB bandwidth.

It is preferable in some applications to work with the logarithm of H(f) where we define

$$\ln H(f) \equiv \alpha(f) + j\beta(f) \qquad (2.2.23)$$

where the system gain is

$$\alpha(f) = \ln|H(f)| \qquad (2.2.24)$$

The phase of the system is $\beta(f)$. The gain and phase components of the transfer function of a linear time-invarient minimum-phase system are uniquely related to

each other according to:

$$\beta(f) = \frac{1}{\pi} \int_{-\infty}^{\infty} \frac{\alpha(\lambda)}{\lambda - f} \, d\lambda \qquad (2.2.25)$$

$$\alpha(f) = \alpha(\infty) - \frac{1}{\pi} \int_{-\infty}^{\infty} \frac{\beta(\lambda)}{\lambda - f} \, d\lambda \qquad (2.2.26)$$

The Paley-Wiener criterion gives the necessary and sufficient condition for the existence of the minimum phase $\beta(f)$ corresponding to a given gain function $\alpha(f)$ by requiring

$$\int_{-\infty}^{\infty} \frac{|\alpha(f)|}{1+(2\pi f)^2} \, df < \infty \qquad (2.2.27)$$

This is a frequency domain analog of the causality requirement in the time domain. For the Paley-Wiener condition to be valid $|H(f)|$ must be square integrable.

An important aspect of signal processing is the characterization of random signals that cannot be described by explicit mathematical relationships [Bendat and Piersol, 1971 and 1980]. A random process is an ensemble of time functions together with a probability rule that assigns a probability to each event associated with an observation of these functions. Consider a random process $\tilde{m}(t)$ and a set of times $t_i$, $i=1,\ldots,n$ in the time

interval on which the process is defined. The ability to specify the joint probability distribution function of $\tilde{m}_{t_i}$ provides a complete characterization of the random process. If the joint probability distribution function is invariant under shifts of the time origin, then the random process is strictly stationary.

The autocorrelation function of a random process $\tilde{m}(t)$ is defined (in terms of two random variables $\tilde{m}_t$ and $\tilde{m}_s$ obtained by observing $\tilde{m}(t)$ at times t and s) by

$$\phi_{\tilde{m}}(t,s) = E[\tilde{m}_t \tilde{m}_s]$$

$$= \int_{-\infty}^{\infty} \int_{-\infty}^{\infty} \tilde{m}_t \tilde{m}_s p_{\tilde{m}_t \tilde{m}_s}(\tilde{m}_t, \tilde{m}_s) d\tilde{m}_t \, d\tilde{m}_s \qquad (2.2.28)$$

For a stationary process the autocorrelation function is only a function of the difference between the observation times t and s, $\tau = t-s$. Thus

$$\phi_{11}(\tau) = \phi_{\tilde{m}}(\tau) = E[\tilde{m}_{t+\tau} \tilde{m}_t] \qquad (2.2.29)$$

A random process is wide-sense stationary if

$$E[\tilde{m}_t] = \text{constant}$$

$$E[\tilde{m}_t \tilde{m}_s] = \phi_{\tilde{m}}(t-s) \qquad (2.2.30)$$

Cross-correlation of two random processes $\tilde{m}_1(t)$ and

$\tilde{m}_2(t)$ may be defined by

$$\phi_{12}(t,s) = E[\tilde{m}_{1_t}\ \tilde{m}_{2_s}] \qquad (2.2.31)$$

and

$$\phi_{21}(t,s) = E[\tilde{m}_{2_t}\ \tilde{m}_{1_s}] \qquad (2.2.32)$$

The correlation matrix of $\tilde{m}_1(t)$ and $\tilde{m}_2(t)$ is defined by

$$\phi(t,s) = \begin{bmatrix} \phi_{11}(t,s) & \phi_{12}(t,s) \\ \phi_{21}(t,s) & \phi_{22}(t,s) \end{bmatrix} \qquad (2.2.33)$$

For $\tilde{m}_1(t)$ and $\tilde{m}_2(t)$ to be jointly wide-sense stationary it is necessary to have

$$\phi(t,s) = \phi(t-s) \qquad (2.2.34)$$

The <u>time average</u> of a sample function m(t) is defined as

$$\langle m(t) \rangle = \lim_{T\to\infty} \frac{1}{2T} \int_{-T}^{T} m(t)\, dt \qquad (2.2.35)$$

The time autocorrelation function is defined by

$$\langle m(t+\tau)m(t)\rangle = \lim_{T\to\infty} \frac{1}{2T} \int_{-T}^{T} m(t+\tau)m(t)dt \quad . \tag{2.2.36}$$

A random process such that any time average of one sample function is equal to the corresponding time average of any other sample function is called a regular random process. Regularity is the time-average analog of stationarity based on expectation. A random process is ergodic if time averages of a sample function of the process can be used as approximations to the corresponding ensemble averages or expectations of the process.

A process $\tilde{m}(t)$ is a Gaussian random process if every linear functional $\tilde{m}_1$ of $\tilde{m}(t)$ is a Gaussian random variable. The linear functional $\tilde{m}_1$ is given for every $g(t)$

$$\tilde{m}_1 = \int_{o}^{T} g(t)\, \tilde{m}(t)\, dt \tag{2.2.37}$$

provided that the mean square value of $\tilde{m}_1$ is finite. The output of a stable linear filter is a Gaussian random process $\tilde{y}(t)$ if the input $\tilde{m}(t)$ is a Gaussian random process.

When the input random process to a stable linear time-invariant filter is wide-sense stationary the output process $\tilde{y}(t)$ is also wide-sense stationary. The mean of the

output is:

$$E[\tilde{y}] = E[\tilde{m}]\ H(o) \qquad (2.2.38)$$

where H(o) is the d.c. gain of the system, and $E[\tilde{m}]$ is the mean of $\tilde{m}(t)$. The mean square value of the output is

$$E[\tilde{y}^2(t)] = \int_{-\infty}^{\infty} h(\tau_1)h(\tau_2)\phi_{\tilde{m}}(\tau_2-\tau_1)d\tau_1 d\tau_2 \qquad (2.2.39)$$

The frequency-domain equivalent of the above time-domain relation is obtained in terms of the spectral density or power spectrum $G_m(f)$ as

$$E[\tilde{y}^2(t)] = \int_{-\infty}^{\infty} |H(f)|^2\ G_{\tilde{m}}(f)\ df \qquad (2.2.40)$$

The spectral density $G_{\tilde{m}}(f)$ is the Fourier transform of the autocorrelation funotion $\phi_{\tilde{m}}(\tau)$

$$G_{\tilde{m}}(f) = \int_{-\infty}^{\infty} \phi_{\tilde{m}}(\tau)\ \exp.(-j2\pi f\tau)d\tau \qquad (2.2.41)$$

Since $G_{\tilde{m}}(f)$ and $\phi_{\tilde{m}}(\tau)$ are a Fourier transform pair then

$$\phi_{\tilde{m}}(\tau) = \int_{-\infty}^{\infty} G_{\tilde{m}}(f) \exp.(j2\pi f\tau)\, df \qquad (2.2.42)$$

The mean square value of a wide-sense stationary random process equals the area under the spectral density curve

$$\psi_m^2 = E[\tilde{m}^2(t)]$$

$$= \int_{-\infty}^{\infty} G_{\tilde{m}}(f)\, df \qquad (2.2.43)$$

The spectral density of the output of a linear filter with transfer function H(f) is related to the spectral density of the input by

$$G_y(f) = |H(f)|^2\, G_m(f) \qquad (2.2.44)$$

## 2.3 Acoustic signal source characteristics

Dynamite, exploded in shotholes is the major acoustic energy source used in land based exploration efforts. Other non-explosive energy sources, such as mechanical impactors and similar low-energy sources, are also used. In marine seismic work explosive-type acoustic energy sources are used. Non-explosive type sources include sparkers which generate seismic waves by the sudden discharge of current between electrodes, boomers and air guns are also used in the operation. In boomer type sources a metallic diaphragm (plate) is set in motion through discharge of a capacitor bank through a flat coil next to the plate. The eddy current effect causes a sudden strong movement of the plate against the water that generates a sharp pressure pulse. In the sparker type seismic waves are generated by the sudden discharge of current between electrodes in the water.

The source signal, used in producing the seismic reflection data analyzed in this thesis, is a repetitive impulse-like pressure acoustic wave, produced by an electrodynamic source (boomer) with maximum energy output of 600 Joules. The source is contained in the deep towed body (fish), known as the Huntec D.T.S. (Deep Towed System) as shown in Figure 2.3.1. Details of the design, performance evaluation and properties of the system are reported in a number of articles [Hutchins et.al.,1976],[McKeown,1975].

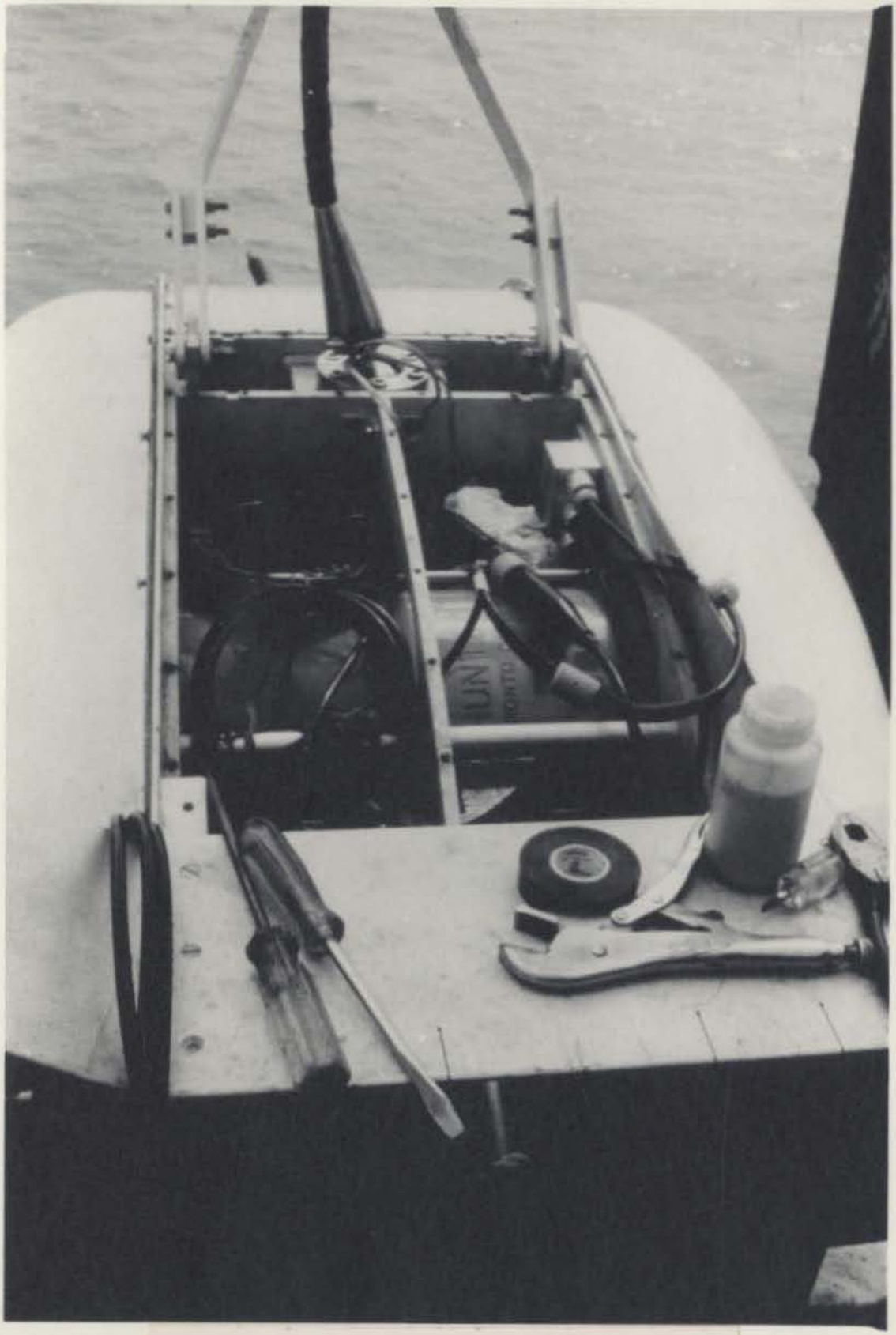

Figure 2.3.1 Deep towed system

The boomer is usually fired 1 to 4 times per second.

The source signal pressure waveform m(t) is shown in Figure 2.3.2.a. The mean value of the signal is zero. The autocorrelation $\phi_m(\tau)$ of the source signal m(t), is shown in Figure 2.3.2.b. It is seen that the autocorrelation function diminishes to zero as the correlation time delay increases. The time corresponding to the autocorrelation function becoming identically zero provides the value of the signal duration which is about 0.6 milliseconds. The amplitude of the Fourier spectrum of the source signal is $|M(f)|$ as shown in Figure 2.3.2.c, the phase angle of the Fourier spectrum of the source signal is $\theta(f)$ as shown in Figure 2.3.2.d. The power spectrum of the source signal is shown in Figure 2.3.2.e. This reveals that the signal is a broad-band signal, the power spectrum is above 10% of its peak value in the range 1.0 KHz to 6.0 KHz.

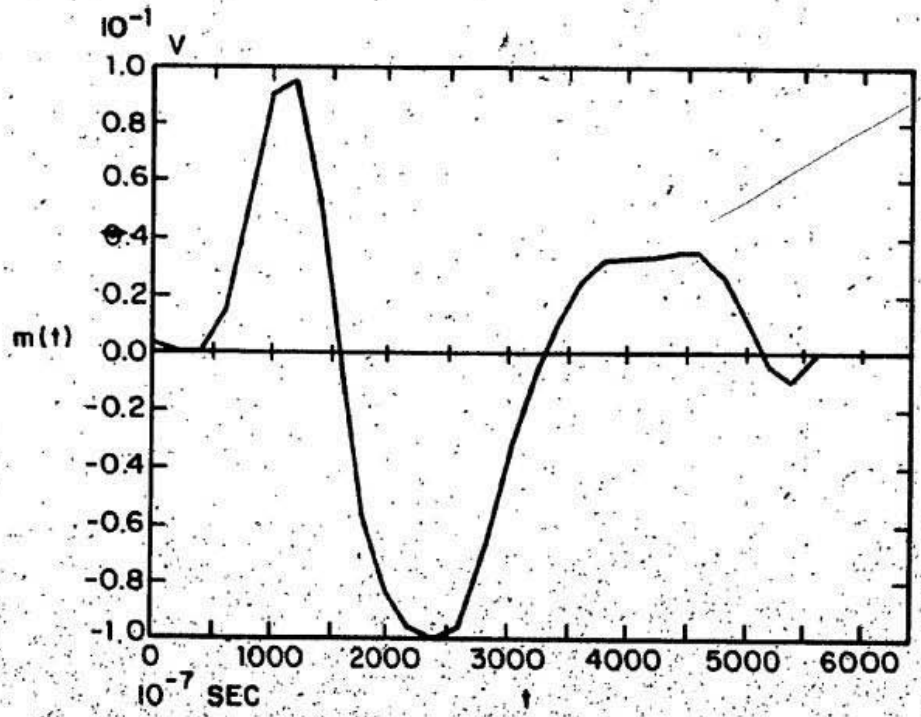


Figure 2.3.2.a The source signal waveform m(t)

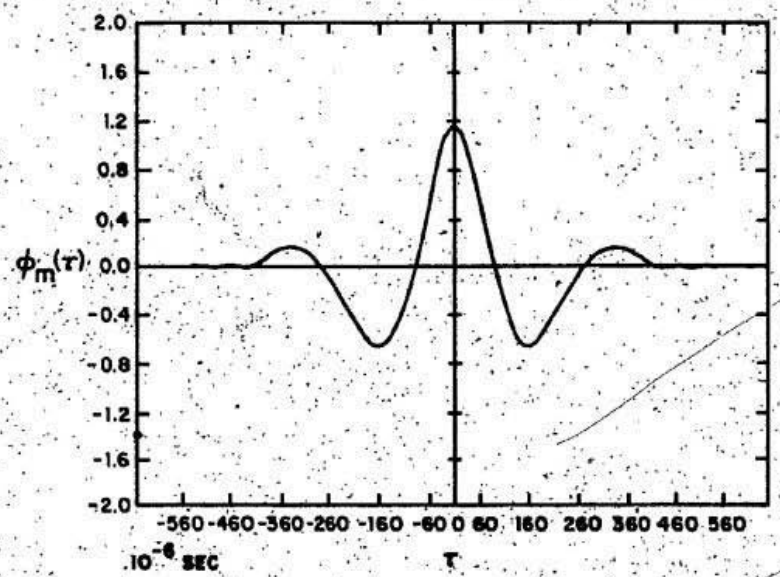


Figure 2.3.2.b The autocorrelation $\phi_{mm}(\tau)$ of the source signal m(t)

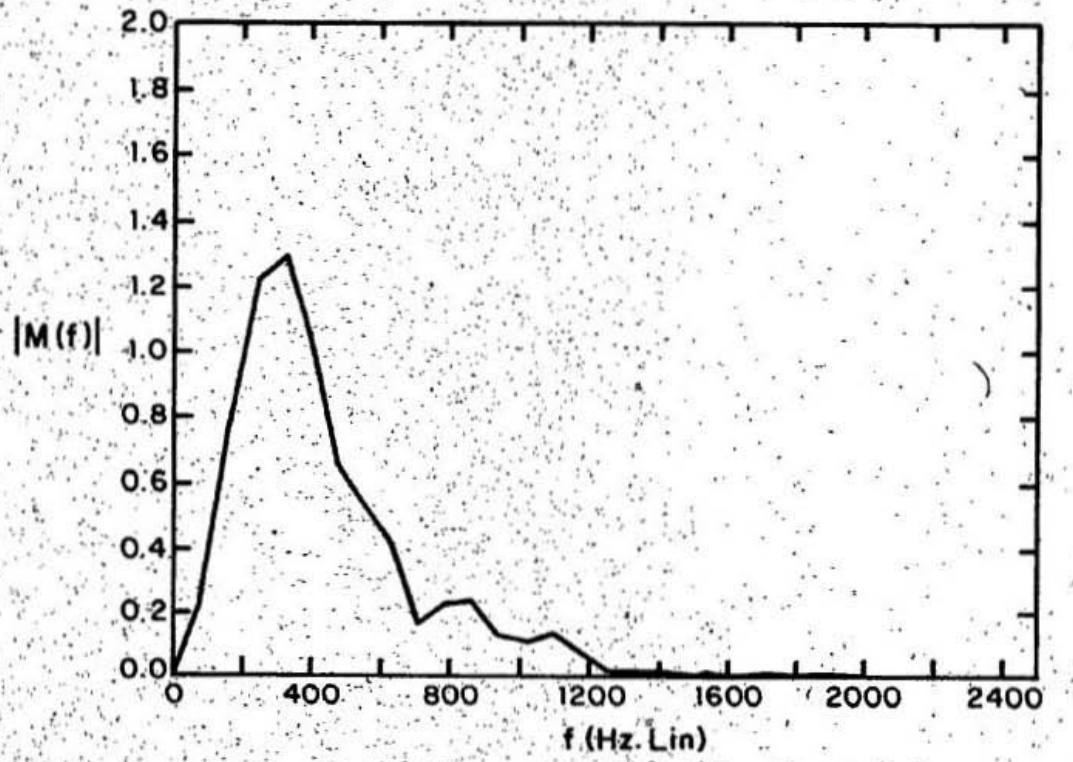


Fig. 2.3.2.c Magnitude of the Fourier spectrum |M(f)| of the source signal

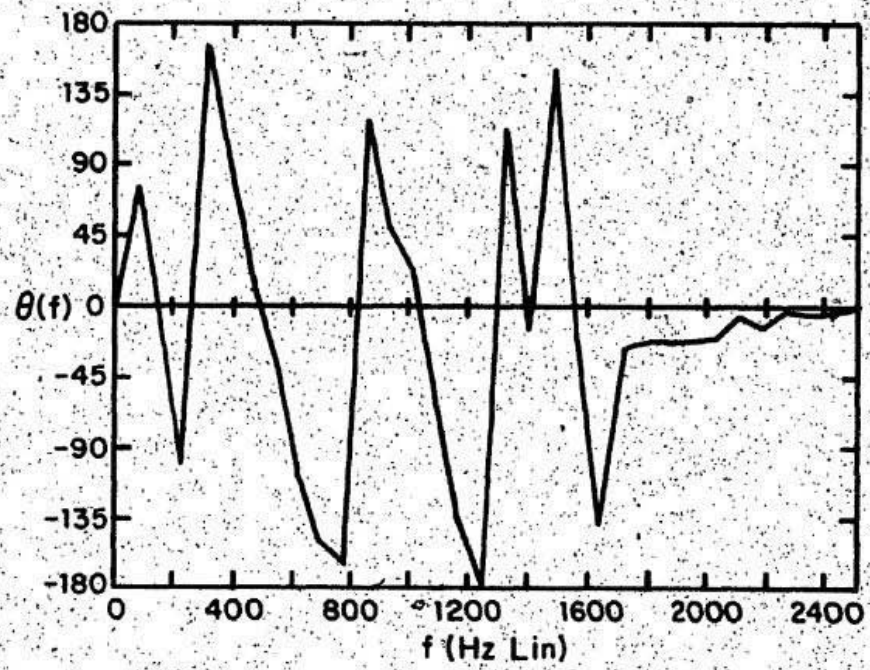


Fig. 2.3.2.d The phase angle of the Fourier spectrum θ(f) of the source signal

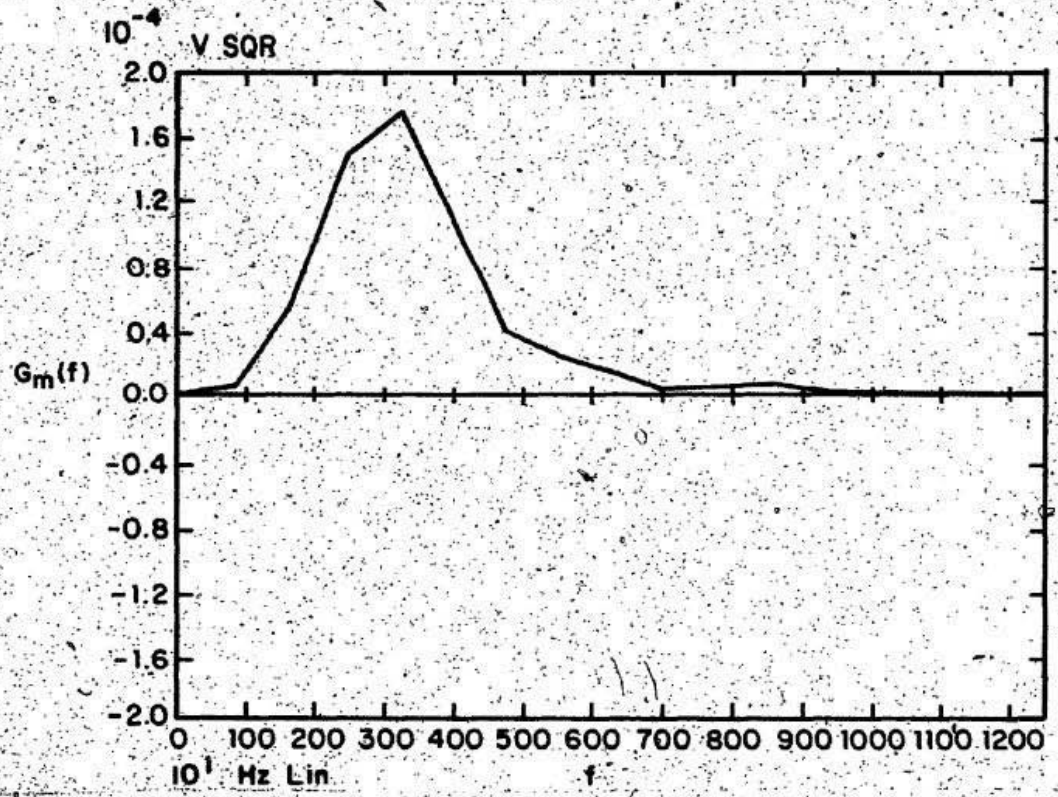


Fig. 2.3.2.e The power spectral density $G_m(f)$ of the source signal.

## 2.4 Some properties of acoustic wave propagation

The treatment of the propagation of sound in a single homogeneous and isotropic medium can be simplified by assuming plane wave propagation. This provides mathematically tractable models with a reasonable degree of accuracy in describing the physical phenomenon. The characteristic property of such waves is that the acoustic pressures and particle displacements have common phases and amplitudes at all points on any given plane perpendicular to the direction of wave propagation. Two particular forms of the acoustic plane wave equation in one dimension relate to the particle displacement $\zeta$ and pressure p.

$$\frac{\partial^2 \zeta(x,t)}{\partial t^2} = c^2 \frac{\partial^2 \zeta(x,t)}{\partial x^2} \qquad (2.4.1)$$

$$\frac{\partial^2 p(x,t)}{\partial t^2} = c^2 \frac{\partial^2 p(x,t)}{\partial x^2} \qquad (2.4.2)$$

c is the velocity of sound propagation in the medium, which is constant in a lossless homogeneous medium for all frequency components of a signal.

A solution of the equation for one variable is usually sufficient. This is due to the fact that all the variables are related, for example the pressure p is given in terms of particle displacement by

$$p(x,t) = -\rho c^2 \frac{\partial \zeta(x,t)}{\partial x} \qquad (2.4.3)$$

where $\rho$ is the density of the medium. The particle velocity u is

$$u(x,t) = \frac{\partial \zeta(x,t)}{\partial t} \qquad (2.4.4)$$

The general solutions of equations (2.4.1) and (2.4.2) are of the form

$$\zeta(x,t) = \zeta_+(t - \frac{x}{c}) + \zeta_-(t + \frac{x}{c}) \qquad (2.4.5)$$

Similarly

$$p(x,t) = p_+(t - \frac{x}{c}) + p_-(t + \frac{x}{c}) \qquad (2.4.6)$$

The first right hand side terms in Equations (2.4.5) and (2.4.6) represent forward moving waves while the second terms represent, backward moving waves. The particular forms of the functions $\zeta_+$, $\zeta_-$, $p_+$ and $p_-$ depend on the form of the source function.

From the available experimental data, the source signals are short pulses. Since in most cases the transient solutions are difficult to obtain directly, a synthesis of steady state solutions is made by using the Fourier integral theorem

$$p(x,t) = \frac{1}{2\pi} \int_{-\infty}^{\infty} P(x,\omega)\, e^{+j\omega t}\, d\omega \qquad (2.4.7)$$

where $P(x,\omega)$ is the Fourier transform of $p(x,t)$,

$$P(x,\omega) = \int_{-\infty}^{\infty} p(x,t)\, e^{-j\omega t}\, dt \qquad (2.4.8)$$

Thus a useful form of solution is that due to harmonic input. In complex form we thus have

$$\zeta(x,t) = \zeta_+(x,t) + \zeta_-(x,t) \qquad (2.4.9)$$

where

$$\zeta_+(x,t) = \xi_+\, e^{j(\omega t - kx)} \qquad (2.4.10)$$

$$\zeta_-(x,t) = \xi_-\, e^{j(\omega t + kx)} \qquad (2.4.11)$$

with

$$k = \omega/c \qquad (2.4.12)$$

Using Equations (2.4.3) and (2.4.4), we can see that

$$p(x,t) = j\,\rho\, c\,\omega(\xi_+(x,t) - \xi_-(x,t)) \qquad (2.4.13)$$

$$u(x,t) = j\,\omega(\xi_+(x,t) + \xi_-(x,t)) \qquad (2.4.14)$$

These complex relations show that, when plane waves are traveling in the positive x direction, p and u are in phase and leading the displacement by one quarter of a cycle ($90^\circ$ phase angle). In the negative x direction u leads $\zeta$ by $90^\circ$ but p lags $\zeta$ by $90^\circ$.

The concept of the acoustic impedance emerges if we write the expressions for p and u as

$$p(x,t) = p_+(x,t) + p_-(x,t) \qquad (2.4.15)$$

$$u(x,t) = u_+(x,t) + u_-(x,t) \qquad (2.4.16)$$

Where

$$p_+(x,t) = j\ \rho\ c\ \omega\ \xi_+(x,t) \qquad (2.4.17)$$

$$p_-(x,t) = -j\ \rho\ c\ \omega\ \xi_-(x,t) \qquad (2.4.18)$$

$$u_+(x,t) = j\ \omega\ \xi_+(x,t) \qquad (2.4.19)$$

$$u_-(x,t) = j\ \omega\ \xi_-(x,t) \qquad (2.4.20)$$

In analogy with the complex Ohms law, the ratio of pressure to particle velocity is defined as the acoustic impedance Z. For the forward moving wave

$$Z_+ = p_+/u_+ = +\ \rho\ c \triangleq Z, \qquad (2.4.21)$$

while for the backward moving wave we have

$$Z_- = p_-/u_- = -\ \rho\ c \triangleq -Z \qquad (2.4.22)$$

The acoustic impedance represents a useful quantifier of one of the acoustical properties of a medium.

If the acoustic pressure is not in phase with particle velocity then the acoustic impedance is complex valued. This is utilized in treating the reflection of plane waves in a fluid at the surface of a solid. The

acoustic impedance in this case is assumed to be analogous to the sinusoidal steady state impedance of an electrical passive element

$$Z_n = R_n + j X_n \qquad (2.4.23)$$

where $R_n$ is its resistive component and $X_n$ is its reactive component. And they are frequency dependent.

Knowledge of certain medium parameters such as density, velocity of sound propagation and/or acoustic impedance can provide information on the type of medium. The phenomenon of sound wave reflection and transmission at the interface between two media is useful in identifying the parameters.

Reflection at the interface of two media

At the interface between two media certain boundary conditions have to be satisfied. These are pressure compatibility and particle velocity continuity. Consider the interface between two media. The medium of incidence is characterized by a density $\rho_1$ and propagation velocity $c_1$, the second medium is characterized by $\rho_2$ and $c_2$. A reflected wave into medium 1 and a transmitted (or refracted) wave in medium 2 will result. Pressure waves are principally considered because most hydrophones are pressure-sensitive devices.

Assume that the incident angle measured from the

normal to an interface is $\theta_1$ and that $\theta_2$ is the corresponding angle of the transmitted wave, as shown in Figure 2.4.1. The two angles are related by Snell's Law as

$$\frac{\sin\theta_1}{c_1} = \frac{\sin\theta_2}{c_2} \qquad (2.4.24)$$

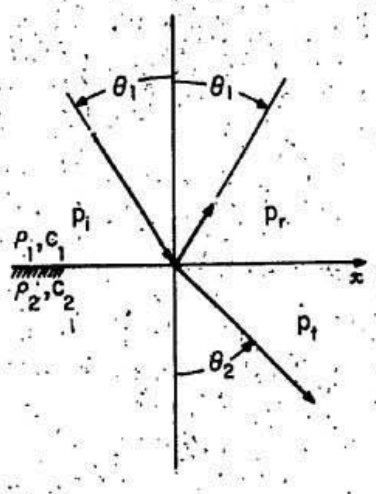


Figure 2.4.1 Pressure wave reflection geometry

The pressure reflection and transmission coefficients R and

T are defined by

$$\bar{R} = \frac{\bar{p}_r}{\bar{p}_i} \qquad (2.4.25)$$

and

$$\bar{T} = \frac{\bar{p}_t}{\bar{p}_i} \qquad (2.4.26)$$

The incident pressure is denoted by $p_i$, while $p_r$ denotes the reflected pressure, and $p_t$ is the transmitted pressure. Fig. 2.4.2 shows a schematic illustration of the reflection process for a single acoustic interface.

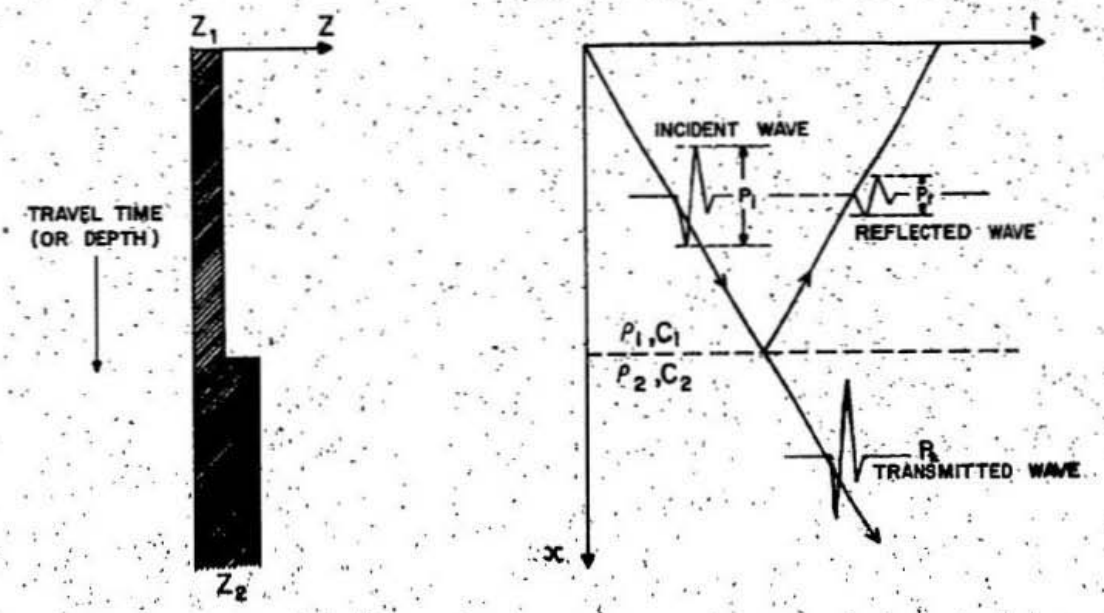


Figure 2.4.2 A schematic illustration of the reflection process for a single acoustic interface.

In terms of the media specifications we have

$$R = \frac{Z_2 \cos\theta_1 - Z_1 \cos\theta_2}{Z_2 \cos\theta_1 + Z_1 \cos\theta_2} \qquad (2.4.27)$$

For normal wave incidence $\theta_1 = \theta_2 = 0^\circ$, hence the reflection coefficient is given by

$$R = \frac{\rho_2 c_2 - \rho_1 c_1}{\rho_2 c_2 + \rho_1 c_1} \qquad (2.4.28)$$

Note that R is a real number in the case of a two-fluids interface.

The situation with a fluid-solid interface is different. In this case the phasor incident and reflected pressures in medium 1 are related by

$$\frac{\bar{p}_r}{\bar{p}_i} = \frac{Z_n - \rho_1 c_1}{Z_n + \rho_1 c_1} \qquad (2.4.29)$$

Thus the reflection coefficient will be complex [Waters, 1978].

$$\bar{R} = \frac{(R_n - \rho_1 c_1) + jX_n}{(R_n + \rho_1 c_1) + jX_n} \qquad (2.4.30)$$

Its magnitude is

$$|R| = \left[\frac{(R_n - \rho_1 c_1)^2 + X_n^2}{(R_n + \rho_1 c_1)^2 + X_n^2}\right] \qquad (2.4.31)$$

In marine seismic applications two interfaces with strong reflection coefficients are encountered. The air-water interface has a reflection coefficient of almost -1, while the water-sediment interface has typically reflection coefficients of magnitude up to the order of 0.8,[Damotte, 1971].

## 2.5 Some properties of marine sediments

The physical properties of the sediments affect the reflection of the sound pressure at the sea floor. The important properties are the density $\rho$ and the compressional wave velocity c. These depend on the water content in the sediment, often represented by the porosity $\eta$, and the properties of the solid component of the sediment. Many papers are available from the areas of geology, geophysics and soil mechanics, treating elastic, and visco-elastic properties of dry and water-saturated rocks and sediments.

A fundamental expression for the velocity of a compressional wave in an elastic medium is given by

$$c_p = \left(\frac{k + 4/3\ \mu}{\rho}\right)^{1/2} \qquad (2.5.1)$$

where k is the bulk modulus or incompressibility $(1/\beta)$, $\mu$ is the shear (rigidity) modulus, $\rho$ is the density, and $\beta$ is the compressibility of the sediments.

To obtain the medium bulk modulus k, it is practical to use Stoll's form of Gassman's equation (2.5.1), giving the compressibility $\beta$ by

$$\beta = \beta_s \frac{(\beta_s - \beta_f) + \eta k_s\ \beta_f(\beta_s - \beta_\omega)}{(\beta_s - \beta_f) + \eta(\beta_s - \beta_\omega)} \qquad (2.5.2)$$

Here one needs to know four components: porosity $\eta$, the bulk modulus of the pore water $k_\omega = \frac{1}{\beta_\omega}$, the aggregate bulk modulus of the solids $k_s$ and the frame bulk modulus $k_f$. $k_\omega$ is calculated from

$$k_\omega = \rho c_\omega^2 \qquad (2.5.3)$$

Subscript $\omega$,s, and f on $\beta$'s, Equation(2.5:2) identify similarly the compressibility parameters for the respective media. Typical bulk modulus values as given in [Clay and Medwin, 1977] are

| | |
|---|---|
| medium sand | $k_s = 51\ N/m^2$ |
| silt-clay | $k_s = 50\ N/m^2$ |
| clayey-silt | $k_s = 54\ N/m^2$ |

The frame bulk modulus $k_f$ varies with the porosity. A typical relationship given by Hamilton, [Hamilton, 1971] is shown in Figure 2.5.1

The dynamic rigidity $\mu$ for different media varies with the porosity. Experimental data, due to Hamilton, is shown in Figure 2.5.2.

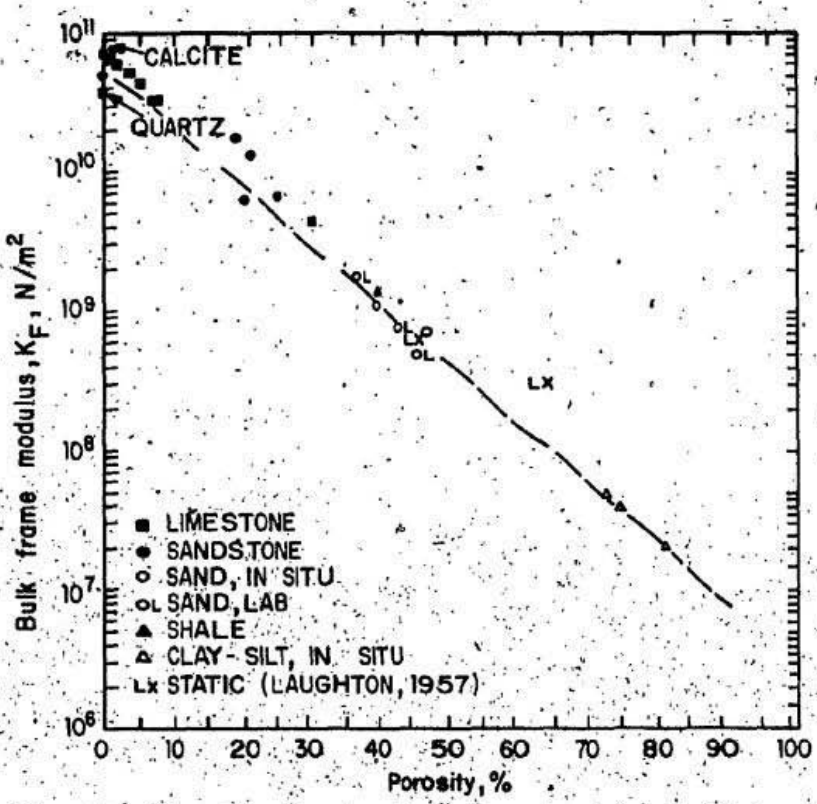


Figure 2.5.1 Dynamic bulk frame modulus $k_f$ (Hamilton, 1971a).

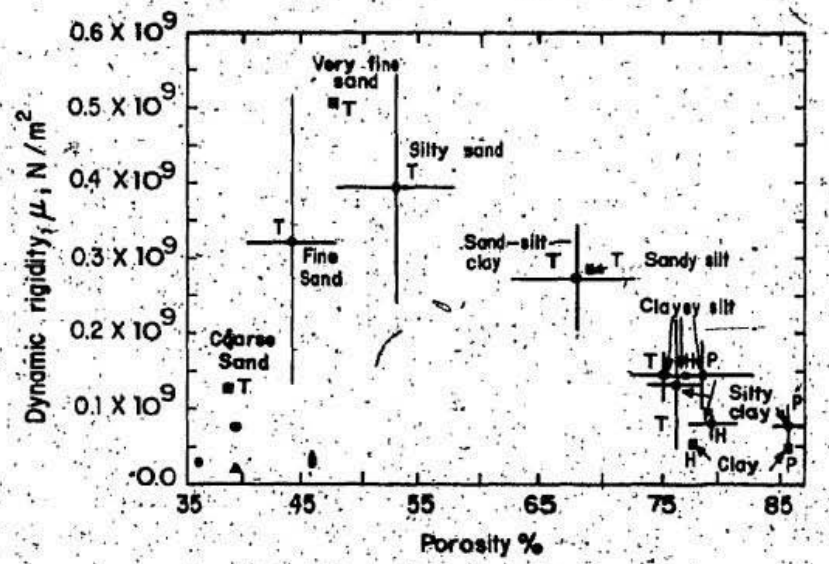


Figure 2.5.2 Dynamic rigidity μ versus porosity (Hamilton, 1971a).

## 2.6 Noise considerations

A general definition of noise is given in IEEE Standard Dictionary of Electrical and Electronic Terms, as unwanted disturbances superposed upon a useful signal that tend to obscure its information content. Within this context, the ocean environment, ship machinery and ship and towed body motion as well as receiving equipment act as sources of noise in the acoustic signals received by the hydrophones. Accordingly a broad classification of noise types is:

i - Ambient or background noise.

ii - Motion induced noise due to ship and towed body.

iii - Sonar system electrical self noise.

A large number of sources contribute to the background noise. Among these wind, and the induced waves, bubbles and droplets are significant factors above 100 Hz. Machinery of nearby and distant ships are also sources of noise in the frequency range 10 to 150 Hz. Seismic activity contributes noise in the frequency band less than 10 Hz. [Clay and Medwin, 1977]

Mechanical vibrations and motion (heave) of the ship and the towed body are additional sources of noise. The sonar system self noise is essentially due to fluctuations of the current through components as well as

thermal-resistor noise due to voltage fluctdtions.

The noise effects indicated above exist whether or not an acoustic pressure test signal is present. There are further sources of noise that arise due to the presence of the signal. These may be attributed to the components of the medium's response which are not accounted for by the model used. For the purposes of this thesis we have the following:

1 - Scattering and diffraction

Scattering is due to secondary waves resulting from the incidence of a primary wave on small regions of different acoustical properties than those of the transmitting medium. Diffraction is caused by wave motion beyond an obstacle which has cut off portions of the advancing wave-front. In scattering the anomalous region acts as a source of secondary waves under the influence of an incident primary wave. In diffraction problems the disected wave-front is the source for the description of propagation in the medium ahead of it. [Officer, 1958]

2 - Ringing and reverberation

Multiple reflections (reverberations) occur within the water layer in marine seismic exploration. The water-air interface is a strong reflector (with reflection coefficient close to -1). If the water-bottom interface is also a strong reflector, then the water layer traps the energy. The seismic pulse will be successively reflected

between the two interfaces. As a consequence, reflections from deep below the water layer may be masked by the water reverberations.

It is important to note that for the shallow marine application the useful reflection signals of interest are received much earlier than the arrival time of masking signals due to surface and surface-bottom multiples.

3 - Irregular interface

The submarine topography will not generally be horizontal. Irregular sloping bottoms are the real physical interface. To consider the true bottom profile presents a difficult problem. Instead, approximations are used. The simplest is the horizontal approximation. A better approximation is an inclined linear profile. The most realistic approximations are the smooth curve and a piecewise linear approximation as shown in Figure 2.6.1.

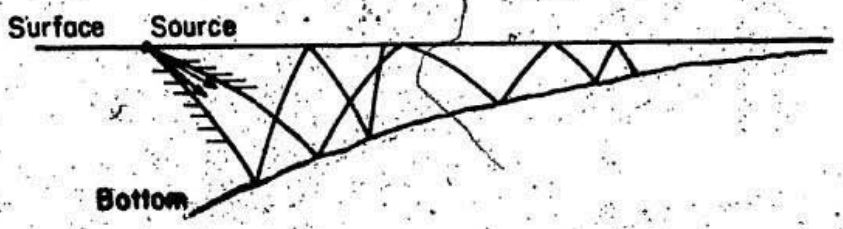


Figure 2.6.1 Bottom profile "a piecewise linear approximation"

## 2.7 Attenuation in layered media

The propagation of elastic plane waves through rock and strata is observed to be accompanied by attenuation or absorption and pulse shape spreading. According to the Encyclopedic Dictionary of Exploration Geophysicists, there is more than one definition for attenuation [Clay and Medwin, 1977] one definition is a reduction in the amplitude of seismic waves such as produced by divergence, reflection and scattering, and absorption. This attenuation varies with depth and frequency of the propagating wave. At low frequencies, attenuation decreases with depth and increases almost linearly with frequency.

A simple model to account for attenuation effects is based on assuming a complex velocity of propagation

$$\bar{c}(\omega) = c(\omega)/\gamma(\omega) \qquad (2.7.1)$$

Normally $\gamma$ is a small angle; thus the following approximation is used

$$\cos\gamma \approx 1 \qquad (2.7.2)$$

$$\sin\gamma \approx \gamma \qquad (2.7.3)$$

The pressure wave is given by

$$p(x,t) = p_o\, e^{j\omega(t-\frac{x}{c})} + p_o\, R\, e^{j\omega(t+\frac{x}{c})} \qquad (2.7.4)$$

where the first term is the incident pressure wave propagating in the forward direction and the second is the reflected pressure wave propagating in the backward direction. Note that R may be complex. With a complex c we obtain

$$p(x,t) = p_o\, e^{j\omega\left(t-\frac{x(1-j\gamma)}{|c|}\right)} + p_o\, R\, e^{j\omega\left(t+\frac{x(1-j\gamma)}{|c|}\right)} \qquad (2.7.5)$$

One defines the attenuation coefficient $\alpha$ by

$$\alpha = \omega\gamma/|c| \qquad (2.7.6)$$

As a result

$$p(x,t) = p_o\, e^{-\alpha x}\, e^{j\omega\left(t-\left|\frac{x}{c}\right|\right)} + p_o\, R\, e^{\alpha x}\, e^{j\omega\left(t+\left|\frac{x}{c}\right|\right)} \qquad (2.7.7)$$

Thus the forward incident (downward) pressure is a wave that attenuates downward with the distance. The backward reflected (upward) pressure is a wave that attenuates upward with the distance. Figure 2.7.1 shows the components of the waves considered in two media.

The evaluation of the attenuation coefficient $\alpha$ can be performed in terms of the specific dissipation constant $1/Q$ through the relation

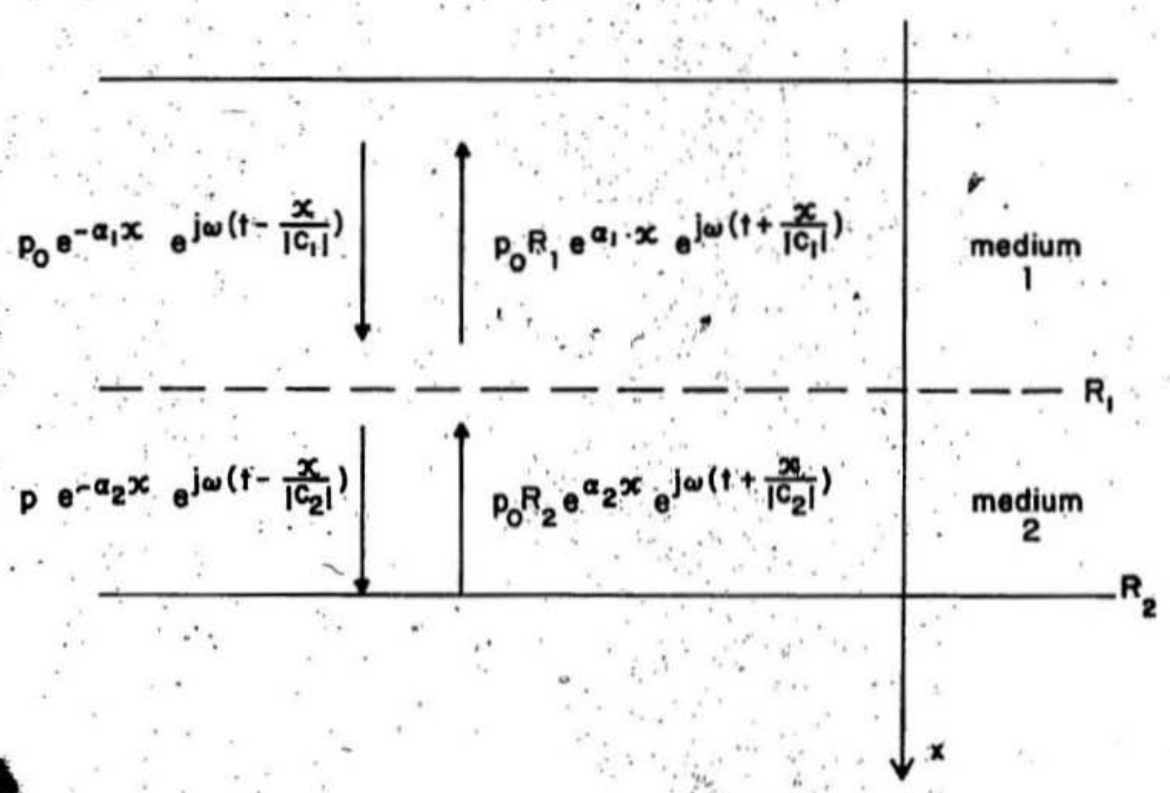


Figure 2.7.1
The components of the waves considered in two media

$$\alpha = \frac{\pi f}{Qc} \qquad (2.7.8)$$

Results of experimental determination of Q for many types of solids has been documented [Waters, 1978].

# CHAPTER 3

## A SURVEY OF APPROACHES TO SEISMIC MODELING

### 3.1 Introduction

The purpose of this chapter is to review a number of important approaches to modeling the response of the subsurface to acoustic or seismic excitation. Models of this nature are known as synthetic seismograms. Here the mathematical form of the input excitation function (normally an impulse or a sinusoidal function) is known. The modeling task can be generally stated as tracing the input wave as it travels through the medium to the receiving equipment.

Several modeling assumptions are common to all models described here. A flat completely elastic layered medium structure with plane acoustic wave propagation is assumed. Normal wave incidence is assumed. This is appropriate for the available field results where the source and the down looking receivers are in close proximity. The models considered differ in the degree of detail and mathematical refinement.

Many factors have contributed to the advances in synthetic seismograms development. Among these factors is the introduction of the digital computers. The field has benefitted from this tool as did virtually all areas of scientific and technological activities. Another major

factor is the advent of the continuous velocity logs. These logs show the velocity of the sound propagation in the formation as function of depth. Peterson and his co-workers [Peterson, Fillippone and Croker, 1955] were the first to use these tools to predict the reflection signal record. They based their development on the earlier work of Thomson [Thomson, 1950], where the first matrix formulation of the propagation process was introduced. The next section deals with Peterson's model which models the reflection process by the incremental changes in the logarithm of layer acoustic impedance. According to Wuenschel [Wuenschel, 1960], Peterson's model offers a remarkably close approximation to field seismograms in many cases. The model however does not allow for multiple reflections.

The second model reviewed is due to Berryman, Goupillaud and Waters (1958). In this case multiple reflections are considered and the velocity function is assumed to be approximated by straight line segments. The model is a frequency response type and provides an iterative sequence for calculating the reflection coefficients of the medium. There is a potential for many refinements on this model mainly in the form of the velocity function approximation. Other possible refinements can be made in the details of the computations. This is of importance since a computational approach to calculating a Fourier

integral is necessary with this model.

The third model considered is that of Baranov and Kunetz [Baranov and Kunetz, 1960]. In this approach, an elegant space-time-diagram procedure is utilized. Here points on a quadrangle are considered and conditions at the extreme point are easily calculated in terms of known values at three other points.

Thomson's and Peterson's formulations were utilized by Wuenschel. The attractive matrix formulation given in this model includes multiples and enables the consideration of problems where source and receiver are in different layers. Wuenschel's formulation, given in the Laplace operator notation, uses particle velocity and stress in each layer as the variables. This is reviewed in Section 3.5. It is thought that this formulation can provide the basis for an electric transmission line equivalent formulation that deals with a more generalized problem.

Goupillaud's model dealt with in Section 3.6 was developed parallel to that of Wuenschel. Apart from the trivial difference of using frequency domain formulation, Goupillaud uses the up-going and down-going propagating pressure waves as the formulation variables. A matrix recursion is obtained. Many subsequent refinements can be traced to Goupillaud's form.

A linear filter model has been introduced by Sengbush,

Lawrence, and McDonal (SLM) [Sengbush, et al., 1961]. It is based on modifications of Peterson's work to accommodate velocity dependent densities of the layers. This is reviewed in Section 3.7. Extrapolating the (SLM) approach one can speculate on further refinements by considering various density-velocity dependence models.

E. A. Robinson's contributions to seismic modeling are in the area of time-series analysis and digital filtering. These are based on a model developed in the Z-transform domain that enables a concise time-series representation of the phenomenon. The details of this model are given in Section 3.8.

Time-domain quasi-state space models were developed by Mendel et. al. These find their bases in earlier work cited above. This is reviewed in Section 3.9.

Vetter and El-Hawary, (1979) concentrate on the input-output relationship and in particular the decomposition of the output into tractable wavelet components. Contributions of layer characteristics to individual components are underlined by considering the different types of reflection processes in the medium. This enables a correlation between system response and structural detail. This approach is reviewed briefly in the concluding section of this chapter.

## 3.2 The Peterson, Fillippone and Croker model

In this early work by Peterson, Fillippone and Croker (1955) an earth model based on approximating the reflection coefficient is proposed. For normal incidence, plane wave propagation between media 1 and 2, the reflection coefficient is given according to equation (2.4.5) by

$$R = \frac{Z_2 - Z_1}{Z_2 + Z_1} \qquad (3.2.1)$$

The incremental change in impedance $\Delta Z$ is introduced as

$$\Delta Z \triangleq Z_2 - Z_1 \qquad (3.2.2)$$

Thus approximately we have

$$R \cong \frac{\Delta Z}{2Z} \qquad (3.2.3)$$

where

$$Z \cong Z_2 \cong Z_1 \qquad (3.2.4)$$

As a result, the reflection coefficient can be expressed as

$$R = \frac{1}{2} \Delta[\ell n(z)] \qquad (3.2.5)$$

The interpretation of the above expression is that the amplitude of the wave reflected by each incremental change in the acoustic impedance is proportional to the corresponding incremental change in the value of the logarithm of acoustic impedance.

Consider the case of three layers giving rise to

two changes in acoustic impedance as shown in Figure (3.2.1). The upper step change represents an increase in the value of the acoustic impedance while the lower one corresponds to a decrease. Consequently the two reflected pulses have opposite polarity. The signal received by the hydrophones (the seismograph) is shown in the diagram. The analytic expression for this signal is:

$$y(t) = m(t) + R_1 m(t-\tau_1) + R_2 m(t-\tau_2) \qquad (3.2.6)$$

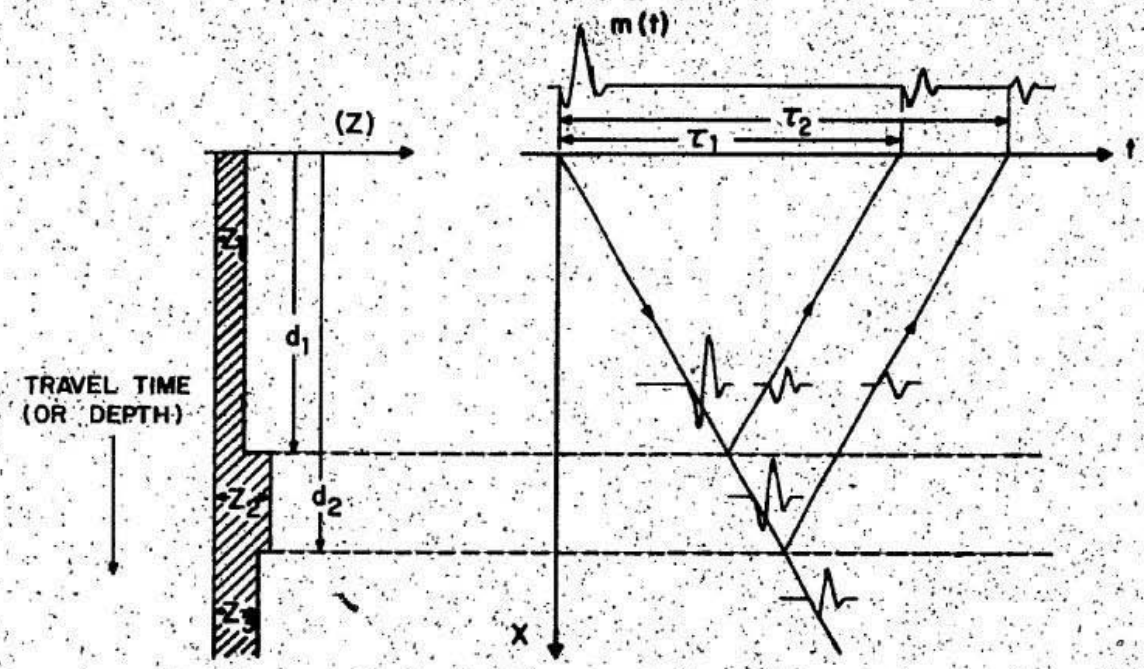


Fig. 3.2.1 A Schematic illustration of the reflection process for two acoustic interfaces.

The delay times $\tau_1$ and $\tau_2$ correspond to the wave travel times

$$\tau_1 = 2\, d_1/c_1 \qquad (3.2.7)$$

$$\tau_2 = \tau_1 + 2\,\frac{(d_2-d_1)}{c_2} \qquad (3.2.8)$$

The reflection coefficients are

$$R_1 = \frac{1}{2}\,\Delta[\ell n(Z)]$$

$$= \frac{1}{2}\,[\ell n(Z_2) - \ell n(Z_1)] \qquad (3.2.9)$$

$$R_2 = \frac{1}{2}\,[\ell n(Z_3) - \ell n(Z_2)] \qquad (3.2.10)$$

In the practical situation where the acoustic impedance varies almost continuously with depth, we may use a stepwise approximation. The steps occur at infinitesimally small depth intervals corresponding to the shortest wave length of interest. This situation is shown in Figure 3.2.2. In this case we write

$$y(t) = m(t) + \sum_{i=1}^{N} R_i\, m(t-\tau_i) \qquad (3.2.11)$$

where N is the number of layers.

$$\tau_i = \tau_{i-1} + 2\,\frac{(d_i-d_{i-1})}{c_i} \qquad (3.2.12)$$

$$R_i = \frac{1}{2}[\ell n(Z_{i+1}) - \ell n(Z_i)] \qquad (3.2.13)$$

Thus a synthetic seismograph can be obtained from a given impedance record.

A minor modification to the derivation given above results from the observation that Equations (3.2.1) and (3.2.2) can be combined to give

$$R = \frac{(\Delta Z/2Z_i)}{1 + (\Delta Z/2Z_1)} \qquad (3.2.14)$$

Thus for

$$Z \cong Z_1$$

one gets

$$R \cong \frac{\Delta\ \ell n(Z)}{2+\Delta\ \ell n(Z)} \qquad (3.2.15)$$

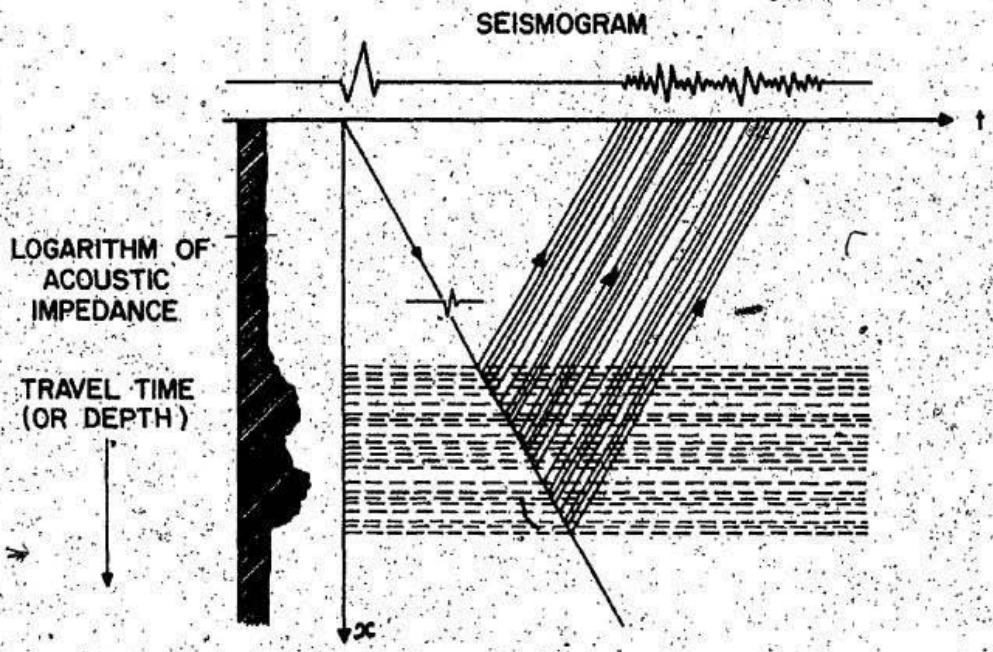


Fig. 3.2.2 A Schematic illustration of the reflection of a seismic pulse from an acoustic impedance distribution exhibiting continuous variation.

## 3.3 The Berryman, Goupillaud and Waters model

Berryman, Goupillaud and Waters (BGW)(1958) present a method for calculating the reflection response (synthetic seismogram) of layered media assuming variable velocity distribution. Their model is based on the particle displacement equation

$$\frac{\partial^2 \zeta(x,t)}{\partial t^2} = c^2 \frac{\partial^2 \zeta(x,t)}{\partial x^2} + 2c \frac{\partial c}{\partial x} \frac{\partial \zeta(x,t)}{\partial x} \qquad (3.3.1)$$

Assuming a sinusoidal input, one has

$$\zeta(x,t) = \xi(x,t)e^{j\omega t} \qquad (3.3.2)$$

As a result $\xi(x)$ satisfies

$$\frac{d}{dx}\left(c^2 \frac{d\xi(x,t)}{dx} + \omega^2 \xi(x,t)\right) = 0 \qquad (3.3.3)$$

A new variable $\Pi(x)$ is introduced

$$\Pi(x) = c^2 \frac{d\xi(x,t)}{dx} \qquad (3.3.4)$$

Note that the pressure $p(x,t)$ can thus be obtained as

$$p(x,t) = \rho\Pi(x)e^{j\omega t} \qquad (3.3.5)$$

Eliminating $\xi$ from equation (3.3.3) gives

$$c^2 \frac{d^2\Pi}{dx^2} + \omega^2\Pi = 0 \qquad (3.3.6)$$

This is the main equation used in the (BGW) derivation.

Assuming a linear velocity distribution in the kth layer.

$$c(x) = c_k + b_k\,(x-x_k), \qquad (3.3.7)$$

with $c_k$, $b_k$ and $x_k$ being constants one obtains by substituting for c in equation (3.3.6) the following

$$[c_k + b_k(x-x_k)]^2 \frac{d^2\Pi_k}{dx_k^2} + \omega^2\Pi_k = 0 \qquad (3.3.8)$$

The general solution of this second order differential equation is

$$\Pi_k(x) = \Pi_k^+ \exp.\{\tfrac{1}{2}(1-\beta_k)\ln(1+(b_k(x-x_k)/c_k))\} + \Pi_k^- \exp.\{\tfrac{1}{2}(1+\beta_k)\ln(1+(b_k(x-x_k)/c_k))\} \qquad (3.3.9)$$

where

$$\beta_k = \sqrt{1-(4\omega^2/b_k)} \qquad (3.3.10)$$

The constants of integration are $\Pi_k^+$ and $\Pi_k^-$.

To simplify the notation the variable $\gamma_k$ is introduced as

$$\gamma_k = \ln(1 + (b_k(x-x_k)/c_k)) \qquad (3.3.11)$$

Thus

$$\Pi_k(x) = \Pi_k^+ \exp.\{\tfrac{1}{2}(1-\beta_k)\gamma_k\}$$

$$+ \Pi_k^- \exp.\{\tfrac{1}{2}(1+\beta_k)\gamma_k\} \qquad (3.3.12)$$

The displacement $\xi$ in terms of $\Pi$ is given by

$$\xi(x) = -\frac{1}{\omega^2}\frac{d\Pi}{dx} \qquad (3.3.13)$$

As a result

$$\xi_k(x) = \frac{-b_k e^{\gamma_k/2}}{2\omega^2[c_k+b_k(x-x_k)]}[\Pi_k^+(1-\beta_k)e^{-\beta_k\gamma_k/2}$$

$$+ \Pi_k^-(1+\beta_k)e^{+\beta_k\gamma_k/2}] \qquad (3.3.14)$$

The ratio of displacement $\xi$ to $\Pi$ defines the new variable A(x).

$$A_k(x) = \xi_k(x)/\Pi_k(x) \qquad (3.3.15)$$

Utilizing equations (3.3.12) and (3.3.14), one obtains

$$A_k(x) = \frac{-b_k}{2\omega^2(c_k+b_k(x-x_k))}\left[1-\beta_k\frac{1-R_k e^{\beta_k\gamma_k}}{1+R_k e^{\beta_k\gamma_k}}\right]$$

$$(3.3.16)$$

Where the coefficient $R_k$ is defined by

$$R_k = \Pi_k^- / \Pi_k^+ \qquad (3.3.17)$$

The boundary condition requiring continuity of $\xi(x)$ and $\Pi(x)$ at the interfaces results in a continuity requirement on $A(x)$. Thus for $x = x_k$, the interface between the (k-1) and kth layer, one has in the kth layer

$$A_k(x_k) = \frac{-b_k}{2\omega^2 c_k} \left[1-\beta_k \frac{1-R_k}{1+R_k}\right] \qquad (3.3.18)$$

In the (k-1)th layer

$$A_{k-1}(x_k) = \frac{-b_{k-1}}{2\omega^2[c_{k-1}+b_{k-1}(x_k-x_{k-1})]} \left[1-\beta_{k-1} \frac{1-R_{k-1}\, e^{\beta_{k-1}\gamma_{k-1}}}{1+R_{k-1}\, e^{\beta_{k-1}\gamma_{k-1}}}\right] \qquad (3.3.19)$$

By continuity of velocity

$$c_k = c_{k-1} + b_{k-1}(x_k-x_{k-1}) \qquad (3.3.20)$$

Thus

$$A_{k-1}(x_k) = \frac{-b_{k-1}}{2\omega^2 c_k}\left[1-\beta_{k-1}\frac{1-R_{k-1}\, e^{\beta_{k-1}\,\ell n\,\frac{c_k}{c_{k-1}}}}{1+R_{k-1}\, e^{\beta_{k-1}\,\ell n\,\frac{c_k}{c_{k-1}}}}\right]$$

(3.3.21)

Equating (3.3.19) and (3.3.21), one obtains

$$b_k\left[1-\beta_k\frac{1-R_k}{1+R_k}\right] = b_{k-1}\left[1-\beta_{k-1}\frac{1-R_{k-1}\, e^{\beta_{k-1}\,\ell n\,\frac{c_k}{c_{k-1}}}}{1+R_{k-1}\, e^{\beta_{k-1}\,\ell n\,\frac{c_k}{c_{k-1}}}}\right]$$

(3.3.22)

The above relation is reduced to a form giving $R_{k-1}$ in terms of $R_k$ and the layer characteristics as

$$R_{k-1} = \frac{b_{k-1}\beta_{k-1}+(b_k-b_{k-1})+b_k\beta_k\frac{1-R_k}{1+R_k}}{b_{k-1}\beta_{k-1}-(b_k-b_{k-1})+b_k\beta_k\frac{1-R_k}{1+R_k}} \cdot e^{-\beta_{k-1}\ell n(c_k/c_{k-1})}$$

(3.3.23)

In the case of regions of constant velocity the formula for the coefficients is obtained from the solution to the equation (3.3.6) as

$$R_{k-1} = \left(\frac{r_k + R_k}{1 + r_k R_k}\right) e^{-j2(x_k - x_{k-1})/c_{k-1}} \qquad (3.3.24)$$

where

$$r_k = \frac{c_{k-1} - c_k}{c_{k-1} + c_k} \qquad (3.3.25)$$

To produce a synthetic seismogram, the bottom layer is assumed to have no reflection and thus $R_N = 0$. Calculations are done backwards, thus $R_{N-1}$ is calculated according to either equation (3.3.23) or equation (3.3.24), then $R_{N-2}, \ldots, R_o$. This last reflection coefficient gives the reflection response for the specific frequency $\omega$. The overall synthetic seismogram is obtained through the use of the Fourier integral.

## 3.4 The Baranov and Kunetz model

Baranov and Kunetz (BK) (1960) assumed a layered medium with the wave equation in terms of displacement $\zeta(x,t)$ in each layer given by

$$\frac{\partial^2 \zeta(x,t)}{\partial x^2} = \frac{1}{c^2} \frac{\partial^2 \zeta(x,t)}{\partial t^2} \qquad (3.4.1)$$

In terms of the Laplace transformed displacement $\xi(s,x)$, the general solution of the wave equation is

$$\xi(s,x) = \xi^+ e^{-\frac{sx}{c}} + \xi^- e^{+\frac{sx}{c}} \qquad (3.4.2)$$

Baranov and Kunetz use this expression to derive a finite difference equation model of the process.

Consider two layers k and k+1, with velocity of propagation $c_k$ and $c_{k+1}$ respectively. The layer thickness corresponds to equal one-way travel time $\tau$

$$\frac{d_k}{c_k} = \frac{d_{k+1}}{c_{k+1}} = \tau \qquad (3.4.3)$$

Assume that the interface between the two layers is at a depth x. The displacement equation at the top of the kth layer denoted by point M in Figure 3.4.1 is given by

$$\xi_M = \xi_k(s,(x-d_k)) \qquad (3.4.4)$$

This turns out to be

$$\xi_M = \xi_k^+ e^{-s(\frac{x}{c_k} - \tau)} + \xi_k^- e^{+s(\frac{x}{c_k} - \tau)} \qquad (3.4.5)$$

For point B at the interface two expressions for displacement can be written. The first is obtained by assuming that the point B is in the kth layer.

$$\xi_B = \xi_k(s,x) \qquad (3.4.6)$$

This gives

$$\xi_B = \xi_k^+ e^{-\frac{sx}{c_k}} + \xi_k^- e^{+\frac{sx}{c_k}} \qquad (3.4.7)$$

The second is obtained by assuming B is in the (k+1)th layer

$$\xi_B = \xi_{k+1}(s,x) \qquad (3.4.8)$$

This gives

$$\xi_B = \xi_{k+1}^+ e^{-\frac{sx}{c_{k+1}}} + \xi_{k+1}^- e^{+\frac{sx}{c_{k+1}}} \qquad (3.4.9)$$

For point N, in the (k+1)th layer one obtains

$$\xi_N = \xi_{k+1}(s, x+d_{k+1}) ,$$

giving then

$$\xi_N = \xi_{k+1}^+ e^{-s(\frac{x}{c_{k+1}} + \tau)} + \xi_{k+1}^- e^{+s(\frac{x}{c_{k+1}} + \tau)} \qquad (3.4.10)$$

The pressure in terms of displacement is given by equation (2.3.3.)

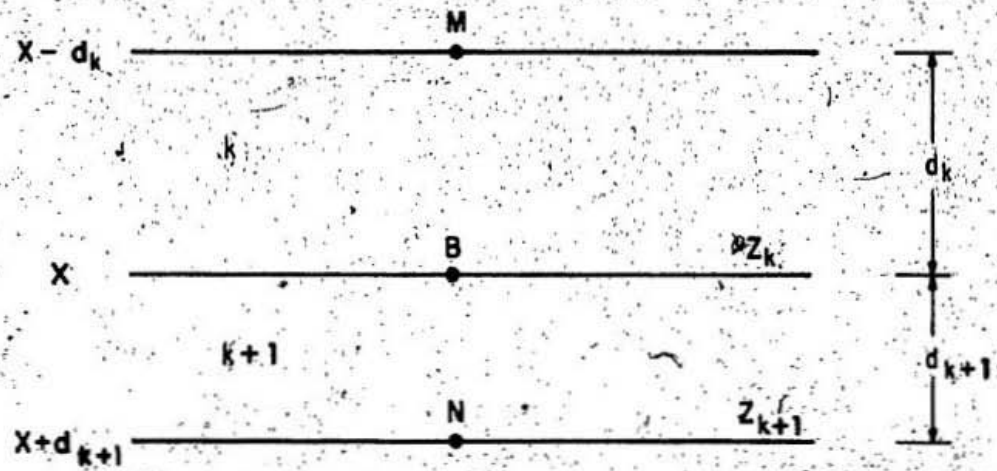


Figure 3.4.1 Layer's configuration for the Baranov and Kunetz procedure

The continuity of pressure at point B gives.

$$Z_k[\xi_k^+ e^{-\frac{sx}{c_k}} - \xi_k^- e^{+\frac{sx}{c_k}}] = Z_{k+1}[\xi_{k+1}^+ e^{-\frac{sx}{c_{k+1}}} - \xi_{k+1}^- e^{+\frac{sx}{c_{k+1}}}] \qquad (3.4.11)$$

A difference equation in displacements is obtained by combining equation (3.4.5), (3.4.7), (3.4.9), (3.4.10) and (3.4.11) to give

$$Z_k \xi_M + Z_{k+1} \xi_N = (1/2)[e^{\tau s}+e^{-\tau s}][Z_k+Z_{k+1}]\xi_B \qquad (3.4.12)$$

Using the definition of the reflection coefficient equation (3.2.1) one rewrites the above as

$$(1+R_k)\xi_M + (1-R_k)\xi_N = (e^{\tau s}+e^{-\tau s})\xi_B \qquad (3.4.13)$$

The Baranov and Kunetz difference equation is thus obtained. In terms of space and time variables this is written as

$$(1+R_k)\zeta(t,(x-c_k\tau)) + (1-R_k)\zeta(t,(x+c_{k+1}\tau))$$

$$= \zeta((t-\zeta),x) + \zeta((t+\tau),x) \qquad (3.4.14)$$

In order to utilize the (BK) difference equation, use is made of the space-time diagram. This is the t-x plane with the propagation characteristic. The time taken by a wavefront initiated at t = 0 and x = 0 to arrive at a depth x is given by

$$t_x = \int_0^x \frac{dx}{c(x)} \qquad (3.4.15)$$

where c(x) is the velocity of propagation. For a region of constant velocity the (t-x) characteristic curve is a straight line.

The (t-x) curve divides the plane into two regions I and II as shown in Fig. 3.4.2

Region I

$$\zeta = o, \qquad t < \int_o^x \frac{dx}{c(x)} \qquad (3.4.16)$$

Here not enough time has elapsed for the displacement wave to arrive.

Region II

$$\zeta \neq o, \qquad t \geq \int_o^x \frac{dx}{c(x)} \qquad (3.4.17)$$

The displacement wave has reached this region.

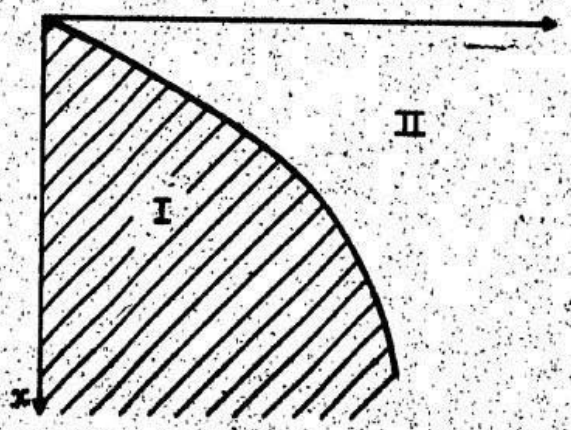


Fig. 3.4.2 The (t-x) curve

Figure 3.4.3 shows a portion of the space-time diagram assuming that the time axis has been divided into equal time intervals of length $\tau$. The displacements at the quadrangle points A, M, N and B are obtained using the Baranov and Kunetz difference equation by substituting

$$\zeta_M = \zeta(t,(x-d_k)) \qquad (3.4.18)$$

$$\zeta_A = \zeta((t-\tau),x) \qquad (3.4.19)$$

$$\zeta_B = \zeta((t+\tau),x) \qquad (3.4.20)$$

$$\zeta_N = \zeta(t,(x+d_{k+1})) \qquad (3.4.21)$$

As a result,

$$(1+R_k)\zeta_M + (1-R_k)\zeta_N = \zeta_A + \zeta_B \quad . \qquad (3.4.22)$$

This can be written as

$$\zeta_B = (1+R_k)\zeta_M + (1-R_k)\zeta_N - \zeta_A \quad . \qquad (3.4.23)$$

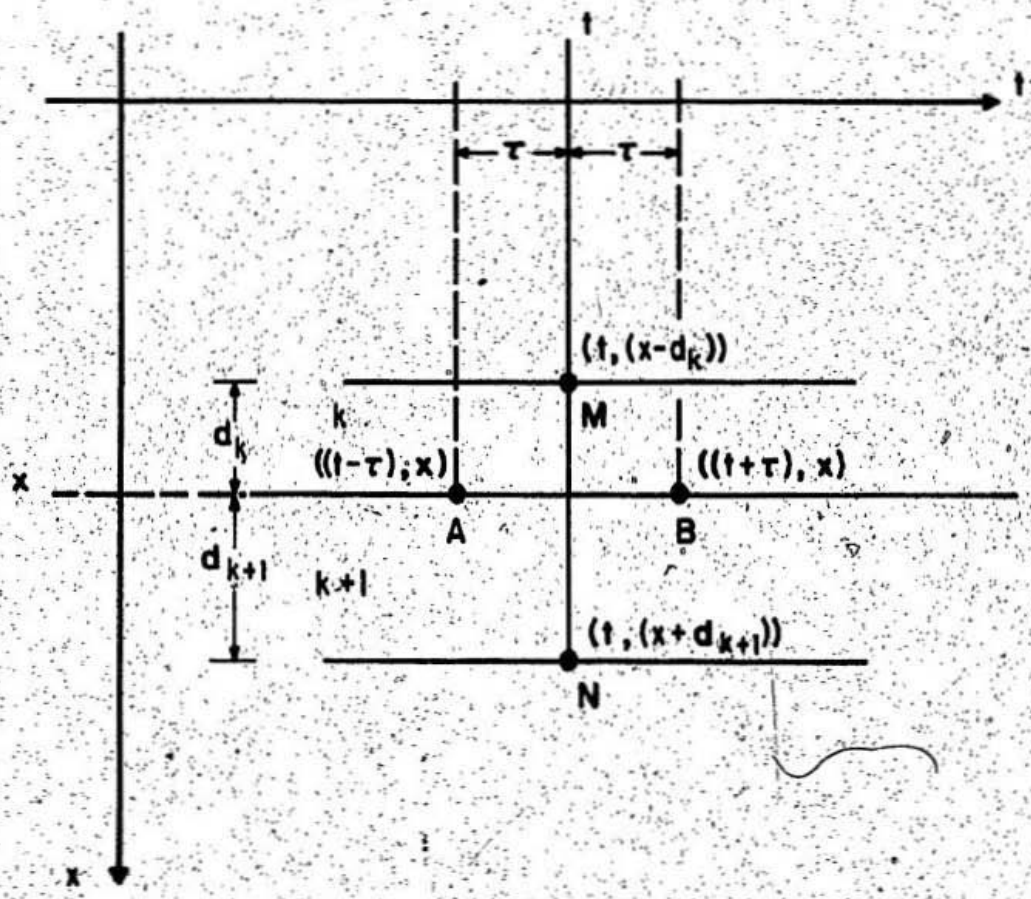


Figure 3.4.3 The space-time diagram for Baranov and Kunetz procedure.

Equation (3.4.23) is used to obtain the displacement at B, using information acquired at A, M, and N in the Baranov and Kunetz's procedure, which is described next.

The time axis of the space-time diagram is divided into equal intervals of duration $\tau$ each. The inter-

sections of the (t-x) characteristic with the verticals at $t = \tau, 2\tau, 3\tau, \ldots$ etc. define the grid points. The procedure is then to obtain the displacements at points of choice successively by constructing quadrangles AMNB such that displacements at A, M, and N are known to calculate that at B. Consider for example the situation shown in Figure 3.4.4 . The displacements at $A_o$ and $N_o$ are zero, since the two points are in region I of the space-time diagram. The displacement at $M_o$ is simply that of the source $M_o(o)$. Thus

$$\zeta(B_o) = (1+R_1)\, M_o(o) \qquad (3.4.24)$$

The procedure continues on working away from the (t-x) characteristic to obtain the synthetic seismogram which is the displacements at x = o for all time values.

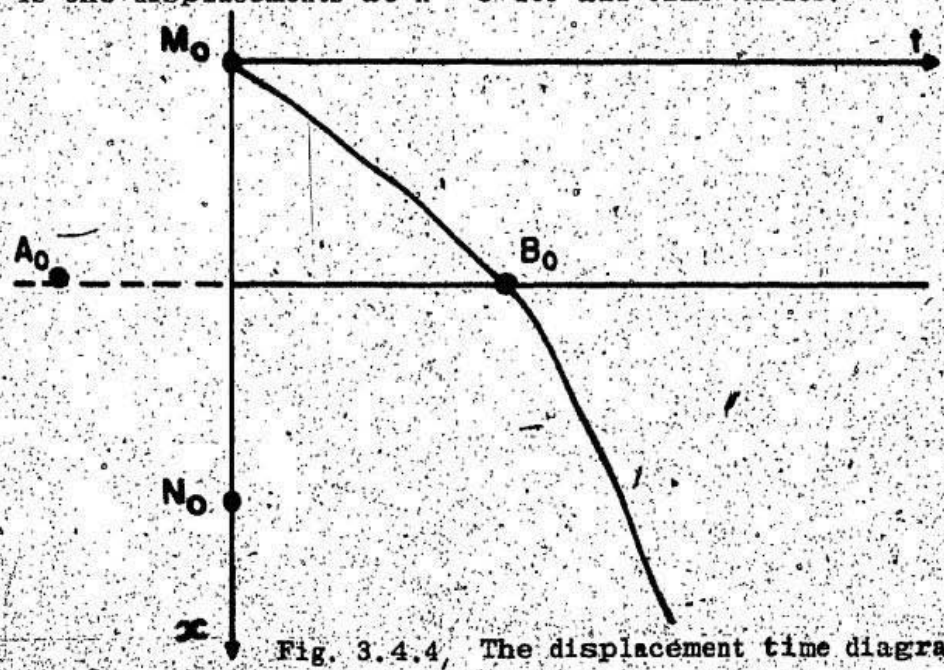


Fig. 3.4.4, The displacement time diagram

## 3.5 Wuenschel's model (1960)

Wuenschel's formulation utilizes the matrix notation introduced by W.T. Thomson (1950). The approach consists basically in relating the particle velocity and pressure variables at the interfaces of the multilayered medium. This is based on the displacement wave equation in terms of spatial displacement x and the Laplace operator s, given by

$$\frac{\partial^2 \xi(s,x)}{\partial x^2} = \frac{s^2}{c^2} \xi(s,x) \qquad (3.5.1)$$

The solution is given by

$$\xi(s,x) = \xi_i e^{-sx/c} + \xi_r e^{+sx/c}, \qquad (3.5.2)$$

in which $\xi_i$ and $\xi_r$ are the incident and reflected amplitudes respectively. As a result, the particle velocity U(s,x) and pressure P(s,x) are obtained as

$$U(s,x) = \xi_i \, s \, e^{-sx/c} + \xi_r \, s \, e^{sx/c} \qquad (3.5.3)$$

$$P(s,x) = Z[-\xi_i \, s \, e^{-sx/c} + \xi_r \, s \, e^{sx/c}] \qquad (3.5.4)$$

Consider now the two layers (k-1) and k with interface at x = o. Assume the kth layer's thickness is $d_k$. One can write, for x = o, at the bottom of the interface between (k-1) and k layers

$$U_{k-1} = s[\xi_i + \xi_r] \qquad (3.5.5)$$

$$P_{k-1} = Z_k . s[\xi_r - \xi_i] \qquad (3.5.6)$$

At $x = d_k$, one writes at the top of the interface between k and (k+1) layers

$$U_k = s[\xi_i e^{-sd_k/c_k} + \xi_r e^{sd_k/c_k}] \qquad (3.5.7)$$

$$P_k = Z_k s[-\xi_i e^{-sd_k/c_k} + \xi_r e^{sd_k/c_k}] \qquad (3.5.8)$$

Eliminating $\xi_i$ and $\xi_r$, one obtains

$$\begin{bmatrix} U_k \\ P_k \end{bmatrix} = \underline{a}_k \begin{bmatrix} U_{k-1} \\ P_{k-1} \end{bmatrix} \qquad (3.5.9)$$

The matrix $\underline{\alpha}_k$ is the Wuenschel's layer matrix given by

$$\underline{\alpha}_k = \begin{bmatrix} \left(\frac{e^{(sd_k/c_k)} + e^{-(sd_k/c_k)}}{2}\right) & \frac{1}{Z_k}\left(\frac{e^{(sd_k/c_k)} - e^{-(sd_k/c_k)}}{2}\right) \\ Z_k\left(\frac{e^{(sd_k/c_k)} - e^{-(sd_k/c_k)}}{2}\right) & \left(\frac{e^{(sd_k/c_k)} + e^{-(sd_k/c_k)}}{2}\right) \end{bmatrix} \qquad (3.5.10)$$

For an N-layer medium, assuming continuity of velocity and pressure along the interfaces one can write

$$\begin{bmatrix} U_N \\ P_N \end{bmatrix} = \underline{\alpha}_N \underline{\alpha}_{N-1} \cdots \underline{\alpha}_1 \begin{bmatrix} U_o \\ P_o \end{bmatrix} \qquad (3.5.11)$$

This situation is shown in Figure 3.5.1 . Assuming

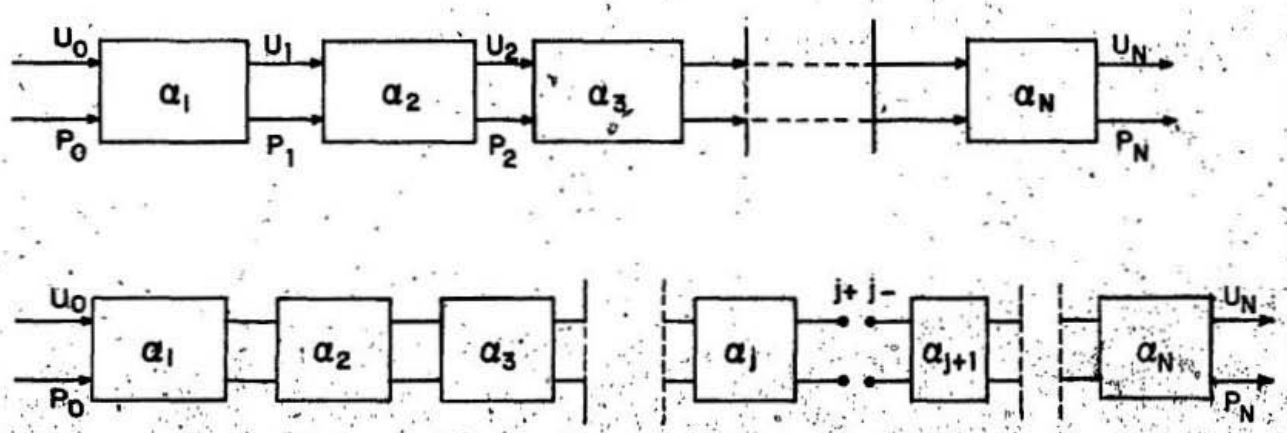


Figure 3.5.1 The Wuenschel's layer matrix for distinct layers

a discontinuity at the jth interface due for example to the placement of the source at that location, the following two equations can be used.

$$\begin{bmatrix} U_N \\ \\ P_N \end{bmatrix} = \underline{\alpha}_N \, \underline{\alpha}_{N-1} \cdots \underline{\alpha}_{j+1} \begin{bmatrix} U_{j+} \\ \\ P_{j+} \end{bmatrix} \qquad (3.5.12)$$

$$\begin{bmatrix} U_{j-} \\ \\ P_{j-} \end{bmatrix} = \underline{\alpha}_j \, \underline{\alpha}_{j-1} \cdots \underline{\alpha}_1 \begin{bmatrix} U_o \\ \\ P_o \end{bmatrix} \qquad (3.5.13)$$

Here (j+) and (j-) represent the positive and negative sides of the jth interface.

Muenschel's formulation enables one to express the particle velocity in terms of the forcing function of the source as follows. Assume that the (N+1)th layer has an acoustic impedance of $Z_{N+1}$. Thus the variables emerging from the Nth layer are related by

$$P_N = -Z_{N+1} U_N$$

As a result

$$\begin{bmatrix} U_N \\ \\ -Z_{N+1} U_N \end{bmatrix} = \underline{\alpha}_N \, \underline{\alpha}_{N-1} \cdots \underline{\alpha}_1 \begin{bmatrix} U_o \\ \\ P_o \end{bmatrix} \qquad (3.5.14)$$

Let $\underline{A}$ denote the overall transition matrix

$$\underline{A} = \underline{\alpha}_N \underline{\alpha}_{N-1} \cdots \underline{\alpha}_1 \qquad (3.5.15)$$

$$\underline{A} = \begin{bmatrix} A_{11} & A_{12} \\ A_{21} & A_{22} \end{bmatrix} \qquad (3.5.16)$$

It is easy to verify that

$$U_o = \frac{(A_{22}/Z_{N+1}) + A_{12}}{(A_{21}/Z_{N+1}) + A_{11}} (-\underline{p}_o) \qquad (3.5.17)$$

Thus the particle velocity at the source is expressed in terms of the forcing function of the source with a single factor of proportionality which is a function of the characteristic impedances of the individual layers and the transit time across the layers.

Wuenschel details the formulation procedures for four problems of interest in reflection seismology. These are the surface source - surface detector with and without stress - free surface, surface source - buried detector and buried source - buried detector problems. These are all easily worked out with some slight algebraic manipulations.

## 3.6 Goupillaud's model (1961)

This model is closely related to that of Wuenschel's. Instead of using pressure and particle velocity as variables, Goupillaud considers the relationship between the displacement variables associated with the reflected and transmitted waves. Consider the kth layer bounded by interfaces k and k+1 and having a one-way travel time $\tau_k$, as shown in Figure 3.6.1. At the (k+1) interface the following two relations are used.

$$D_{k+1} = -R_k U_{k+1} + T_k D'_k \qquad (3.6.1)$$

$$U'_k = T'_k U_{k+1} + R_k D'_k \qquad (3.6.2)$$

$R_k$ and $T_k$ are the reflection and transmission coefficients in the kth layer respectively. Note that

$$T_k = 1 + R_k \qquad (3.6.3)$$

$$T'_k = 1 - R_k \qquad (3.6.4)$$

D and U denote the down-going and up-going propagating wave amplitudes. The prime denotes a time-shift. Thus

$$D'_k = D_k e^{-j\omega\tau_k} \qquad (3.6.5)$$

$$U'_k = U_k e^{j\omega\tau_k} \qquad (3.6.6)$$

Equations (3.6.1) and (3.6.2) can be manipulated to give quantities at the kth interface in terms of those at the (k+1)th. This gives

$$T_k \, D_k' = D_{k+1} + R_k \, U_{k+1} \qquad (3.6.7)$$

$$T_k \, U_k' = R_k \, D_{k+1} + U_{k+1} \qquad (3.6.8)$$

Combining equations the following matrix equation is obtained

$$\begin{bmatrix} D_k \\ U_k \end{bmatrix} = \frac{1}{T_k} \begin{bmatrix} e^{j\omega\tau_k} & R_k e^{j\omega\tau_k} \\ R_k e^{-j\omega\tau_k} & e^{-j\omega\tau_k} \end{bmatrix} \begin{bmatrix} D_{k+1} \\ U_{k+1} \end{bmatrix} \qquad (3.6.9)$$

The layer matrix $M_k$ is thus given by

$$M_k = \frac{1}{T_k} \begin{bmatrix} e^{j\omega\tau_k} & R_k e^{j\omega\tau_k} \\ R_k e^{-j\omega\tau_k} & e^{-j\omega\tau_k} \end{bmatrix} \qquad (3.6.10)$$

$M_k$ is commonly known as the Goupillaud matrix [Claerbout, 1976]

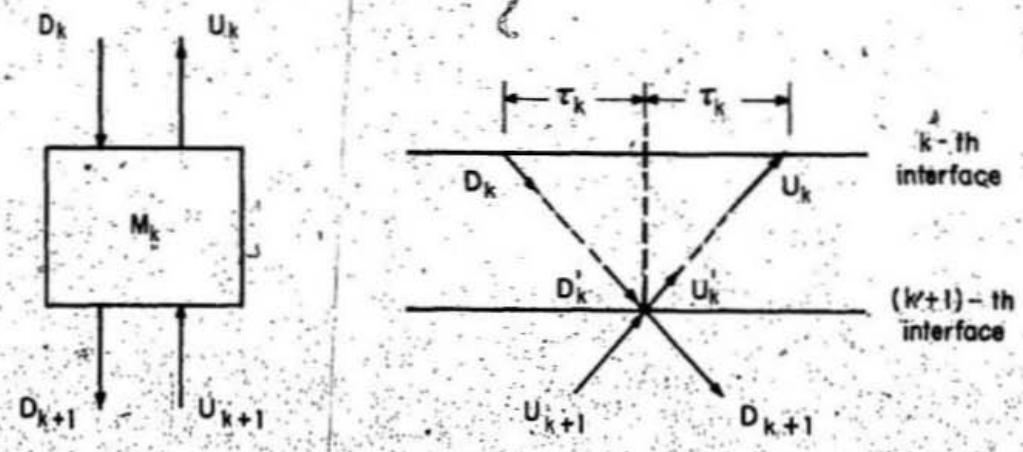


Figure 3.6.1 Variable definitions for Coupillaud's model

For a system of N interfaces the process of transmission and reflections can thus be described by

$$\begin{bmatrix} D_o \\ \\ U_o \end{bmatrix} = [M_o]\,[M_1] \ldots\ldots [M_{N-1}] \begin{bmatrix} D_N \\ \\ U_N \end{bmatrix} \qquad (3.6.11)$$

This can be written more compactly as

$$\begin{bmatrix} D_o \\ U_o \end{bmatrix} = M_o^{N-1} \begin{bmatrix} D_N \\ U_N \end{bmatrix} \qquad (3.6.12)$$

where the system matrix $M_o^{N-1}$ is given by

$$M_o^{N-1} = [M_o]\,[M_1]\,.....\,[M_{N-1}] \qquad (3.6.13)$$

If the Nth interface is completely absorptive, $U_N = o$, and for a unit impulse input $D_o = 1$, the system response is described by

$$\begin{bmatrix} 1 \\ U_o \end{bmatrix} = M_o^{N-1} \begin{bmatrix} D_N \\ o \end{bmatrix} \qquad (3.6.14)$$

The system matrix $M_o^{N-1}$ is a 2x2 matrix, of the form

$$M_o^{N-1} = \begin{bmatrix} M_{11} & M_{12} \\ M_{21} & M_{22} \end{bmatrix} \qquad (3.6.15)$$

As a result, one has

$$D_N = \frac{1}{M_{11}} \qquad (3.6.16)$$

$$U_o = M_{21}\, D_N \qquad (3.6.17)$$

This gives the transmission and reflection response of the overall system.

The expression for the transmission response is given by

$$D_N = \frac{T_o T_1 T_2 \ldots T_N \exp.\{-j\omega \sum_o^N \tau_i\}}{1+\Delta_1+\Delta_2+\ldots} \qquad (3.6.18)$$

where

$$\Delta_1 = \sum_{i=o}^{N-1} \left( \sum_{\substack{j=1 \\ j\neq i}}^{N} R_i R_j \right) \exp.\{-2j\omega[\sum_o^i \tau_j - \sum_o^i \tau_i]\} \qquad (3.6.19)$$

$$\Delta_2 = \sum_{i=0}^{N-3} \left( \sum_{\substack{j=1 \\ j\neq i}}^{N-2} \sum_{\substack{k=2 \\ k\neq j}}^{N-1} \sum_{\substack{\ell=3 \\ \ell\neq k}}^{N} R_i R_j R_k R_\ell \right) \exp.\{-2j\omega[\sum_o^\ell \tau - \sum_o^k \tau_k + \sum_o^j \tau_j - \sum_o^i \tau_i]\} \qquad (3.6.20)$$

The reflection response $U_o$ is given by

$$U_o = \Big[ \sum_{i=o}^{N} R_i \exp.\{-2j\omega \sum_{o}^{N} \tau_i\} +$$

$$\sum_{i=o}^{N-2} \Big( \sum_{\substack{j=1 \\ j\neq i}}^{N-1} \sum_{\substack{k=2 \\ k\neq i}}^{N} R_i R_j R_k \Big) \exp.\{-2j\omega( \sum_{o}^{k} \tau_k$$

$$- \sum_{o}^{j} \tau_j + \sum_{o}^{i} \tau_i \} + \ldots.] / (1+\Delta_1+\Delta_2+ \ldots)$$

(3.6.21)

Use of the Goupillaud's matrix representation enables one to split a complete system into any number of complementary portions. A specific example is shown in Figure 3.6.2, where the first (j+1)-layers are lumped together in one system representing the shallow portion described by the matrix $M_o^j$. The remaining layers representing the deep portion are described by $M_{j+1}^{N-1}$. This provides the basis for separating the shallow portion's response from the deep layer response as described in [Goupillaud, 1961].

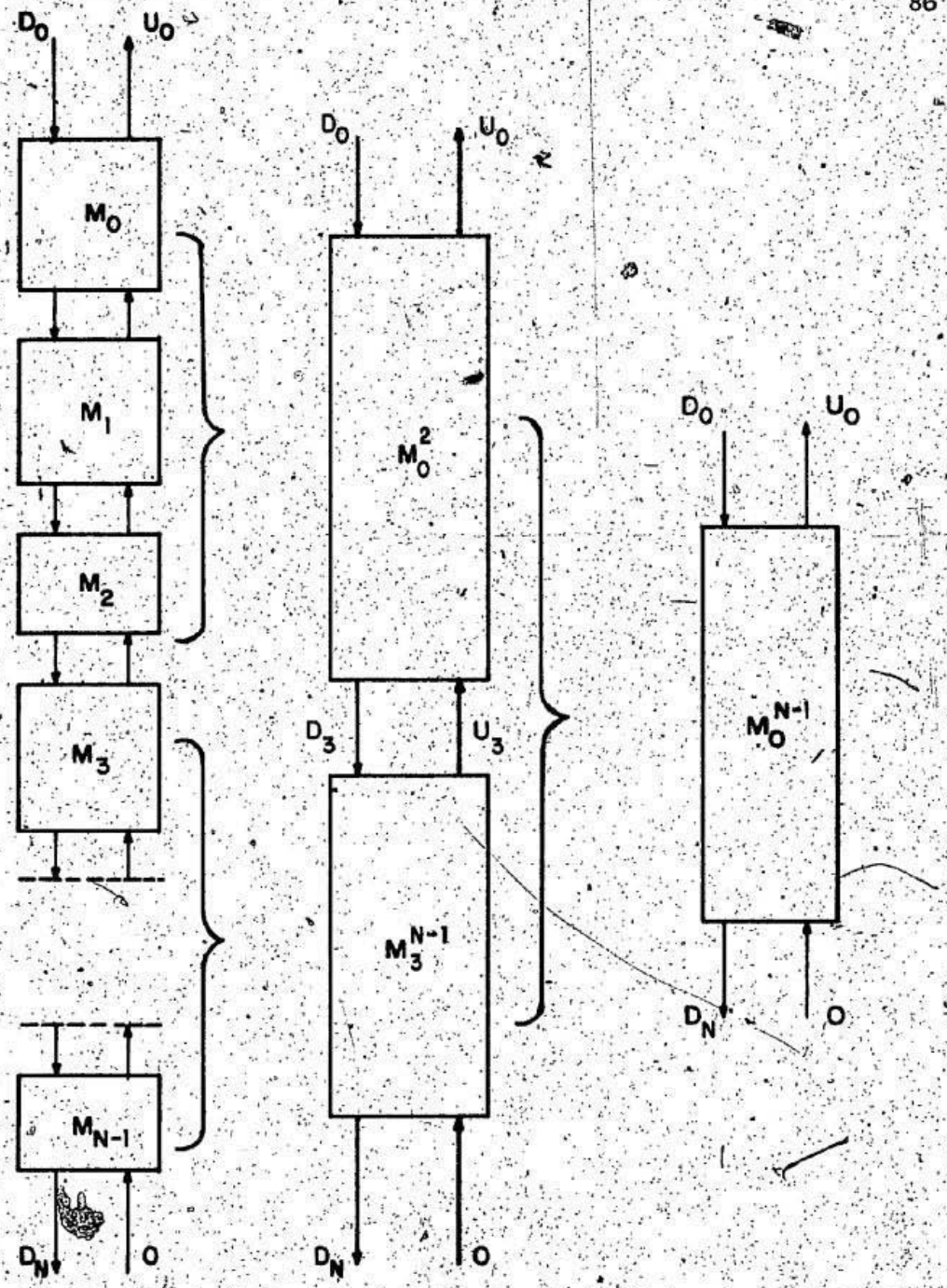


Figure 3.6.2 Block diagram of Goupillaud's model

## 3.7 Sengbush, Lawrence, and McDonal (1961)

The reflection coefficient model Peterson et. al. is modified in the approach developed by Sengbush, Lawrence, and McDonal (1961). It is assumed that the layer's density is velocity-dependent. The proposed relation is

$$\rho = k\, c^m \tag{3.7.1}$$

where k and m are constants. As a result

$$Z = k\, c^{m+1} \tag{3.7.2}$$

The reflection coefficient in terms of velocity of propagation is thus given by

$$R = \frac{m+1}{2} \Delta \ln c \tag{3.7.3}$$

In this case the reflection coefficient is proportional to the change in the logarithm of velocity.

The extension to the continuous case gives rise to Sengbush's reflectivity function $\tilde{r}(t)$. This is developed as the limiting case

$$\tilde{r}(t) = \lim_{\Delta t \to o} \frac{R}{\Delta t} \tag{3.7.4}$$

With

$$R = \frac{\Delta c}{2c+\Delta c} \tag{3.7.5}$$

we obtain

$$\tilde{r}(t) = \lim_{t \to o} \frac{\Delta c}{\Delta t} \frac{1}{[2c+(\frac{\Delta c}{\Delta t})\Delta t]}$$

$$= \frac{1}{2c} \frac{dc}{dt}$$

$$= \frac{1}{2} \frac{d \ \ell n \ c(t)}{dt} \qquad (3.7.6)$$

The factor (1/2) is dropped in Sengbush's definition of reflectivity

$$\tilde{r}(t) = \frac{d \ \ell n \ c(t)}{dt} \qquad (3.7.7)$$

As a result of the above, a velocity log can be converted into a reflectivity function in three steps. The first converts the depth to two-way travel time rendering c(t) from c(x). The logarithm of c(t) is then calculated, followed by a differentiation to give $\tilde{r}(t)$.

Consider the output waveform for primary reflections written as

$$y(t) = \sum_{i=1}^{N} R_i \ m(t-\tau_i) \qquad (3.7.8)$$

The reflection coefficients are functions of depth or delay time which is signified by writing

$$R_i = R_i(\tau_i) \qquad (3.7.9)$$

Thus the output is

$$y(t) = \sum_{i=1}^{N} R_i(\tau_i)\, m(t-\tau_i) \qquad (3.7.10)$$

This summation is a convolution and as a result we can see that the reflection process is a linear filtering process.

The model can be extended from N discrete layers to a continuous velocity distribution in the limit as the layer thickness approaches zero. Then the output can be expressed as

$$y(t) = \int_{o}^{t} \tilde{r}(\tau)\, m(t-\tau)d\tau \qquad (3.7.11)$$

The reflection process is essentially a convolution. The normal way is to consider the source signal (shot pulse) as an input and the reflectivity function as the filter's impulse response. Sengbush et. al. interchange the input and filter by treating the reflectivity function $\tilde{r}(t)$ as the input and the shot pulse as the filter. The filtering that acts upon $\tilde{r}(t)$ is divided into two parts, the shot pulse m(t) and the filtering external to the earth, e(t). The latter includes the combined effect of all instruments plus hydrophone coupling.

$$y(t) = \tilde{r}(t) * e(t) * m(t) \qquad (3.7.12)$$

To simplify the notation let

$$b(t) = e(t) * m(t) \qquad (3.7.13)$$

Thus

$$y(t) = \tilde{r}(t)*b(t) \qquad (3.7.14)$$

This is shown in Fig. 3.7.1.a

Alternatively

$$y(t) = m(t)*e(t)*\tilde{r}(t) \qquad (3.7.15)$$

as shown in Fig. 3.7.1.b

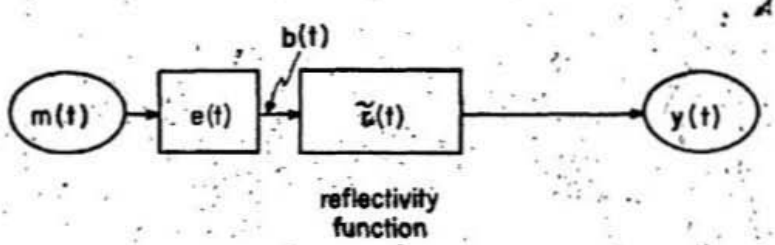


Fig. 3.7.1.a Reflection process model according to Eq. (3.7.12)

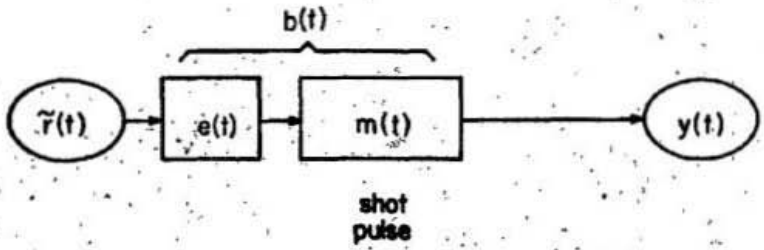


Fig. 3.7.1.b Reflection process model according to Eq. (3.7.15)

The consequences of the linear filter model given by Sengbush et. al. are important. For given a velocity function the corresponding reflections can be inferred using the linearity (superposition) properties. A simple example is shown in Figure 3.7.2. Assume that the reflection due to a step change in velocity is a replica of the shot pulse. The reflection due to an impulse (derivative of step) is a replica of a differentiated shot pulse. Similarly since a ramp is the integral of a step, the reflection due to a ramp change in velocity is a replica of an integrated shot pulse.

A three-layer case where the first and third layers have the same velocity, with the velocity of the mid-layer larger, is considered. The velocity function is a square pulse. It is clear that there are two reflections, a positive one at $t_1$ and a negative reflection at $t_2$. The total response is the superposition of the two. Assume that the middle layer has a two-way travel time $\Delta t$ and that the shot pulse has a period T between peaks. Figure 3.7.3 shows the outcome for three ratios at $(\Delta t/T)$. For $\Delta t >> T$, two isolated step responses can be seen. The resulting reflections are distinct and each has the same waveform as the shot pulse. The polarity of the second reflection is opposite to that of the first. For $\Delta t = 1/2\ T$,

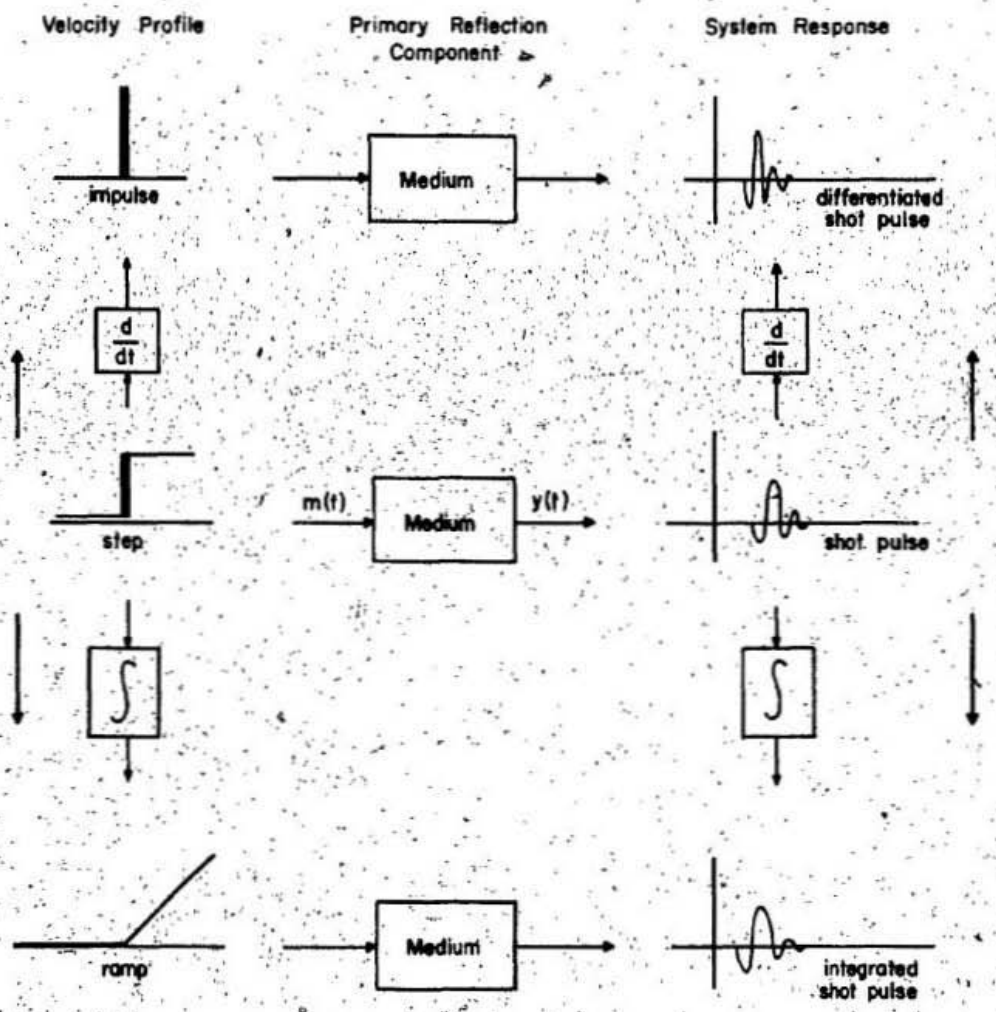


Figure 3.7.2

Implications of the linear filter model for impulse, step and ramp response

the resulting reflection has a maximum amplitude of twice the amplitude of reflection from a step. This is called tuning. For $\Delta t \ll T$, the composite reflection decreases, approaching that due to an impulse.

Sengbush et.al. utilize the above to construct charts showing the variation of the reflection amplitudes with the ratio $\Delta t/T$ for square-pulse velocity functions, ramp transition velocity functions. Synthetic records are obtained by using velocity logs as the input to a filter whose impulse response corresponds to the shot pulse.

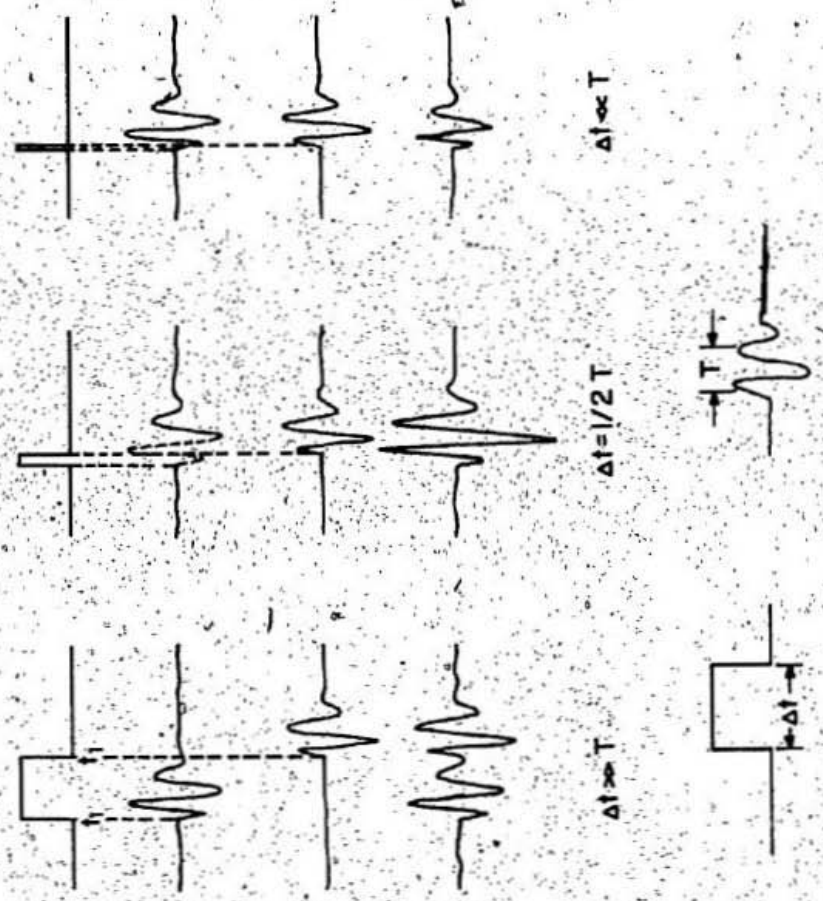


Fig. 3.7.3 Reflections from square-pulse velocity functions, showing the three critical Δt/T ratios.

## 3.8 Robinson's model (1967)

This model is developed in terms of Z-transform notation. Either of Wuenschel's or Goupillaud's approaches can be used to arrive at Robinson's form. The latter, however, provides a more direct way. Assume that the layers have one way travel times of

$$\tau_k = 0.5 \qquad (3.8.1)$$

Recall also from the theory of Z-transforms that

$$Z = e^{-j\omega} \qquad (3.8.2)$$

The Goupillaud's matrix equation can be written as

$$\begin{bmatrix} D_k(Z) \\ U_k(Z) \end{bmatrix} = \frac{Z^{-1/2}}{T_k} \begin{bmatrix} 1 & R_k \\ R_k Z & Z \end{bmatrix} \begin{bmatrix} D_{k+1}(Z) \\ U_{k+1}(Z) \end{bmatrix} \qquad (3.8.3)$$

This form is also known as the scattering equation.

The inverse relation giving $D_{k+1}$, $U_{k+1}$ in terms of $D_k$ and $U_k$ is given by

$$\begin{bmatrix} D_{k+1}(Z) \\ U_{k+1}(Z) \end{bmatrix} = \frac{Z^{-1/2}}{T'_k} \begin{bmatrix} Z & -R_k \\ -R_k Z & 1 \end{bmatrix} \begin{bmatrix} D_k(Z) \\ U_k(Z) \end{bmatrix} \tag{3.8.4}$$

where

$$T'_k = 1 - R_k \tag{3.8.5}$$

The matrix $N_k$ is defined as

$$\underline{N}_k = \begin{bmatrix} Z & -R_k \\ -R_k Z & 1 \end{bmatrix} \tag{3.8.6}$$

As a result, assuming continuity at the interfaces, one has

$$\begin{bmatrix} D_{k+1}(Z) \\ U_{k+1}(Z) \end{bmatrix} = \frac{Z^{-k/2}}{T'_k \cdots T'_2 T'_1} \underline{N}_k \cdots \underline{N}_2 \underline{N}_1 \begin{bmatrix} D_1(Z) \\ U_1(Z) \end{bmatrix} \tag{3.8.7}$$

The process of matrix multiplication indicated above can be simplified by taking advantage of properties inherent in their definition. Consider the matrix product $\underline{N}_2\underline{N}_1$

$$N^{(2)} = \underline{N}_2\underline{N}_1 = \begin{bmatrix} Z & -R_2 \\ -R_2 Z & 1 \end{bmatrix} \begin{bmatrix} Z & -R_1 \\ -R_1 Z & 1 \end{bmatrix} \tag{3.8.8}$$

Let

$$\underline{N}^{(2)} = \begin{bmatrix} n_{11}^{(2)} & n_{12}^{(2)} \\ n_{21}^{(2)} & n_{22}^{(2)} \end{bmatrix} \tag{3.8.9}$$

Then

$$n_{11}^{(2)}(Z) = Z^2 + R_1 R_2 Z \tag{3.8.10}$$

$$n_{12}^{(2)}(Z) = -(R_2 + R_1 Z) \tag{3.8.11}$$

$$n_{21}^{(2)}(Z) = -(R_1 Z + R_2 Z^2) \tag{3.8.12}$$

$$n_{22}^{(2)}(Z) = 1 + R_1 R_2 Z \tag{3.8.13}$$

An important relation exists between the matrix elements, namely

$$n_{11}^{(2)}(Z) = Z^2 \, n_{22}^{(2)}(Z^{-1}) \tag{3.8.14}$$

$$n_{21}^{(2)}(Z) = Z^2\, n_{12}^{(2)}(Z^{-1}) \qquad (3.8.15)$$

Consider now the matrix $N^{(1)} = N_1$, here

$$\underline{N}^{(1)} = \underline{N}_1 = \begin{bmatrix} Z & -R_1 \\ -R_1 Z & 1 \end{bmatrix} = \begin{bmatrix} n_{11}^{(1)}(Z) & n_{12}^{(1)}(Z) \\ n_{21}^{(1)}(Z) & n_{22}^{(1)}(Z) \end{bmatrix} \qquad (3.8.16)$$

The following relation holds

$$n_{11}^{(1)}(Z) = Z\, n_{22}^{(1)}(Z^{-1}) \qquad (3.8.17)$$

$$n_{21}^{(1)}(Z) = Z\, n_{12}^{(1)}(Z^{-1}) \qquad (3.8.18)$$

In general for $\underline{N}^{(k)}$ one has

$$n_{11}^{(k)}(Z) = Z^k\, n_{22}^{(k)}(Z^{-1}) \qquad (3.8.19)$$

$$n_{21}^{(k)}(Z) = Z^k\, n_{12}^{(k)}(Z^{-1}) \qquad (3.8.20)$$

Thus

$$\underline{N}^{(k)} = \underline{N}_k \underline{N}_{k-1} \cdots \underline{N}_1 = \begin{bmatrix} Z^k\, n_{22}^{(k)}(Z^{-1}) & n_{12}^{(k)}(Z) \\ Z^k\, n_{12}^{(k)}(Z^{-1}) & n_{22}^{(k)}(Z) \end{bmatrix} \qquad (3.8.21)$$

It is therefore only necessary to evaluate the elements $n_{12}$ and $n_{22}$.

The evaluation of the elements $n_{12}$ and $n_{22}$ can be done easily, if one considers the result of the following

$$\underline{N}^{(k)} = \underline{N}_k \, \underline{N}^{(k-1)} \qquad (3.8.22)$$

Thus

$$\begin{bmatrix} z^k \, n_{22}^{(k)}(z^{-1}) & n_{12}^{(k)}(z) \\ z^k \, n_{12}^{(k)}(z^{-1}) & n_{22}^{(k)}(z) \end{bmatrix}$$

$$\begin{bmatrix} z & -R_k \\ -R_k z & 1 \end{bmatrix} \begin{bmatrix} z^{k-1} \, n_{22}^{(k-1)}(z^{-1}) & n_{12}^{(k-1)}(z) \\ z^{k-1} \, n_{12}^{(k-1)}(z^{-1}) & n_{22}^{(k-1)}(z) \end{bmatrix}$$

(3.8.23)

Performing the matrix multiplication one obtains

$$n_{12}^{(k)}(z) = z n_{12}^{(k-1)}(z) - R_k \, n_{22}^{(k-1)}(z)$$

(3.8.24)

$$n_{22}^{(k)}(Z) = n_{22}^{(k-1)}(Z) - R_k Z n_{12}^{(k-1)}(Z)$$

(3.8.25)

This is the basic recursion procedure for evaluating the matrix products.

The basic model equation is thus

$$\begin{bmatrix} D_{k+1}(Z) \\ U_{k+1}(Z) \end{bmatrix} = \frac{Z^{-k/2}}{\prod_{i=1}^{k} T_i} \begin{bmatrix} Z^k n_{22}^{(k)}(Z^{-1}) & n_{12}^{(k)}(Z) \\ Z^k n_{12}^{(k)}(Z^{-1}) & n_{22}^{(k)}(Z) \end{bmatrix} \begin{bmatrix} D_1(Z) \\ U_1(Z) \end{bmatrix}$$

(3.8.26)

If no up-going waveform is impinging on the bottom interface N, then $U_{N+1}(Z) = o$. Consequently

$$U_1(Z) = \frac{-Z^N n_{12}^{(N)}(Z^{-1})}{n_{22}^{(N)}(Z)} D_1(Z) \quad (3.8.27)$$

For a unit impulse excitation at $k = o$,

$$D_1(Z) = 1 - R_o U_1(Z) \quad (3.8.28)$$

Thus the reflection response $U_1(Z)$ is obtained as

$$U_1(Z) = \frac{-Z^N \, n_{12}^{(N)}(Z^{-1})}{n_{22}^{(N)}(Z) - R_o \, Z^N \, n_{12}^{(N)}(Z^{-1})}$$

(3.8.29)

The reflection response $U_1(Z)$ can be visualized as a layered earth transfer function $G^{(N)}(Z)$ as shown in Figure 3.8.1. As a result

$$G^{(N)}(Z) = \frac{-Z^N \, n_{12}^{(N)}(Z^{-1})}{n_{22}^{(N)}(Z) - R_o \, Z^N \, n_{12}^{(N)}(Z^{-1})}$$

(3.8.30)

where $n_{12}^{(k)}(Z)$ and $n_{22}^{(k)}(Z)$ are derived in equations (3.8.24), (3.8.25), with

$$n_{12}^{(1)}(Z) = -R_1 \qquad (3.8.31)$$

$$n_{22}^{(1)}(Z) = 1 \qquad (3.8.32)$$

$$G^{(o)}(Z) = o \qquad (3.8.33)$$

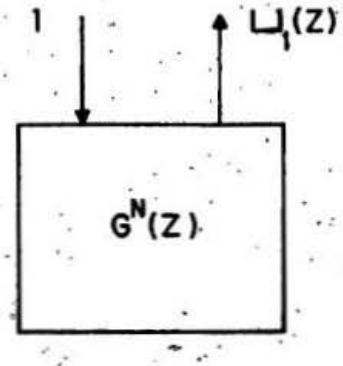


Figure 3.8.1 A layered earth transfer function for Robinson's model

For signal processing purposes the reflection transfer function is written in terms of a characteristic polynomial $A^{(N)}(Z)$ and a reflection polynomial $E^{(N)}(Z)$,

$$A^{(N)}(Z) = n_{22}^{(N)}(Z) - R_o Z^N n_{12}^{(N)}(Z^{-1}) \quad (3.8.34)$$

$$E^{(N)}(Z) = -Z^N n_{12}^{(N)}(Z^{-1}) \quad (3.8.35)$$

Thus

$$G^{(N)}(Z) = \frac{E^{(N)}(Z)}{A^{(N)}(Z)} \quad (3.8.36)$$

$E^N(Z)$ and $A^N(Z)$ can be expressed in polynomial forms as

$$E^{(N)}(Z) = \sum_{j=1}^{N} \epsilon_j^{(N)} Z^j \quad (3.8.37)$$

$$A^{(N)}(Z) = \sum_{j=o}^{N} a_j^{(N)} Z^j \quad (3.8.38)$$

with

$$a_o^{(N)} = 1 \qquad (3.8.39)$$

If one denotes the output by Y(k) and the input by M(k), then the signal time domain representation is

$$Y(k) + \sum_{j=1}^{N} - a_j^{(N)}\, Y(k-j) = \sum_{j=1}^{N} \epsilon_j^{(N)}\, M(k-j) \qquad (3.8.40)$$

Using the defining relations, the coefficients of the characteristic polynomial $a_j^{(N)}$ can be obtained. Silvia (1977) gives the values in terms of the serial correlation defined by

$$\phi_j^{(N)} = \sum_{i=o}^{N} R_i\, R_{i+j} \qquad j \geq 1 \qquad N \geq 1 \qquad (3.8.41)$$

$$\phi_o^{(N)} = 1 \qquad (3.8.42)$$

Table (3.8.1) gives the expressions corresponding to N = 1,...,4. Note that residual terms such as $R_o\, R_1\, R_2\, R_3$ are present. If one assumes a small reflection coefficient approximation, then these residuals may be neglected giving

$$a_j^{(N)} \cong \phi_j^{(N)} \qquad (3.8.43)$$

$$a_j^{(N)} \cong \sum_{i=o}^{N} R_i\, R_{i+j} \qquad (3.8.44)$$

In a similar fashion, the coefficients of the reflection polynomial E(Z) are found, as given in Table (3.8.2). If one uses the same small reflection approximation one has

$$\epsilon_j^{(N)} \cong R_j \qquad (3.8.45)$$

| N | $a_1^{(N)}$ | $a_2^{(N)}$ | $a_3^{(N)}$ | $a_4^{(N)}$ |
|---|---|---|---|---|
| 1 | $\phi_1^{(1)}$ | — | — | — |
| 2 | $\phi_1^{(2)}$ | $\phi_2^{(2)}$ | — | — |
| 3 | $\phi_1^{(3)}$ | $\phi_2^{(3)} + R_0 R_1 R_2 R_3$ | $\phi_2^{(3)}$ | — |
| 4 | $\phi_1^{(4)}$ | $\phi_2^{(4)} + R_4R_3R_2R_1 + R_4R_3R_1R_0 + R_3R_2R_1R_0$ | $\phi_3^{(4)} + R_4R_3R_2R_0 + R_4R_2R_1R_0$ | $\phi_4^{(4)}$ |

Table (3.8.1)

| N | $\Sigma_1^{(N)}$ | $\Sigma_2^{(N)}$ | $\Sigma_3^{(N)}$ | $\Sigma_4^{(N)}$ |
|---|---|---|---|---|
| 1 | $R_1$ | — | — | — |
| 2 | $R_1$ | $R_2$ | — | — |
| 3 | $R_1$ | $R_2 + R_3 R_2 R_1$ | $R_3$ | — |
| 4 | $R_1$ | $R_2 + R_4 R_3 R_1 + R_3 R_2 R_1$ | $R_3 + R_4 R_2 R_1 + R_4 R_3 R_2$ | $R_4$ |

Table (3.8.2)

It can thus be seen that the polynomial $E^{(N)}(Z)$ contains the reflection information required for seismic data processing.

## 3.9 Mendel's model (1976)

A quasi-state space model for layered media has been developed by Mendel et.al. (1975 & 1976). The starting equations are obtained from prior models, for example from Goupillaud's formulation. Equations (3.6.2), (3.6.5) and (3.6.6) can be combined to give in the time-domain.

$$u_k(t+\tau_k) = R_k\, d_k(t-\tau_k) + (1-R_k)u_{k+1}(t) \qquad (3.9.1)$$

Equations (3.6.1), (3.6.5) and (3.6.6) yield

$$d_{k+1}(t) = (1+R_k)d_k(t-\tau_k) - R_k\, u_{k+1}(t) \qquad (3.9.2)$$

The boundary conditions at the surface with input signal m(t), and output y(t) are

$$d_1(t) = (1+R_o)\, m(t) - R_o u_1(t) \qquad (3.9.3)$$

$$y(t) = R_o\, m(t) + (1-R_o)\, u_1(t) \qquad (3.9.4)$$

At the Nth interface, assuming no reflection

$$u_{N+1}(t) = o \qquad (3.9.5)$$

Thus

$$u_N(t+\tau_N) = R_N\, d_N(t-\tau_N) \qquad (3.9.6)$$

and

$$d_{N+1}(t) = (1+R_N)d_N(t-\tau_N) \qquad (3.9.7)$$

Mendel et. al. make the substitution

$$\tilde{d}_k(t) \triangleq d_k(t-\tau_k) \qquad (3.9.8)$$

The result is the so-called, layer ordered (L-O) model

$$\tilde{d}_1(t+\tau_1) = -R_o\, u_1(t) + (1+R_o)\, m(t) \qquad (3.9.9)$$

$$u_1(t+\tau_1) = R_1\, d_1(t) + (1-R_1)\, u_2(t) \qquad (3.9.10)$$

$$\vdots$$

$$\tilde{d}_k(t+\tau_k) = (1+R_{k-1})\tilde{d}_{k-1} - R_{k-1}\, u_k(t) \qquad (3.9.11)$$

$$u_k(t+\tau_k) = R_k\, \tilde{d}_k(t) + (1-R_k)u_{k+1}(t) \qquad (3.9.12)$$

$$\left.\begin{matrix}\\ \\ \end{matrix}\right\} k=2,3,\ldots,N-1$$

$$\tilde{d}_N(t+\tau_N) = (1+R_{N-1})\tilde{d}_{N-1}(t) - R_{N-1}\, u_N(t) \qquad (3.9.13)$$

$$u_N(t+\tau_N) = R_N\, \tilde{d}_N(t) \qquad (3.9.14)$$

The model given above is a dynamical equation with multiple generally incrementally non-equal time delays. Such equations have been designated as causal functional equations.

A quasi-state space representation is given by defining

$$\underline{X}(t) = \text{col.}[u_1(t), \tilde{d}_1(t), \ldots, u_N(t), \tilde{d}_N(t)] \qquad (3.9.15)$$

The 2Nx2N matrix operator $\tilde{\underline{Z}}$ is defined by

$$\tilde{\underline{Z}} \triangleq \text{diag.}[Z_1, Z_1, Z_2, Z_2, \ldots, Z_k, Z_k] \qquad (3.9.16)$$

where $\tilde{Z}_i$ is a scalar operator denoting a $\tau_i$ sec. time delay. $\tilde{Z}_i f(t) = f(t-\tau_i)$. As a result one has

$$\tilde{\underline{Z}}^{-1} \underline{X}(t) = \underline{A}\, \underline{X}(t) + \underline{b}\, \underline{m}(t) \qquad (3.9.17)$$

$$y(t) = \underline{C}^T \underline{X}(t) + R_o\, \underline{m}(t) \qquad (3.9.18)$$

This equation provides a conceptual solution given by

$$\underline{X}(t) = [\tilde{\underline{Z}}^{-1} - \underline{A}]^{-1} \underline{b}\, m(t) \qquad (3.9.19)$$

and

$$y(t) = [C^T[\tilde{\underline{Z}}^{-1} - \underline{A}]^{-1} \underline{b} + R_o]\, m(t) \qquad (3.9.20)$$

The transfer function of the system will be a ratio of two polynomials in $Z_1, Z_2, \ldots, Z_N$ which should reduce to Robinson's formula when $Z_1 = Z_2 = \ldots = Z_N$. As an example, the two layer case (Nahi, et. al. 1978) gives

$$\frac{Y(\tilde{Z})}{M(\tilde{Z})} = \frac{R_o + R_o R_1 R_2 Z_2^2 + R_1 Z_1^2 + R_2 Z_1^2 Z_2}{1 + R_1 R_2 Z_2^2 + R_o R_1 Z_1^2 + R_o R_2 Z_1^2 Z_2^2} \qquad (3.9.21)$$

For the case of equal $Z_i$'s, i.e. $\tau_1 = \tau_2 = \ldots = \tau_N \triangleq \tau$, a state space solution is possible, since the model reduces to

$$\underline{X}[(k+1)\tau] = \underline{A}\,\underline{X}(k\tau) + \underline{b}\,m(k\tau) \qquad (3.9.22)$$

whose solution is

$$\underline{X}[(k+1)\tau] = \underline{A}^{k}\,\underline{X}(o) + \sum_{i=o}^{k} A^{k-i}\,\underline{b}\,m(i\tau) \qquad (3.9.23)$$

No solution to the general case has been documented in the literature.

3.10 Layer indexed reflection model (1979)

In this approach a time domain raypath analysis is utilized to systematically describe the synthetic seismogram. The formulation is a refinement on previous direct methods and accommodates multiple reflection effects of all orders which are not accounted for by methods previously discussed. The approach features a novel wavelet index notation which enables aggregation of all wavelets in a dynamic group [Vetter and El-Hawary, 1979], without adding dimensional complexity.

Consider an N-layer medium, with layer interfaces $0,1,2,\ldots,N$, with source and receiver at the top of interface 0. The received signal $y(t)$ is the composite of wavelets from the many reflection-transmission processes in the medium. It is convenient to group wavelets according to their type as, primary, secondary, tertiary, ... etc., wavelets.

Primary wavelets $y_i$ arise due to a single reflection at a lower interface i. Figure 3.10.1 shows primary wavelets $y_0, y_1, \ldots, y_N$ arriving at the top of interface 0. Consider the wavelet $y_i(t)$ whose path is indicated in the Figure 3.10.1. This is the result of the down-going wave $m(t)$ transmitted downward through interfaces $0,1,\ldots$ to the ith interface as $y_{i-}(t)$, which is then reflected upward as $y_{i+}(t)$. Clearly $y_i(t)$ is the result of $y_{i+}(t)$

propagating upwards. The process can be described by

$$y_{i-}(t) = T_o T_1 \ldots T_{i-1}\, m(t-(\tau_1+\tau_2+\ldots+\tau_i)) \qquad (3.10.1)$$

$$y_{i+}(t) = R_i y_{i-}(t) \qquad (3.10.2)$$

$$y_i(t) = T'_{i-1}\, T'_{i-2} \ldots T'_o\, y_{i+}(t-(\tau_i+\tau_{i-1}+\ldots+\tau_1)) \qquad (3.10.3)$$

Where $\tau_i$ is the one-way travel time for the ith layer, $T_i$ is the down-going transmission coefficient through the ith interface and $T'_i$ is the corresponding up-going transmission coefficient. The reflection coefficient off the top of interface i is denoted $R_i$. Noting that

$$T_i = 1 + R_i \qquad (3.10.4)$$

$$T'_i = 1 - R_i \qquad (3.10.5)$$

we obtain

$$y_i(t) = R_i \prod_{j=o}^{i-1} [1-R_j^2]\, m(t-2 \sum_{j=1}^{i} \tau_j) \qquad (3.10.6)$$

To simplify the notation the scaling factor $a_i$ and total travel time $\gamma_i$ are introduced

$$a_i = R_i \prod_{j=o}^{i-1} [1-R_j^2] \qquad (3.10.7)$$

$$\gamma_i = 2 \sum_{j=1}^{i} \tau_j \qquad (3.10.8)$$

As a result, for primary wavelets one has

$$y_i(t) = a_i \; m(t-\gamma_i) \qquad (3.10.9)$$

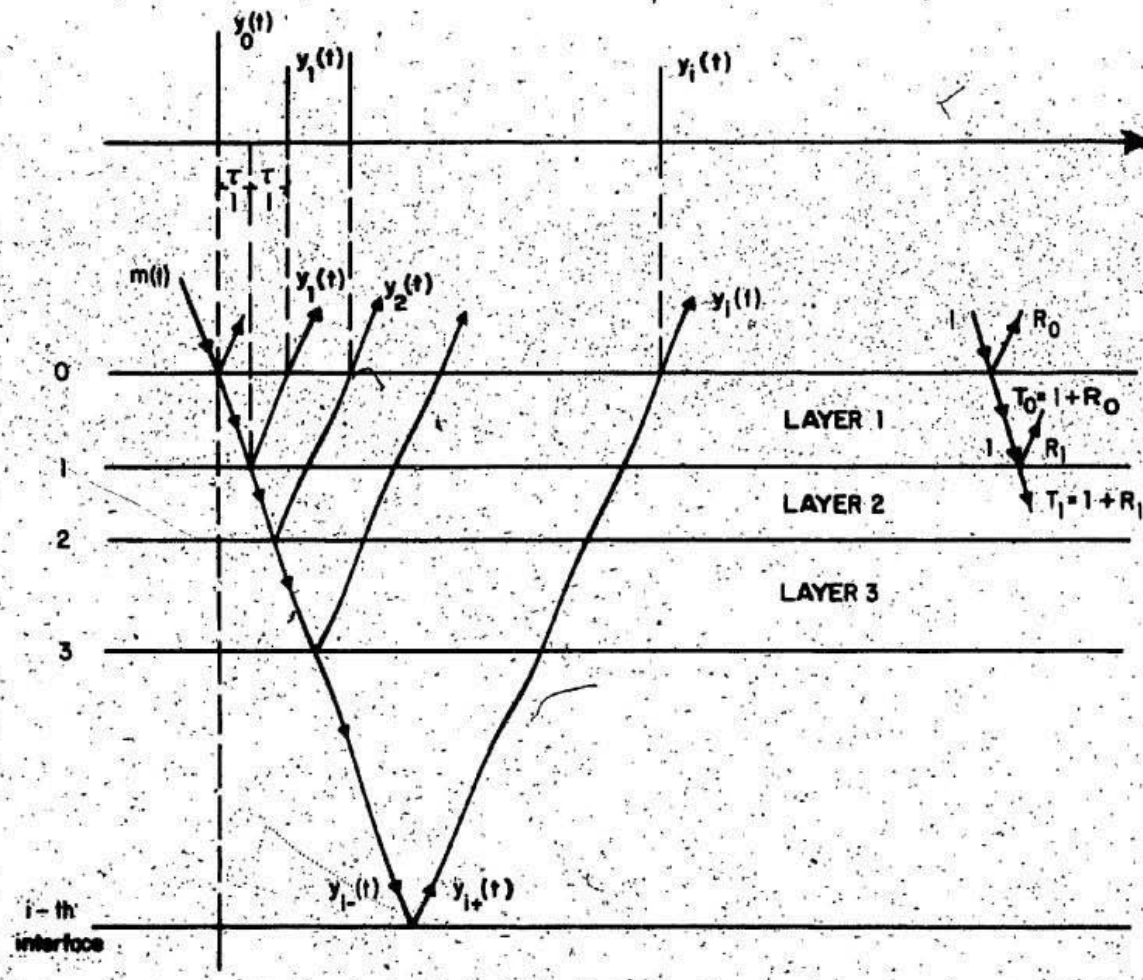


Figure 3.10.1 The wavelet travel path

Secondary wavelets arise from upward reflection off the top of the ith interface followed by a downward reflection off the bottom of the jth interface. This wave is then reflected off the top of the kth interface and is directly transmitted to the surface. Since there are three reflecting interfaces one denotes such a wavelet by $y_{i\,k}^{\,j}(t)$. Figure 3.10.2 shows some possible secondaries and the path for the specific wavelet $y_{i\,k}^{\,j}(t)$, which can be seen to be generated by the following sequence

$$y_{i\,k}^{\,j}(t) = \left(\prod_{\ell=o}^{k-1} T_\ell\right) y_{k+}\left(t - \sum_{\ell=j+1}^{k} \tau_\ell\right) \qquad (3.10.10)$$

$$y_{k+}(t) = R_k\, y_{k-}(t) \qquad (3.10.11)$$

$$y_{k-}(t) = \left(\prod_{\ell=j+1}^{k-1} T_\ell\right) y_{j+}\left(t - \sum_{\ell=j+1}^{k} \tau_\ell\right) \qquad (3.10.12)$$

$$y_{j+}(t) = -R_j\, y_{j-}(t) \qquad (3.10.13)$$

$$y_{j-}(t) = \left(\prod_{\ell=j+1}^{i-1} T_\ell\right) y_{i+}\left(t - \sum_{\ell=j+1}^{i} \tau_\ell\right) \qquad (3.10.14)$$

$$y_{i+}(t) = R_i\, y_{i-}(t) \qquad (3.10.15)$$

$$y_{i-}(t) = \left(\prod_{\ell=o}^{i-1} T_\ell\right) m\left(t - \sum_{\ell=1}^{i} \tau_\ell\right) \qquad (3.10.16)$$

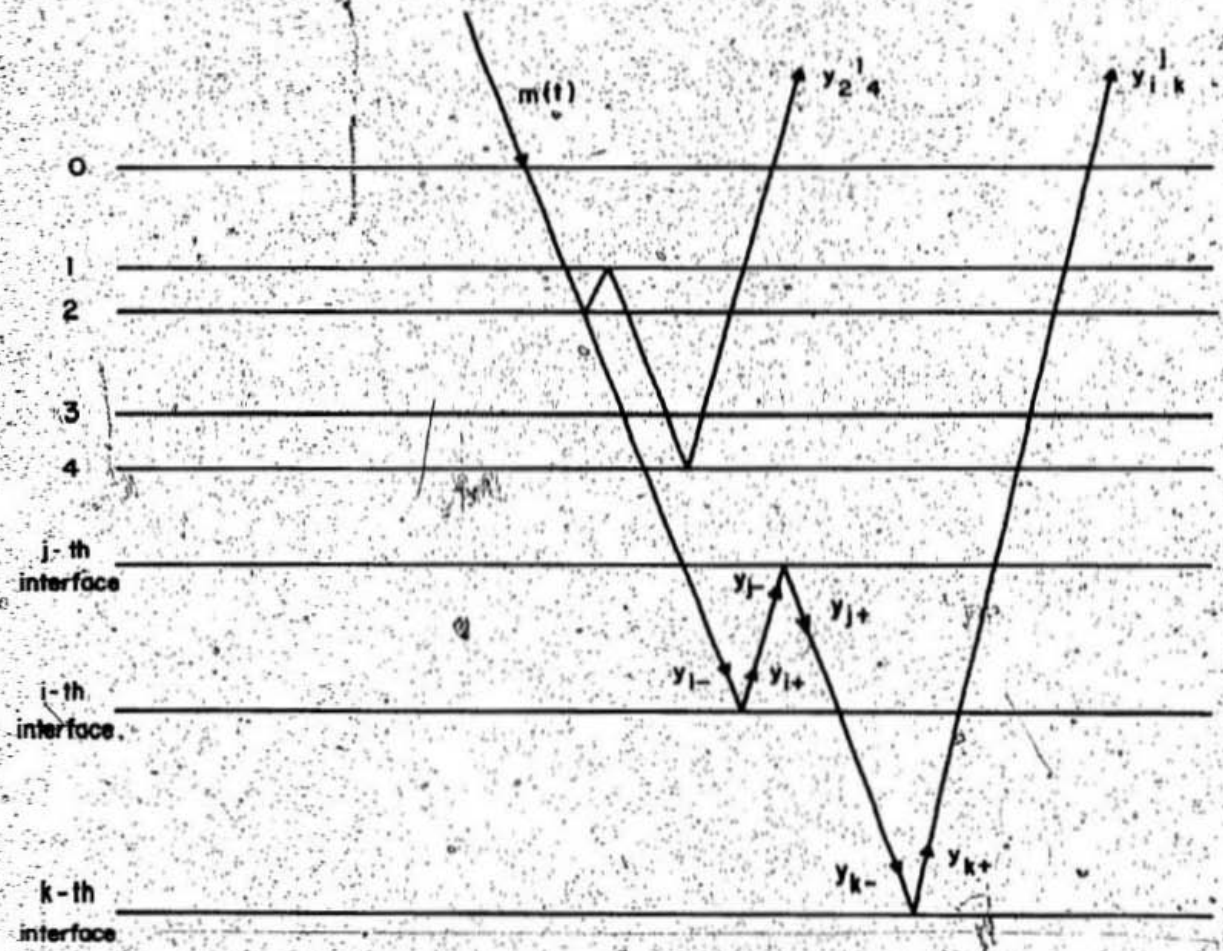


Figure 3.10.2 Some possible secondaries and the path
For the specific wavelet $y_{i\ k}^{\ j}(t)$

The above equations are now combined in a unique form to give the compact expression

$$y_{i\,k}^{\,j}(t) = a_{i\,k}^{\,j}\, m(t-\gamma_{i\,k}^{\,j}) \qquad (3.10.17)$$

The amplitude parameter is given by

$$a_{i\,k}^{\,j} = a_i\, b^{(j)}\, a_k \qquad (3.10.18)$$

where

$$a_i = R_i \prod_{\ell=o}^{i-1} (1-R_\ell^2) \qquad (3.10.19)$$

$$b^{(j)} = -R_j / \left[\prod_{\ell=o}^{j} (1-R_\ell^2)\right] \qquad (3.10.20)$$

The delay parameter is given by

$$\gamma_{i\,k}^{\,j} = \gamma_i - \gamma_j + \gamma_k \qquad (3.10.21)$$

where as before

$$\gamma_i = 2 \sum_{\ell=1}^{i} \tau_\ell \qquad (3.10.22)$$

The above notation enables one to proceed in a systematic manner to describe higher order reflections. Successive indices i, j, k, ℓ, n, ... on the amplitude and delay parameters catalogue the upward, downward, upward, ... reflection history. Associated with a lower index i, k, n are the scale factors $a_i$, $a_k$, and $a_n$, etc.,

while for top index j, ℓ, ... scale factors $b^{(j)}$, $b^{(\ell)}$, ... are used. Thus for tertiary reflections, and similarly for all higher order reflections the structure can be obtained directly as

$$y_{i\,k\,n}^{j\,\ell}(t) = a_{i\,k\,n}^{j\,\ell}\, m(t-\gamma_{i\,k\,n}^{j\,\ell}) \qquad (3.10.23)$$

where

$$a_{i\,k\,n}^{j\,\ell} = a_i\, b^{(j)}\, a_k\, b^{(\ell)}\, a_n \qquad (3.10.24)$$

$$\gamma_{i\,k\,n}^{j\,\ell} = \gamma_i - \gamma_j + \gamma_k - \gamma_\ell + \gamma_n \qquad (3.10.25)$$

With the task of adequately modeling the multiple reflection wavelets done, we proceed to enumerate the possible wavelets involved. Suppose there are N layers. Then the index set of primary wavelets $y_I$ includes all interfaces

$$y_I = \{y_i | i=0,\ldots,N\} \qquad (3.10.26)$$

Secondary wavelets corresponding to the ith interface arise from additional reflections at upper layers j=i-1, i-2,...,0 with a further reflection for a particular j at lower levels k=j+1, j+2,...,N. The set of all secondary wavelets is then given by

$$\{y_{I\,k}^{J}\} = \{y_{i\,k}^{j} \mid \begin{array}{l} i=1,\ldots,N \\ j=o,1,..,i-1 \\ k=j+1,..,N \end{array}\} \qquad (3.10.27)$$

The generalization to higher order reflection wavelets at the receiver is now obvious.

As a result one can now write the received signal as

$$y(t) = \sum_{i=0}^{N} y_i(t) + \sum_{i=1}^{N}\sum_{j=o}^{i-1}\sum_{k=j}^{N} y_{i\,k}^{j}(t)$$

$$+ \sum_{i=1}^{N}\sum_{j=o}^{i-1}\sum_{k=j+1}^{N}\sum_{\ell=o}^{k-1}\sum_{n=\ell+1}^{N} y_{i\,k\,n}^{j\,\ell}(t)$$

$$+ \ldots. \qquad (3.10.28)$$

Some multiply reflected wavelets such as $y_{2\,1}^{o}$ and $y_{1\,2}^{o}$ are received at the same time and have identical amplitudes even though traversing different paths. These waves can only be sensed as an aggregate and are called "index equivalent" or"dynamic analogues" as shown in Figure 3.10.3. This phenomenon is also called reinforcement of multiple reflections, (Ellsworth, 1948, Backus, 1959, Mendel and Lee, 1977). Hron (1971) studied these multi-path and found a method for computing the count number of members in a group.

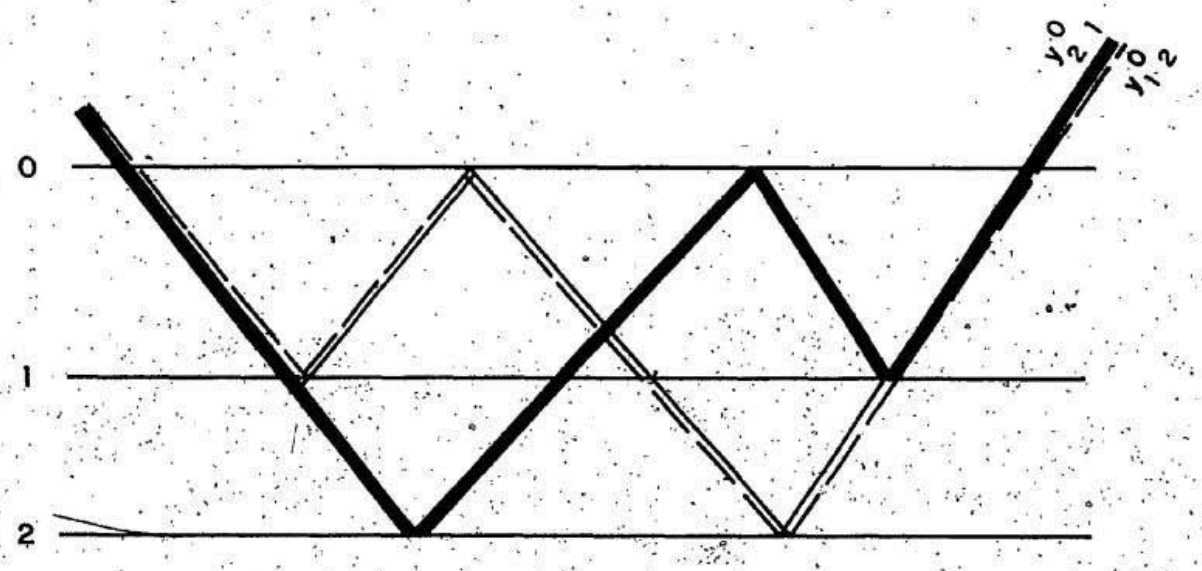


Figure 3.10.3 Index equivalent wavelets.

The received signal can be compacted using the aggregation of the index equivalent wavelet using a "marker wavelet" concept. The wavelet with lowest possible index sequence consistent with the possible raypaths of a group is denoted "marker wavelet" or group identifier. This means that the index structure for marker wavelets is such that any particular index may not be smaller than

its neighbour to the left. Thus $y_{1\ 2}^{\ o}$ is marker for $y_{1\ 2}^{\ o}$ and $y_{2\ 1}^{\ o}$. Similarly $y_{2\ 3\ 3}^{\ 1\ 2}$ is marker for $y_{2\ 3\ 3}^{\ 1\ 2}$ and $y_{3\ 3\ 2}^{\ 2\ 1}$. Also $y_{2\ 3\ 3}^{\ o\ 1}$ is the marker for $y_{3\ 2\ 3}^{\ o\ 1}$, $y_{3\ 3\ 2}^{\ o\ 1}$, $y_{3\ 3\ 2}^{\ 1\ 2}$, $y_{2\ 3\ 3}^{\ 1\ o}$, $y_{2\ 3\ 3}^{\ o\ 1}$ and $y_{3\ 2\ 3}^{\ 1\ o}$. Thus marker secondaries, tertiaries ... etc., are

$$\{y_I J_k\} = \{y_{i\ k}^{\ j} \mid \begin{array}{l} i=1,2,\ldots,N \\ j=o,1,\ldots,i-1 \\ k=i,1+1,\ldots,N \end{array} \} \qquad (3.10.29)$$

As a result y(t) is rewritten as

$$y(t) = \sum_{i=o}^{N} y_i(t) + \sum_{i=1}^{N} \sum_{j=o}^{i-1} \sum_{k=i}^{N} (\mu_{i\ k}^{\ j}) y_{i\ k}^{\ j}(t)$$

$$+ \sum_{i=1}^{N} \sum_{j=o}^{i-1} \sum_{k=i}^{N} \sum_{\ell=j}^{k-1} \sum_{n=k}^{N} (\mu_{i\ k\ n}^{\ j\ \ell}) y_{i\ k\ n}^{\ j\ \ell}(t)$$

$$+ \ldots . \qquad (3.10.30)$$

where $\mu_{i\ k}^{\ j}$, $\mu_{i\ k\ n}^{\ j\ \ell}$ denote marker multiplicities.

The multiplicities $\mu$ are given by [Vetter and El-Hawary, 1979] as

$$\mu_{i_1\ i_2\ i_3 \ldots \ell}^{\ j_1\ j_2\ j_3} = \left(\prod_i C_{(\#i)}^{(\#\#i)}\right)\left(\prod_j C_{(\#j)}^{(\#\#j)}\right) \qquad (3.10.31)$$

where

$$C_B^A = A!/[(B!)(A-B)!] \qquad (3.10.32)$$

i,k distinct index values from $i_1, i_2, \ldots, \ell$.

j,k distinct index values from $j_1, j_2, \ldots$

(#i) Number (count) of index repetitions (upward reflections) at the ith interface.

(#j) Number (count) of index repetitions (downward reflections) at the jth interface.

$$(\#\#i) = 1 + \sum_{\substack{k= \\ j_1, j_2, \ldots < i}} (\#jk) - \sum_{\substack{k= \\ i_1, i_2, \ldots < i}} (\#ik) \qquad (3.10.33)$$

(number of down-up path pairs in layer i)

$$(\#\#j) = \sum_{\substack{k= \\ j_1, j_2, \ldots < j}} (\#jk) - \sum_{\substack{k= \\ i_1, i_2, \ldots < j}} (\#ik) \qquad (3.10.34)$$

Consider for example $\mu_{5\,5\,9}^{3\,3}$. The index i takes on values 5 and 9. Here #5 = 2 and #9 = 1. The index j takes on the value 3, with #3 = 2. Values for (3.10.33) and (3.10.34) become then

$$\#\#3 = 2 - 0 \qquad (3.10.35)$$

$$\#\#5 = 1 + (\#3) - 0 = 3 \qquad (3.10.36)$$

$$\#\#9 = 1 + (\#3) - (\#5) = 1 \qquad (3.10.37)$$

As a result

$$\mu_{5\,5\,9}^{3\,3} = (C_{\#5}^{\#\#5}\ C_{\#9}^{\#\#9})(C_{\#3}^{\#\#3}) \qquad (3.10.38)$$

$$= (C_2^3\ C_1^1)(C_2^2)$$

$$= \left(\frac{3!}{2!1!}\right)(1)(1)$$

$$= 3$$

Computer evaluation of $\mu$ for secondary and tertiary reflections can be conveniently effected by a simple index comparison analysis [Vetter, 1980 & 1981].

3.11 Summary

Models of acoustic wave propagation in lossless layered media systems that have been reviewed in this chapter can be classified into two broad categories, according to the degree of detail involved. Models in the first category are based on the fact that the system is described by the lossless wave equation and boundary conditions, and the nature of the solution of the wave equation requiring that the output be the sum of time shifted and scaled replicas of the source signals. The model in this case is a convolution summation as given by Eq. (3.2.11), which is sometimes referred to as a non-parametric representation [Mendel et. al. 1980]. In the second category are models which utilize a parametric representation involving two signals for each layer. The basis for this type of model is the decomposition of the solution to the wave particle displacement, particle velocity, and pressure) into forward and backward travelling components in each layer.

The non-parametric models reviewed differ in their approach to modeling the reflection coefficients at the interfaces. In the Peterson, Fillippone and Croker model the reflection coefficient is obtained using the incremental change in the logarithm of the acoustic impedance across the interface as discussed in Section (3.2). A recursive formula for the reflection coefficients is given

in the Berryman, Goupillaud and Waters model discussed in Section (3.3). The basis for the recursive formula is the assumption that the velocity of sound propagation is a linear function of distance in each layer. The overall synthetic seismogram is obtained using the Fourier integral representation. Sengbush, Lawrence and McDonal's model discussed in Section (3.7) is based on the assumption of a specific relation between the layer's medium density and the velocity of sound propagation. This leads to an expression for the reflection coefficient in terms of the incremental change in the logarithm of velocity of sound propagation. Section (3.10) discusses a model due to Vetter and El-Hawary that belongs to this category. A raypath analysis is utilized to obtain a model which accommodates multiple reflection effects of all orders.

The second category of models gives rise to cascade type matrix model structure. This is a feature common to all parametric type models reviewed. The models differ in the choice of the two signals associated with each interface. Another difference is in the choice of representation either in discrete-time (Z-transform), continuous time (Laplace transform) or the frequency domain. In the Baranov and Kunetz model reviewed in Section (3.4), the forward and backward compo-

nents of the particle displacement are used together with a Laplace-transform development. Wuenschel's model described in Section (3.5) employs the pressure and particle velocity in arriving at a transmission matrix type model in the s-domain. Section (3.6) describes the model due to Goupillaud which uses the upward and downward propagating pressure wave amplitudes as the model variables. A scattering matrix type representation in the frequency domain is the feature of this model. Robinson's model discussed in Section (3.8) is among the most widely accepted models. It is a scattering-matrix type model developed in the Z-domain for equal layer thickness. Robinson's model is the basis for the predictive convolution method. The quasi-state space model of Mendel is discussed in Section (3.9). This is a time-domain representation in terms of a dynamical equation with multiple time delays referred to as a causal functional equation. Figure 3.11.1 shows the classification of earth models.

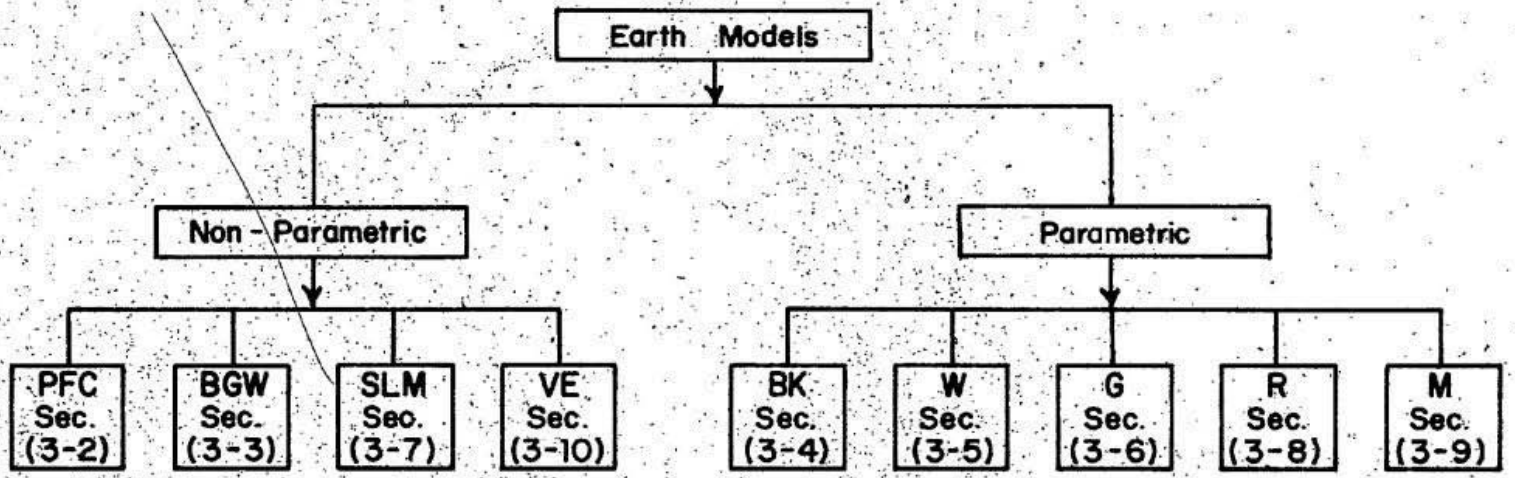


Figure 3.11.1 The classification of earth models

# Chapter 4

## COMPENSATION FOR SOURCE HEAVE BY USE OF A KALMAN FILTER

### 4.1 Introduction

In carrying out shallow marine seismic experiments employing a deep towed signal source and hydrophone receivers (HUNTEC '70 DTS), the unavoidable ship dynamics, coupled to the towed "fish" through the towing cable, and the hydrodynamics of the towed "fish" result in motions with vertical components, as large as two meters peak to peak. Such vertical motions of the source and sensor have the effect of a varying acoustic wave travel path to the sea floor and to the sub-bottom reflectors between successive pings of the source. These effects appear on the aggregate of reflection records along the ship track as apparent undulations of the sea floor and the sub-bottom reflectors. Partial removal of these effects can be done by use of estimates of the vertical source motions from hydrostatic pressure and motion sensors to delay or advance the pulse firing instants relative to a clock pulse reference. This is done such that the source-bottom-sensor pulse travel time corresponds to that of a source and sensor located at a constant depth relative to the mean water surface level as shown in Fig. 4.1.1, [Hutchins, 1978].

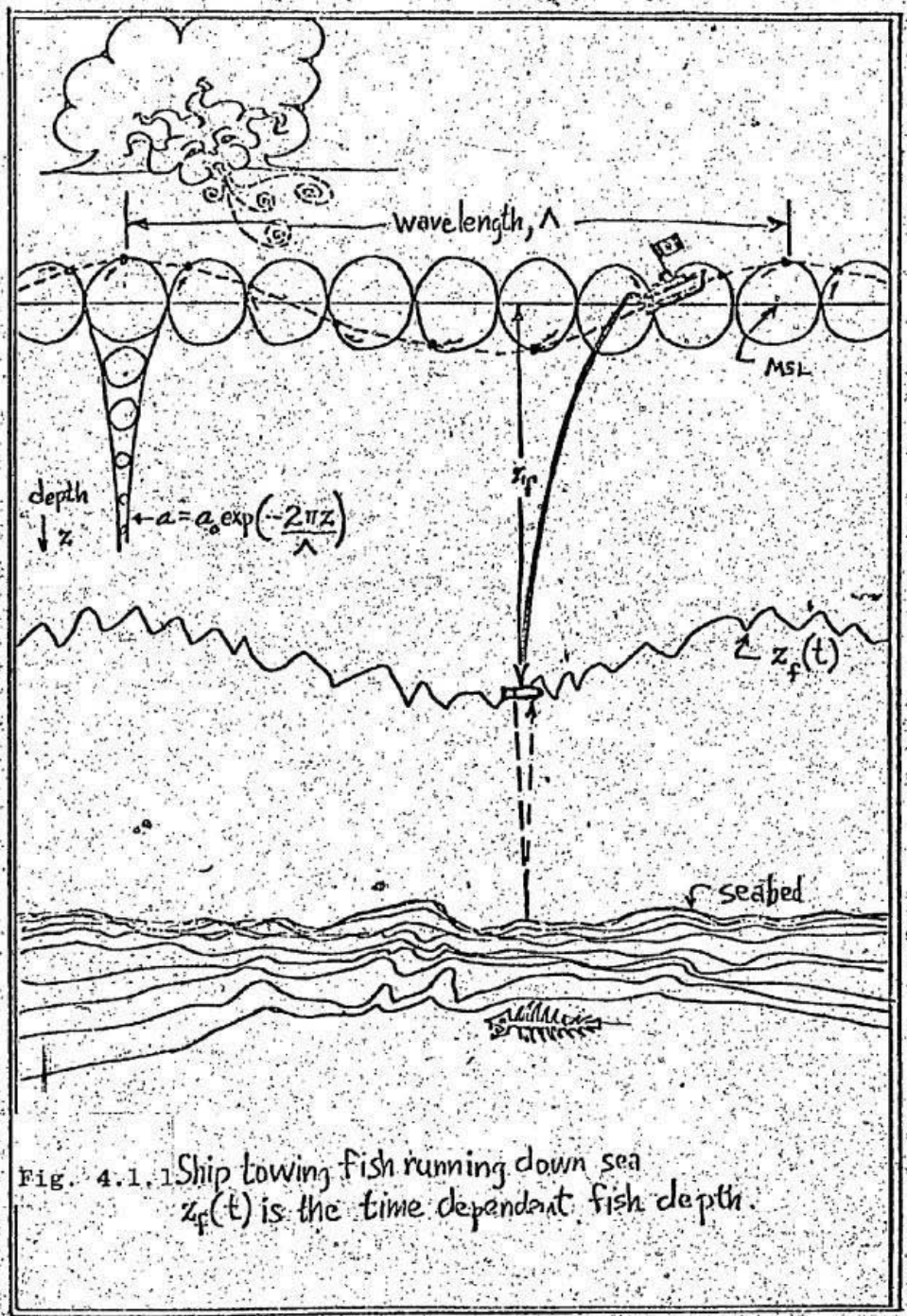


Fig. 4.1.1 Ship towing fish running down sea
$z_f(t)$ is the time dependant fish depth.

After such corrections on the HUNTEC '70 DTS data, there remains a residual undulation effect in the response records of the order of 50 cm. peak-to-peak as shown in Figure 4.1.2. Removal of this heave residual is an important pre-processing task for enhancement of grey scale displays of the raw and filtered reflection data, for extraction of such medium parameters as reflection coefficients and reflector depths, for ping to ping correlation and coherence, etc.

The source/receiver "fish" dynamics exhibit some degree of regularity (governed by wave action, speed, heading and dynamics of the towing vessel, towed "fish" hydrodynamics, current fields, etc.) in terms of a spectral content which can be modeled as that of a narrow band random noise process. This is the basis for the design of a Kalman filter for reducing the residual heave effects, i.e. for delaying and advancing the recording trigger on successive pings so as to effect a smoothing or removal of such undulations. The filtering can be applied to post-experiment data records, or preferably in a real time mode during acquisition of the reflection responses.

The purpose of this chapter is to present a procedure for data filtering to compensate for the heave's

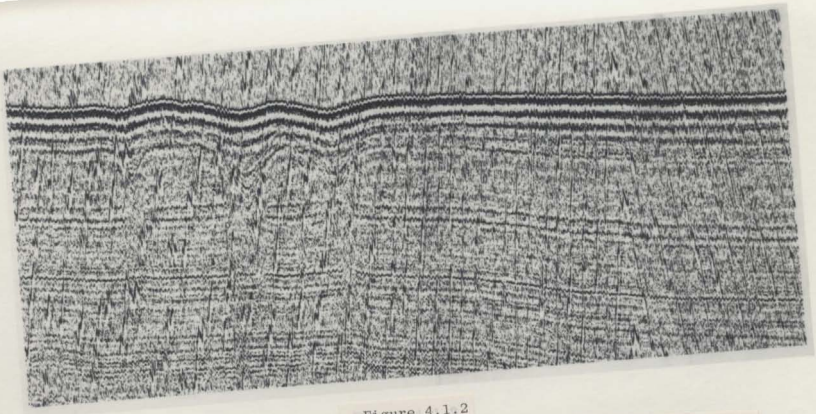

Figure 4.1.2

Grey scale displays for 2 km. of recorded sea bed data with depth of 15 m.

effects of the towed body dynamics. The next section discusses a procedure for extracting the contribution of the heave motion to the received signal. The Fourier transform of the heave component record provides the basis for a proposed linear model for the heave motion. A state-space model in continuous-time and the corresponding discrete-time version for heave motion representation are developed in Section (4.4). This is followed by a formulation of the heave compensation requirement as a Kalman filtering problem in optimal linear estimation theory. A discussion of the computational aspects and practical results are given to conclude this chapter.

## 4.2 Heave Component Extraction

A time record z(t) of the contribution of the towed body's heave motion to the received signals can be obtained from a sequence of return signal records, i=o,1, 2,...,$N_T$, taken at equal time intervals T. For a given record (i), the first peak of the return signal occurs at the two-way travel time of the wave reflected off the sea floor $\tau(i)$. The values of these travel times $\tau(iT)$ are related to the vertical displacement of the towed body plus the travel time to the sea bed by the velocity of sound propagation in water

$$z(iT) = c.\tau(i) \qquad (4.2.1)$$

The above is based on assuming a perfectly horizontal sea floor. It is thus clear that a discrete sequence of the record z(t) can be obtained from the computed time-to-first peak as shown in Figure 4.2.1. The data obtained were such that the pulse firing time is controlled electronically to eliminate the major effects of the fish heave. As a result the displacement of the order of two meters was reduced to the order of 0.5 meters by this compensation.

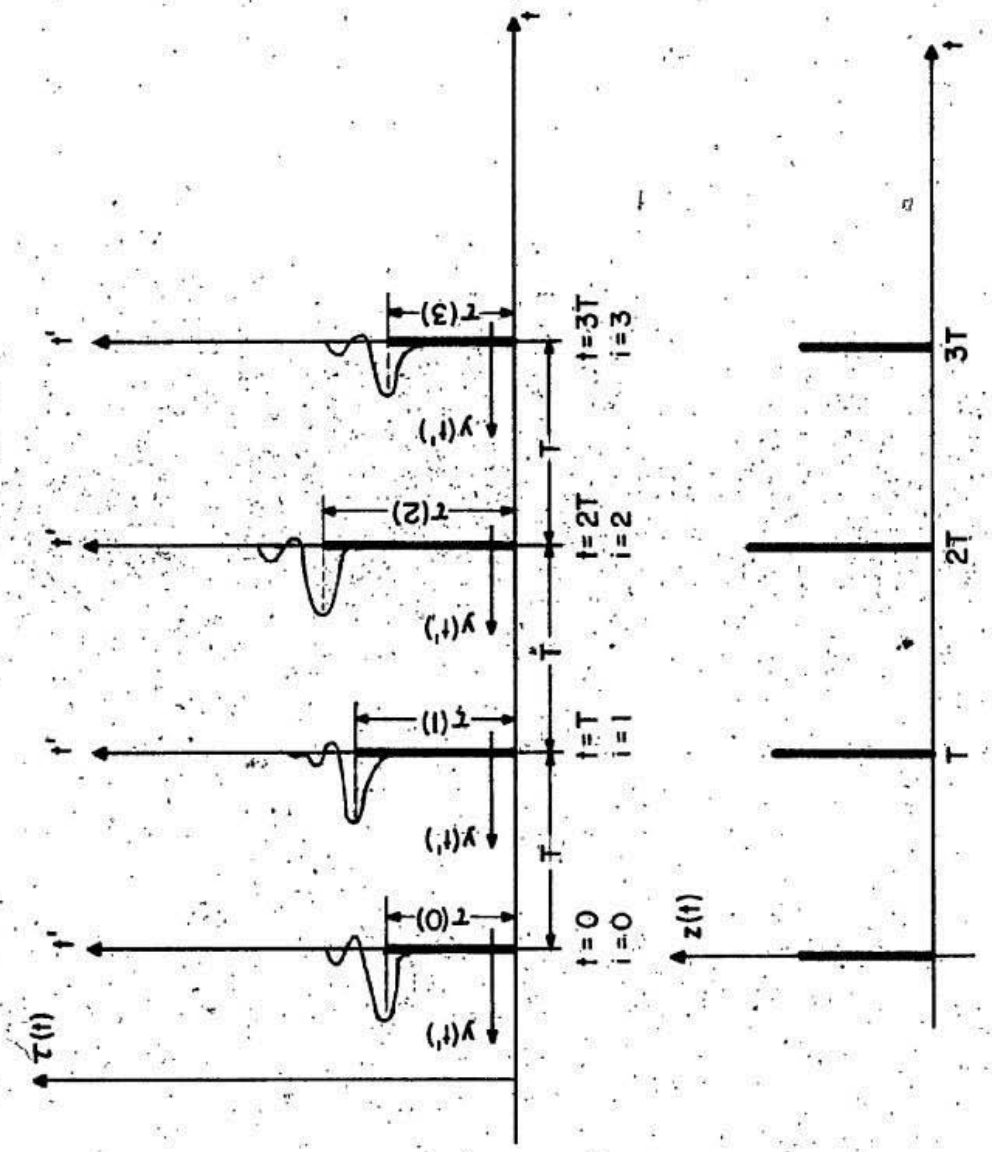


Figure 4.2.1 Construction of z(t) record from a sequence of return signal records.

Figure 4.2.2 shows the data after bandpass filtering (1.5-12.5 KHz). In the figure, (a) shows a sequence of individual records which display the arrival time shift (of time window of 20 m. sec). Part (b) of the figure shows a gray scale display record profile for a 512 meter length of the track. The time interval T between successive pings (record initiation) is 0.5 seconds. This corresponds to about one meter horizontal space separation between echo records at ship speed (an average of 2 m/sec.) The sampling rate for digitization for each individual record is 20 μ.sec.

The vertical displacement plus the travel time to the sea bed (or the corresponding peak delay-time) record, z(t) for the experimental data was obtained for 512 reflection records, initiated at T= 0.5 sec. intervals. This is shown in Figure 4.2.3.

The ship and towed body are assumed to travel at a constant speed v. The record z(t) which contains the heave variation can be calibrated to give the spatial displacement $\tilde{x}$ with a scaling of the time axis such that

$$\tilde{x} = v \cdot t \qquad (4.2.2)$$

The record z(t) can thus be transformed into a record $z(\tilde{x})$ in terms of the spatial displacement $\tilde{x}$.

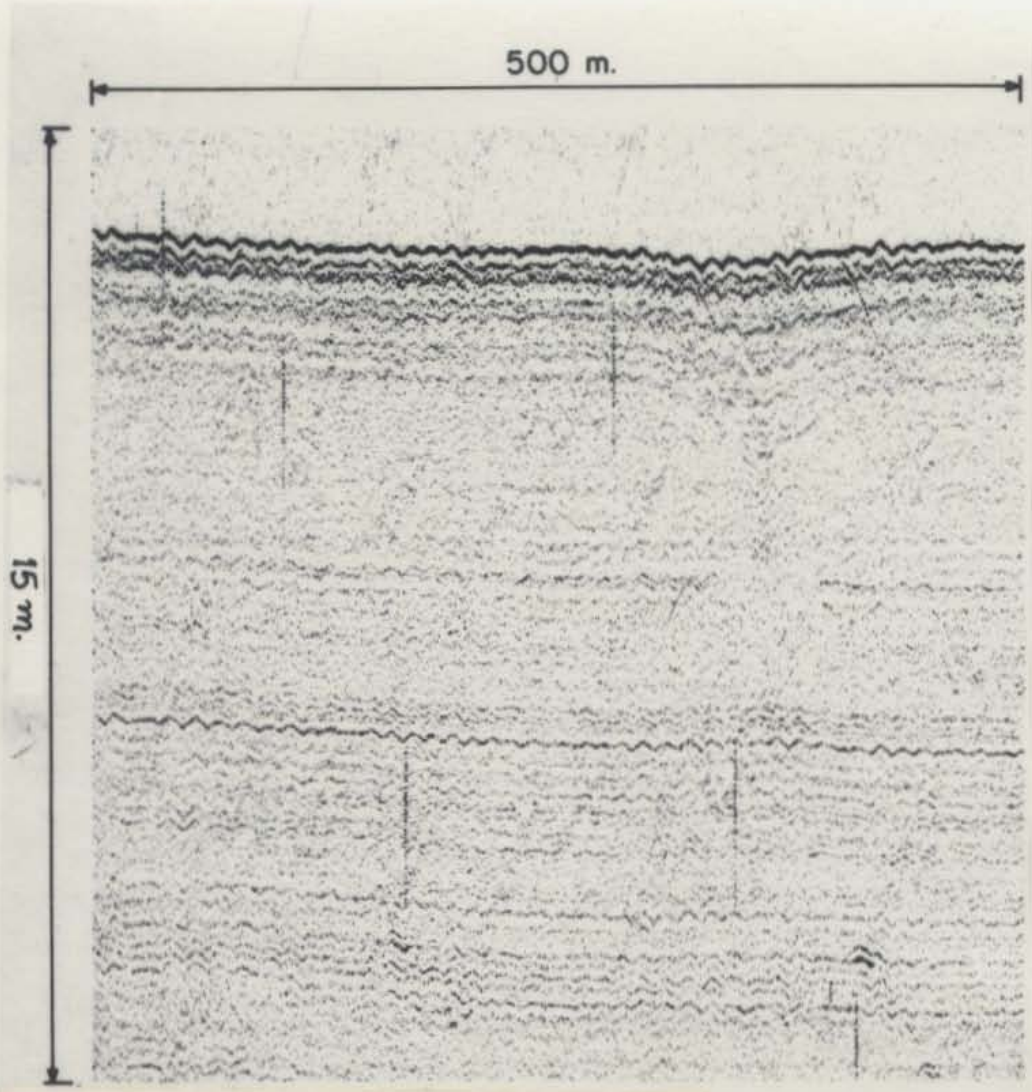


Figure 4.2.2.b A grey scale display record profile

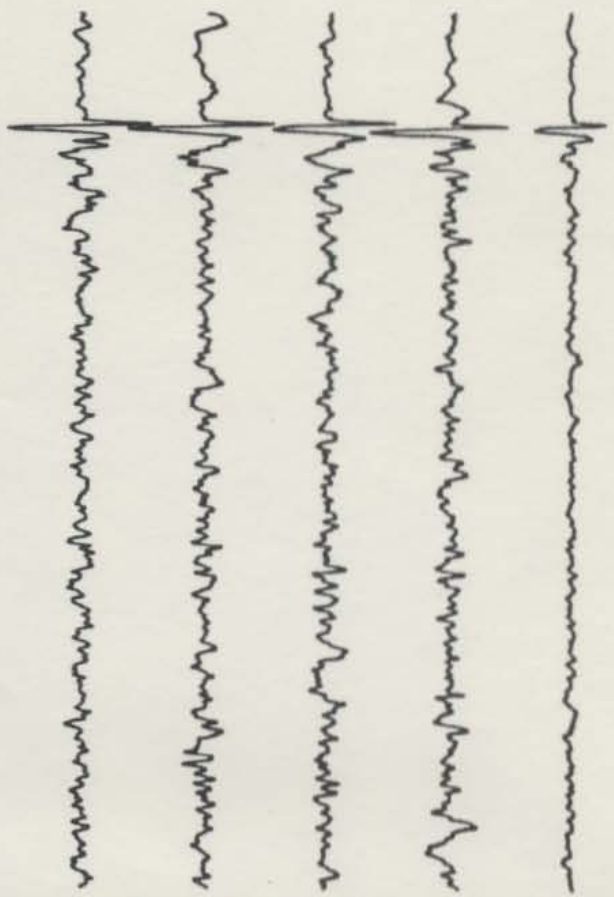

Figure 4.2.2.a A sequence of individual records

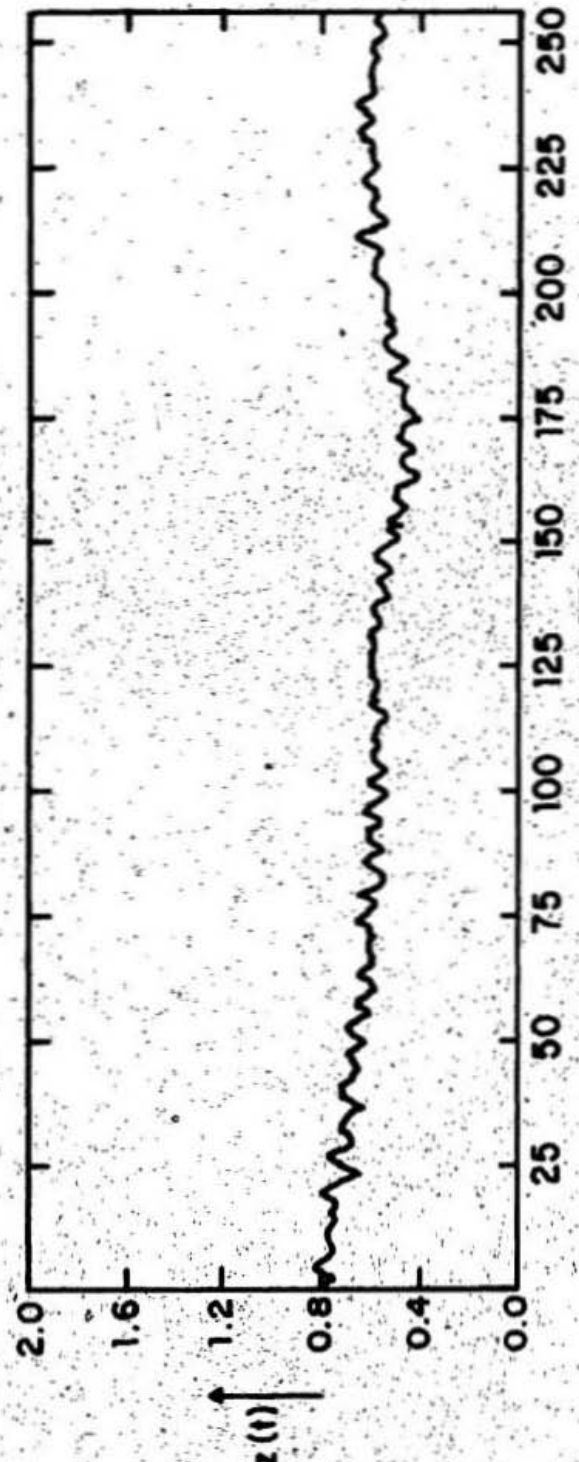


Fig. 4.2.3 Delay times of peaks record

The calibration is done using the relation of Eq.(4.2.2), where v is the ship speed. The record shows a periodic variation with randomness about an average (or trend) value corresponding to the sea bed features without the heave effect. The task is to identify the heave effect and then remove its contribution from the individual return signal records prior to further processing.

Inspection of the heave component record indicates a somewhat periodic motion with about 40-50 periods in 512 data records (corresponding to 512 meters of track length). Thus a rough estimate of the prevailing frequency for the given sea state is 0.08 - 0.10 cycles/meter or spatial period ≈ 10-13 meters.

## 4.3 Model for heave motion

To model the heave motion we have available the record z(t) which exhibits a somewhat periodic random component. Frequency response methods have given successful results in many fields of application. This provides a motivation to consider a frequency response method to identify the model of the physical phenomenon of source heave.

The Fourier transform Z(f) of the record z(t) gives the frequency response of the heave dynamics. This is postulated to be due to a purely random excitation (white noise) due to current and wave effects on the towed body, towed cable, and ship.

In order to avoid aliasing and to improve resolution the Fourier transform of the record with 0.5 seconds sampling rate is obtained through time scaling of $4 \times 10^{-5}$ ratio. This gives a 20 μ.sec. sampling period for processing. This corresponds to a sampling frequency of 50 KHz which is much higher than the anticipated frequency components in the record. The resolution in this case is 97.65 HZ, Figure 4.3.1 shows the magnitude of the Fourier transform Z(f) with a maximum frequency of 24 KHz, this corresponds to 0.96 HZ in the original record or 0.48 cycles/meter spatial frequency. The spatial resolution therefore is $1.953 \times 10^{-3}$ cycles/meter.

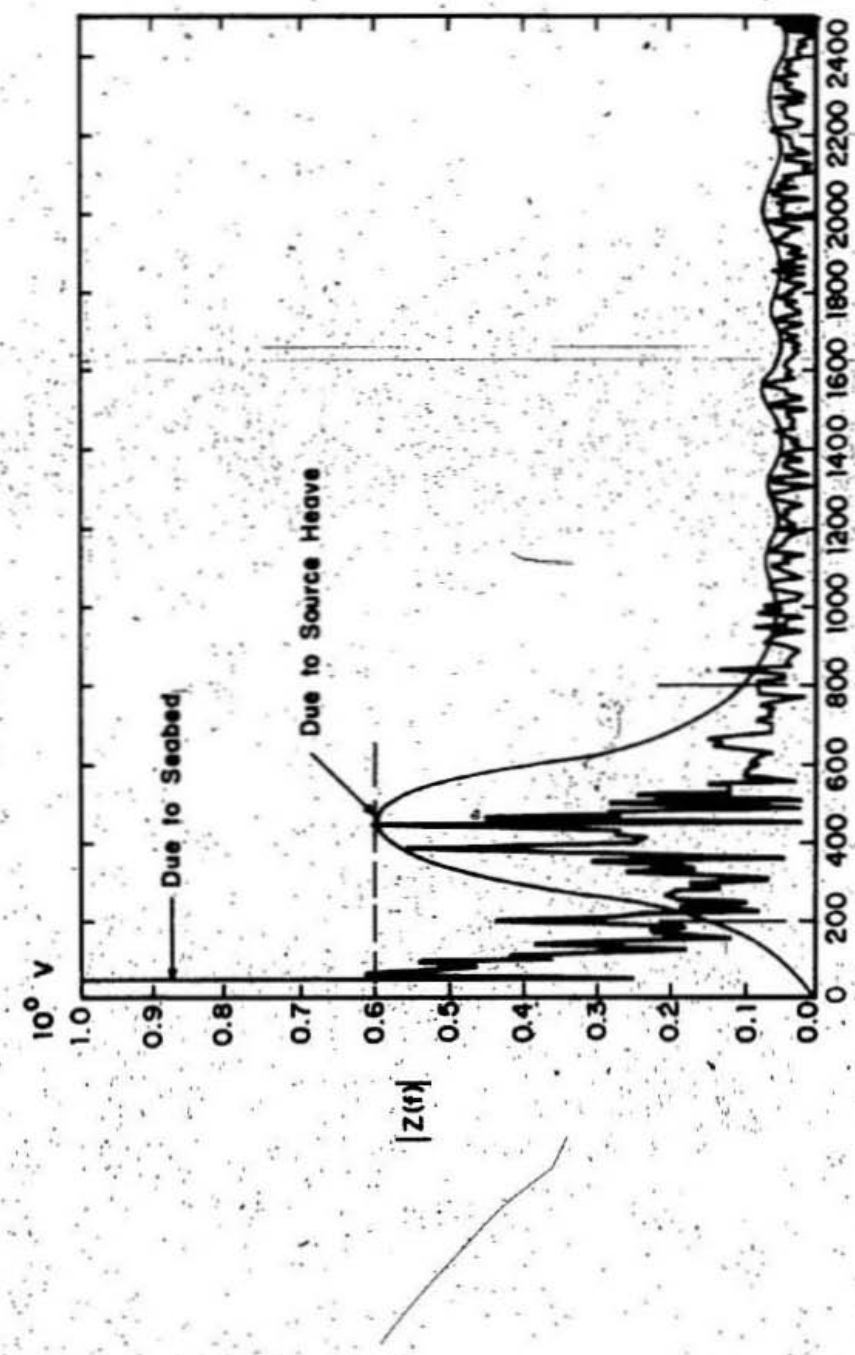


Figure 4.3.1 Fourier Magnitude of the actual response record z(t)

Inspection of the frequency response characteristic reveals the presence of a number of dominant frequencies. This suggests that the response can be modeled by passing the purely random input through a narrow band filter with drifting center frequencies corresponding to the observed dominant frequencies. This particular idealization is shown in Figure 4.3.2. The narrow band filter's response is somewhat similar to that of a simple resonant electric circuit (RLC) which can be modeled using a second-order transfer function.

For the purposes of this study only a narrow band filter corresponding to the envelope of the heave spectrum is postulated to represent the heave dynamics. This can be visualized as a reduced order model for a complex physical phenomenon. It is also consistent with models of heave dynamics found in the literature on marine hydrodynamics such as Bhattacharyya (1978), Price and Bishop's (1974) and, McCormick (1973).

The heave response model in the s-domain is chosen as

$$\frac{Z(s)}{u(s)} = \frac{K}{1 + Q_o\left[\frac{s}{\omega_o} + \frac{\omega_o}{s}\right]} \qquad (4.3.1)$$

The natural (or center) frequency of the system is $\omega_o$ while $Q_o$ is the quality factor which is obtained from

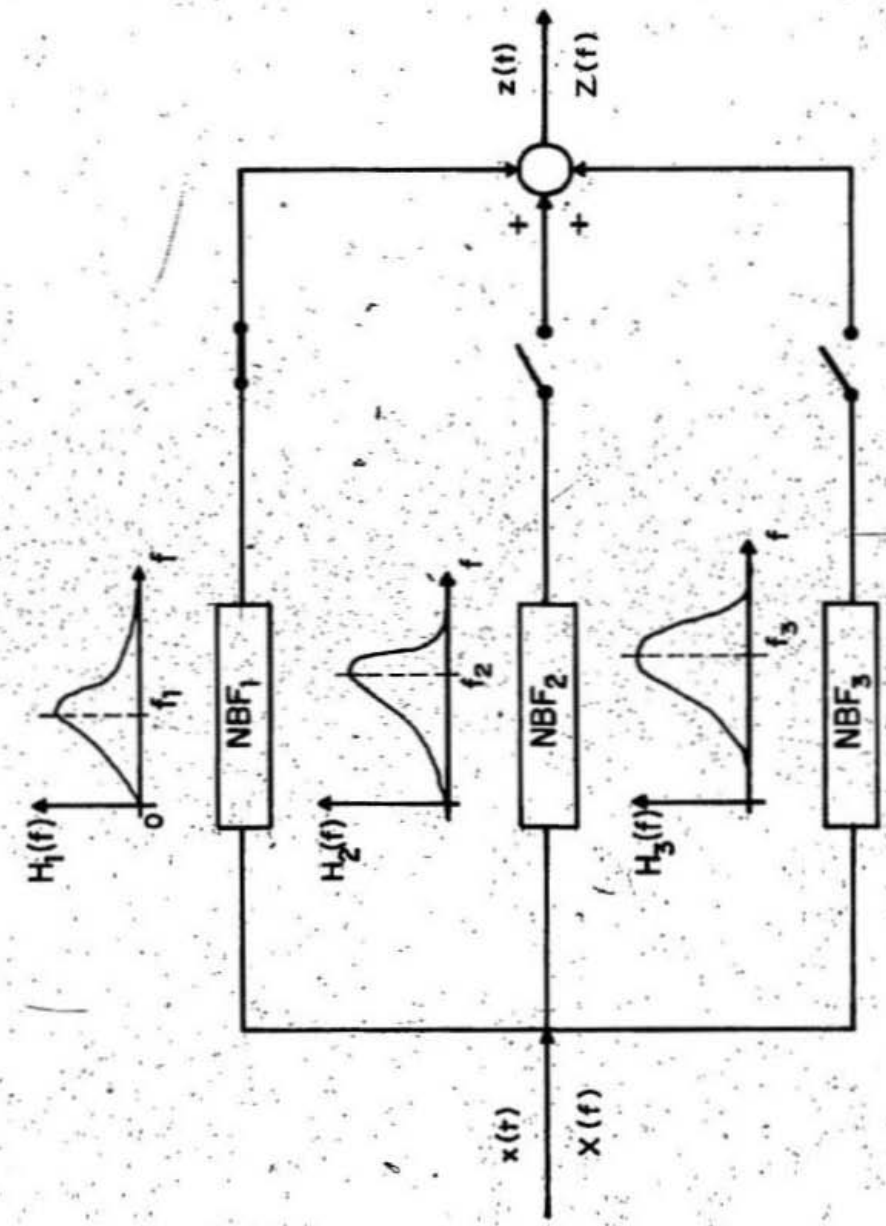


Figure 4.3.2 Narrow band filter with drifting centre frequencies

the half-power points ($f_1$ and $f_2$)

$$Q_o = f_o/(f_2 - f_1) \qquad (4.3.2)$$

The idealized frequency response of the system is shown in Figure 4.3.3.

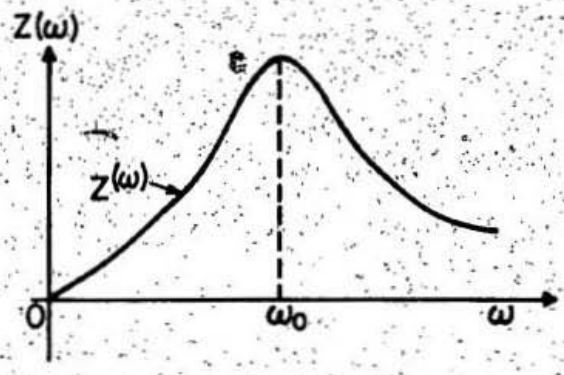


Fig. 4.3.3. The typical frequency response of a parallel GCL circuit.

From Figure 4.3.1, the centre frequency $f_o$ is seen to be at $f_o$ = 4 KHz. The half-power points occur at

frequencies approximately of 3 KHz and 5 KHz. As a result the quality factor is calculated to be $Q_o = 2$ and $\omega_o = 2\pi f_o$ (4.3.3)

Equation (4.3.1) leads to the form

$$T(s) = \frac{cs}{s^2 + as + b} = \frac{Z(s)}{U(s)} \qquad (4.3.4)$$

where the system parameters are

$$a = \omega_o/Q_o \qquad (4.3.5)$$

$$b = (\omega_o)^2 \quad \text{and} \qquad (4.3.6)$$

$$c = k\,\omega_o/Q_o \qquad (4.3.7)$$

This is the lowest order model that provides a reasonable approximation to the actual frequency response in the least square sense. This is verified by comparison of the graph of Figure 4.3.4 with the envelope of the actual response shown in Figure 4.3.1.

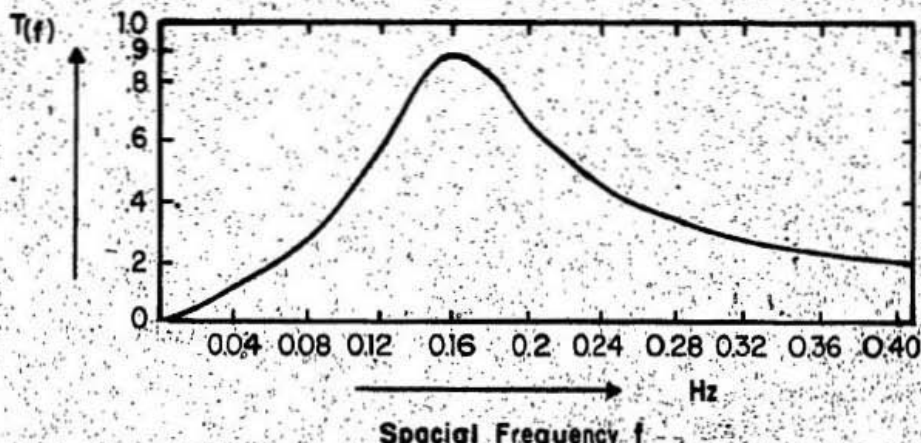


Figure 4.3.4 Simulated frequency response

## 4.4 The Dynamic Model for heave motion

A mathematical model which can serve to describe the dynamic phenomenon is the state equation model, with its attendant observation model, of the general form

$$\frac{d}{dt}\underline{x}(t) = \underline{f}(x(t),b(t),u(t),\omega(t),t) \qquad (4.4.1)$$

A state-space model for the heave process can be obtained by choosing the states $x_1(t)$ and $x_2(t)$ in accordance with their Laplace transform as given by

$$X_1(s) = Q_o\, Z(s)/(K\, \omega_o\, s) \qquad (4.4.2)$$

$$X_2(s) = s\, X_1(s) \qquad (4.4.3)$$

Note that with this choice

$$X_2(s) = (Q_o\, Z(s))/(K\, \omega_o) \qquad (4.4.4)$$

This indicates that the required vertical displacement variable $Z(s)$ is simply obtained by scaling of $X_2(s)$ As a result Eq. (4.3.1) becomes

$$[s^2 + \frac{\omega_o}{Q_o}\, s + \omega_o^2]\, X_1(s) = U(s) \qquad (4.4.5)$$

Now the state space model for this linear system is obtained as

$$\dot{x}_1(t) = x_2(t) \qquad (4.4.6)$$

$$\dot{x}_2(t) = -\omega_o^2 x_1(t) - \frac{\omega_o}{Q_o} x_2(t) + u(t) \qquad (4.4.7)$$

or in vector-matrix form

$$\begin{bmatrix} \dot{x}_1(t) \\ \dot{x}_2(t) \end{bmatrix} = \begin{bmatrix} 0 & 1 \\ -\omega_o^2 & -\frac{\omega_o}{Q_o} \end{bmatrix} \begin{bmatrix} x_1(t) \\ x_2(t) \end{bmatrix} + \begin{bmatrix} o \\ 1 \end{bmatrix} u(t) \qquad (4.4.8)$$

This can be written in the compact form

$$\dot{\underline{x}}(t) = \underline{A}\, \underline{x}(t) + \underline{B}\, u(t). \qquad (4.4.9)$$

where

$$\underline{A} = \begin{bmatrix} o & 1 \\ -\omega_o^2 & -\frac{\omega_o}{Q_o} \end{bmatrix} \qquad (4.4.10)$$

$$\underline{B} = \begin{bmatrix} o \\ 1 \end{bmatrix} \qquad (4.4.11)$$

$$\underline{x}(t) = [o \quad 1]^T \qquad (4.4.12)$$

The numerical values for elements of the matrix $\underline{A}$ are

$$\underline{A} = \begin{bmatrix} 0 & 1 \\ -(8\pi x10^3)^2 & -(4\pi x10^3) \end{bmatrix} \qquad (4.4.13)$$

The state-transition matrix associated with this representation is given by [Ogata,1967]

$$\underline{\Phi}(t_i,t_j) = \begin{bmatrix} a(t_{ij})\sin(\omega_d t_{ij}+\Psi) & \frac{a(t_{ij})}{\omega_o}\sin(\omega_d t_{ij}) \\ -\omega_o a(t_{ij})\sin(\omega_d t_{ij}) & -a(t_{ij})\sin(\omega_d t_{ij}-\Psi) \end{bmatrix} \qquad (4.4.14)$$

where

$$t_{ij} = t_i - t_j \qquad t_i > t_j \qquad (4.4.15)$$

$$a(t) = \frac{\exp.\{\frac{-\omega_o}{2Q_o} t\}}{\sqrt{1 - (\frac{1}{4Q_o^2})}} \qquad (4.4.16)$$

$$\omega_d = \omega_o\sqrt{1 - \frac{1}{4Q_o^2}} \qquad (4.4.17)$$

$$\Psi = \tan^{-1}\sqrt{4Q_o^2 - 1} \qquad (4.4.18)$$

The continuous-time domain solution is given by

$$\underline{x}(t) = \underline{\Phi}(t,t_o)x(t_o) + \int_{t_o}^{t} \underline{\Phi}(t,\tau)\underline{B}(\tau)u(\tau)d\tau \qquad (4.4.19)$$

For estimation purposes, a discrete-time version is needed. Considering the time interval $t_k < t < t_{k+1}$ for k=o,1,...,assuming that $x(t_k)$ is given and that $u(t) = u(k)$ is constant one thus has

$$\underline{x}(t_{k+1}) = \underline{\Phi}(t_{k+1}, t_k)\, \underline{x}(t_k) + \left[\int_{t_k}^{t_{k+1}} \underline{\Phi}(t_{k+1}, \tau)\underline{B}(\tau)d\tau\right] u(k) \tag{4.4.20}$$

Now define

$$\underline{x}(t_{k+1}) = \underline{x}(k+1) \tag{4.4.21}$$

$$\underline{x}(t_k) = \underline{x}(k) \tag{4.4.22}$$

$$\underline{\Phi}(t_{k+1}, t_k) = \underline{\Phi}(k+1,k) \tag{4.4.23}$$

$$\int_{t_k}^{t_{k+1}} \underline{\Phi}(t_{k+1}, \tau)\underline{B}(\tau)d\tau = \underline{\Gamma}(k+1,k) \tag{4.4.24}$$

then

$$\underline{x}(k+1) = \underline{\Phi}(k+1,k)\underline{x}(k) + \underline{\Gamma}(k+1,k)\, u(k) \tag{4.4.25}$$

The discrete state transition matrix $\underline{\Phi}$ is given by

$$\underline{\Phi}(k+1,k)=\begin{bmatrix} a(\Delta)\sin(\omega_d\Delta+\Psi) & \frac{a(\Delta)}{\omega_o}\sin(\omega_d\Delta) \\ -\omega_o a(\Delta)\sin(\omega_d\Delta) & -a(\Delta)\sin(\omega_d\Delta-\Psi) \end{bmatrix} \tag{4.4.26}$$

where

$$\Delta = t_{k+1} - t_k$$

The vector $\Gamma$ is found to be

$$\underline{\Gamma}(k+1,k) = \begin{bmatrix} \frac{1}{\omega_o^2}\left[1 - \frac{e^{-\omega_o\Delta/2Q_o}}{\sqrt{1-\frac{1}{4Q_o^2}}}\sin(\omega_d\Delta+\Psi)\right] \\ \frac{e^{-\omega_o\Delta/2Q_o}}{\omega_o\sqrt{1-\frac{1}{4Q_o^2}}}\sin(\omega_d\Delta) \end{bmatrix} \tag{4.4.27}$$

This completely specifies the discrete transition model for the system.

## 4.5 Kalman filtering for heave motion removal

The available measurements of heave motion (vertical displacement) provide only crude information on the actual system behaviour and may be unsatisfactory for compensation purposes. This is due to the fact that the sensors and the manipulation process are subject to random and systematic errors. The previous section dealt with modeling the dynamic process in a state-space form. The estimation of the state vector from measurement data corrupted by noise can be performed using results from optimal linear estimation theory. Of specific interest is the linear optimal filter commonly referred to as Kalman filter. Filtering refers to estimating the state vector at the current time based upon all past measurements. The optimal estimates minimize the estimation error in a well defined statistical sense. For Kalman filtering the objective is to minimize a weighted scalar sum of the diagonal elements of the error covariance matrix. The process and measurement models and assumptions for Kalman filtering purposes are outlined before presenting the optimal filtering algorithm.

The heave-motion model in state-space form obtained in the previous section is

$$\underline{x}(k+1) = \underline{\Phi}(k+1,k)\underline{x}(k) + \underline{\Gamma}(k+1,k)\underline{w}(k), \tag{4.5.1}$$

where the forcing function u has been replaced by w. Since $\underline{\Phi}$ and $\underline{\Gamma}$ are independent of k, one writes

$$\underline{x}(k+1) = \underline{\Phi}\,\underline{x}(k) + \underline{\Gamma}\,\underline{w}(k) \qquad (4.5.2)$$

The input sequence $\underline{w}(k)$ is assumed to be a gaussian white sequence with zero mean

$$E[\underline{w}(k)] = \underline{o} \qquad (4.5.3)$$

and covariance

$$E[\underline{w}(j)\,\underline{w}^T(k)] = \underline{Q}(k)\,\delta_{jk} \qquad (4.5.4)$$

$\underline{Q}(k)$ is a positive semi-definite 2x2 matrix. Further, $\underline{x}(o)$ is assumed to be a gaussian random vector with zero mean.

$$E[\underline{x}(o)] = \underline{o} \qquad (4.5.5)$$

and known covariance matrix

$$E[\underline{x}(o)\,\underline{x}^T(o)] = \underline{P}(o), \qquad (4.5.6)$$

where $\underline{P}(o)$ is a positive semi-definite 2x2 matrix. It is further assumed that w(k) is independent of $\underline{x}(o)$

$$E\{\underline{x}(o)\,\underline{w}^T(k)\} = o \quad \text{for all } k \qquad (4.5.7)$$

The record of vertical displacement obtained by the procedure outlined in Section (4.2) is a sequence of measurements z(k). In terms of the state-space model for heave motion, the sequence z(k) is given by

$$z(k+1) = \begin{bmatrix} o & \frac{\omega_o}{Q_o} \end{bmatrix} \begin{bmatrix} x_1(k+1) \\ x_2(k+1) \end{bmatrix} + \underline{v}(k+1) \qquad (4.5.8)$$

or in vector form

$$z(k+1) = \underline{H}\, \underline{x}\,(k+1) + \underline{v}(k+1) \qquad (4.5.9)$$

The measurement error sequence $\underline{v}(k)$ is assumed to be a gaussian white sequence with zero mean.

$$E[\underline{v}(k)] = o \qquad (4.5.10)$$

for all k=o,1,..., and a covariance

$$E[\underline{v}(j)\ \underline{v}^T(k)] = \underline{R}(k)\ \delta_{jk} \qquad (4.5.11)$$

where $\delta_{jk}$ is the Kronecker delta. It is also assumed that $\underline{v}(k)$ is independent of $\underline{x}(o)$ for all k,

$$E\{\underline{x}(o)\ \underline{v}^T(k)\} = o \qquad (4.5.12)$$

The noise processes $\underline{w}(k)$ and $\underline{v}(k)$ are assumed independent, hence

$$E\{\underline{v}(j)\ \underline{w}^T(k)\} = o \qquad (4.5.13)$$

for all j and k.

Assume that measurements z(1), z(2),...,z(j) are available from which to estimate $\underline{x}(k)$, denoted by $\hat{\underline{x}}(k|j)$. The estimation problem is referred to as one of prediction if k > j, if k = j as one of filtering, and, if k < j, one of smoothing or interpolation. Of interest here is the filtering problem. Thus, given

measurements $z(1),\ldots,z(k)$ one would like to determine $\hat{\underline{x}}(k|k)$. The filtering error $\tilde{x}$ is defined by

$$\tilde{\underline{x}}(k|k) = \underline{x}(k) - \hat{\underline{x}}(k|k), \qquad (4.5.14)$$

and has a covariance matrix denoted by $\underline{P}(k|k)$. A Kalman filter is a recursive algorithm that finds the optimal filtered estimates on the basis of $\hat{\underline{x}}(o|o)$ and $\underline{P}(o|o)$.

There are many alternative forms for the Kalman filtering algorithm. The following is one form which provides an easy implementation. This is based on details given in Meditch (1969) and Gelb (1974).

1. Given $\underline{P}(k|k)$, $\underline{Q}(k)$, $\underline{\Phi}$ and $\underline{\Gamma}$, the predictor covariance matrix $\underline{P}(k+1|k)$ is computed according to

$$\underline{P}(k+1|k) = \underline{\Phi}\,\underline{P}(k|k)\,\underline{\Phi}^T + \underline{\Gamma}\,\underline{Q}(k)\,\underline{\Gamma}^T \qquad (4.5.15)$$

2. The Kalman Filter Gain Matrix $K(k+1)$ is computed using

$$\underline{K}(k+1) = \underline{P}(k+1|k)\underline{H}^T[\underline{H}\,\underline{P}(k+1|k)\underline{H}^T + \underline{R}(k+1)]^{-1} \qquad (4.5.16)$$

The matrix inverse in the above poses no problem since the matrix is m x m, where m is the number of elements in the measurement vector, in the present case 1.

3. The error covariance matrix $\underline{P}(k+1|k+1)$ is

computed according to

$$\underline{P}(k+1|k+1) = [\underline{I} - \underline{K}(k+1)\underline{H}]\underline{P}(k+1|k) \quad (4.5.17)$$

This is stored until the time of the next measurement when the cycle is repeated.

4. The given estimate $\hat{\underline{x}}(k|k)$ is propagated forward to give the predicted estimate $\hat{\underline{x}}(k+1|k)$ according to

$$\hat{\underline{x}}(k+1|k) = \underline{\Phi}\,\hat{\underline{x}}(k|k) \quad (4.5.18)$$

5. The measurement estimate $\hat{z}(k+1|k)$ is obtained as

$$\hat{z}(k+1|k) = \underline{H}\,\hat{\underline{x}}(k+1|k) \quad (4.5.19)$$

6. The measurement estimate is subtracted from the actual measurement $z(k+1)$ to obtain the measurement residual $\tilde{z}(k+1|k)$

$$\tilde{z}(k+1|k) = z(k+1) - \hat{z}(k+1|k) \quad (4.5.20)$$

7. A correction term involving weighting of the measurement residual by the matrix $\underline{K}(k+1)$ is obtained and is added to the predicted estimate $\hat{\underline{x}}(k+1|k)$ to obtain $\hat{\underline{x}}(k+1|k+1)$

$$\hat{\underline{x}}(k+1|k+1) = \hat{\underline{x}}(k+1|k) + \underline{K}(k+1)\tilde{z}(k+1|k) \quad (4.5.21)$$

This value is stored until the next cycle.

The information flow is shown in Fig. 4.5.1

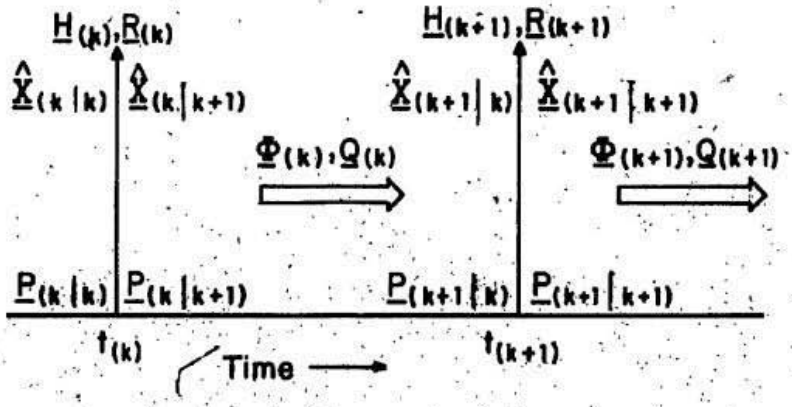


Fig. 4.5.1 Discrete Kalman filter timing diagram.

Filtering is initiated with $\hat{\underline{x}}(o|o) = o$ and $\underline{P}(o|o) = \underline{P}(o)$ is assumed given. It is noted here that if large uncertainty is associated with x(o) then its covariance matrix $\underline{P}(o)$ can be considered as diagonal with arbitrarily large terms, that is $\sigma_{ii}^2(o)=E[\underline{x}_i^2(o)]\to\infty$. In the present application w and v are assumed stationary, and as a result

$$\underline{Q}(k) = \underline{Q}$$

$$\underline{R}(k) = \underline{R}$$

The choice of $\underline{Q}$ and $\underline{R}$ is generally based on experience with the noise process present in the record. If one assumes that the measured variables are uncertain (less reliable) then this is equivalent to large measurement noise and hence a large $\underline{R}$ ($\underline{R}^{-1}$ is small). Assuming that the noise in state vector components are uncorrelated, one thus has a diagonal covariance matrix $\underline{Q}$. For the present application a good choice of $\underline{R}$ is found to be $\underline{R} = (0.1\ z(t)_{av})^2$, and for $\underline{Q}$, one has $\underline{Q} = (1.5\ z(t)_{av})^2\ \underline{I}$, where I is the unity matrix. $z(t)_{av}$ is the average of the observation record.

A computer program was written to implement the Kalman filter procedure described above. The results corresponding to the stretch of the track are shown in Fig. 4.5.2. It may be observed from the corresponding power spectrum in Figure 4.5.3 (B) that the filtering process has the effect of removing the high frequency content of the sea bed profile. Figure 4.5.4.a and Figure 4.5.4.b show an ANAC graphic gray scale display of the features of the area before and after compensation.

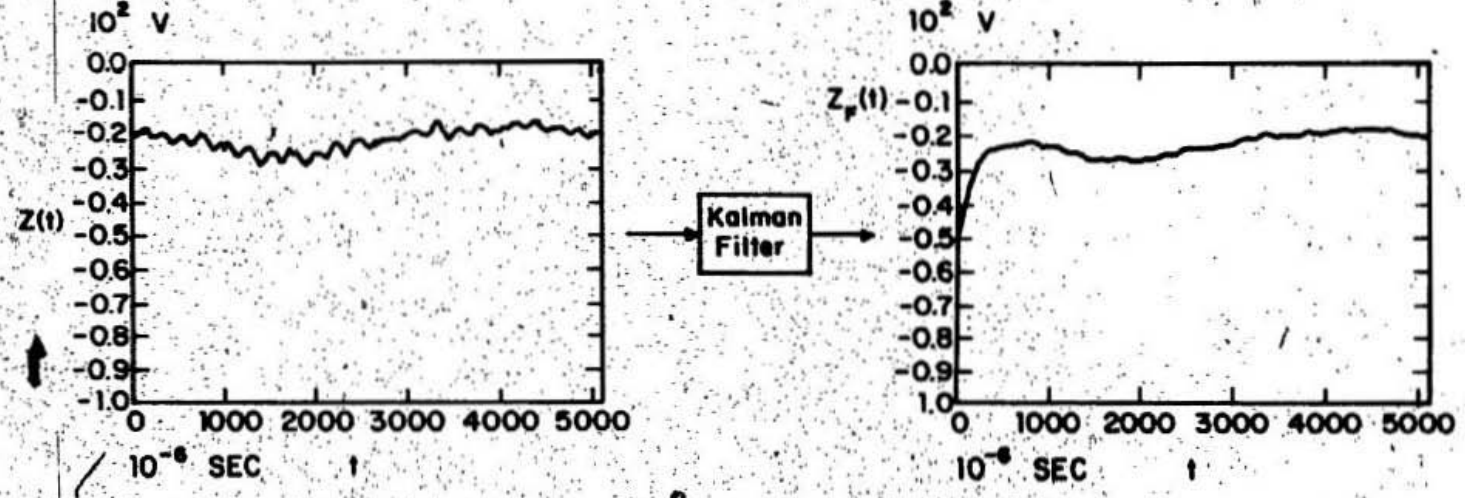


Figure 4.5.2

The unfiltered and filtered waveform after applying Kalman filter

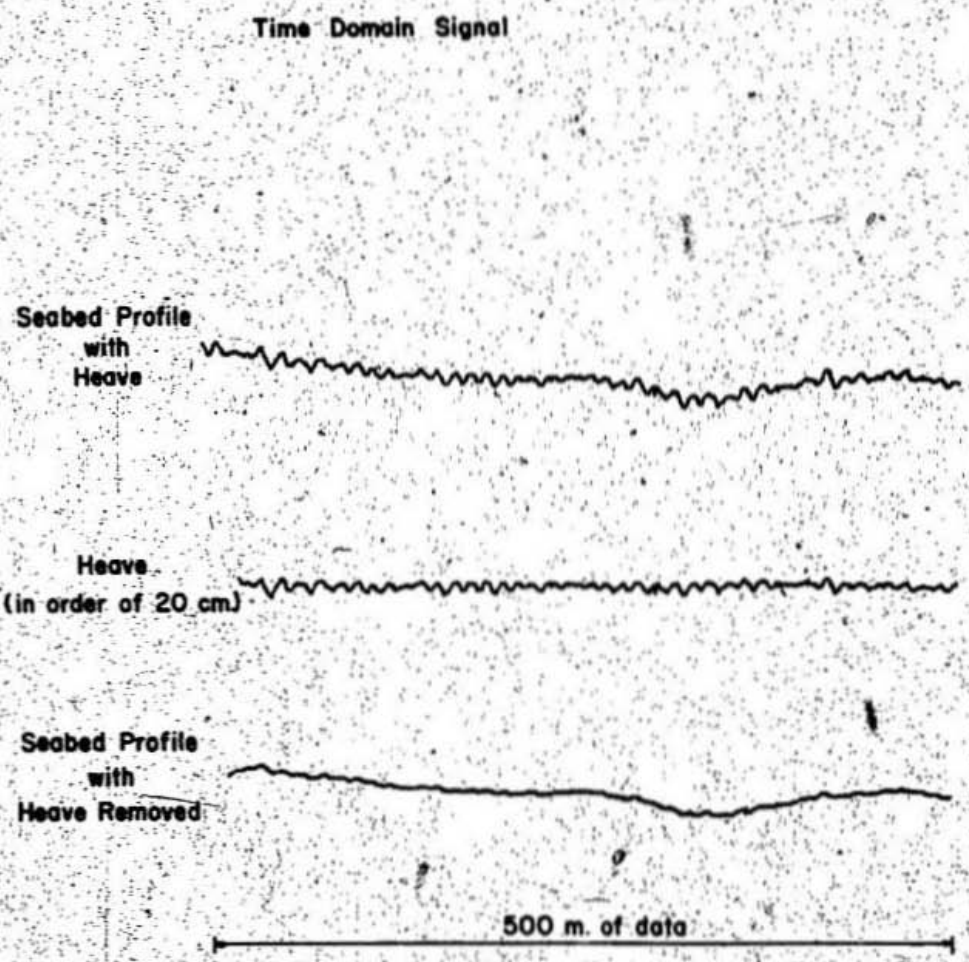


Figure 4.5.3a

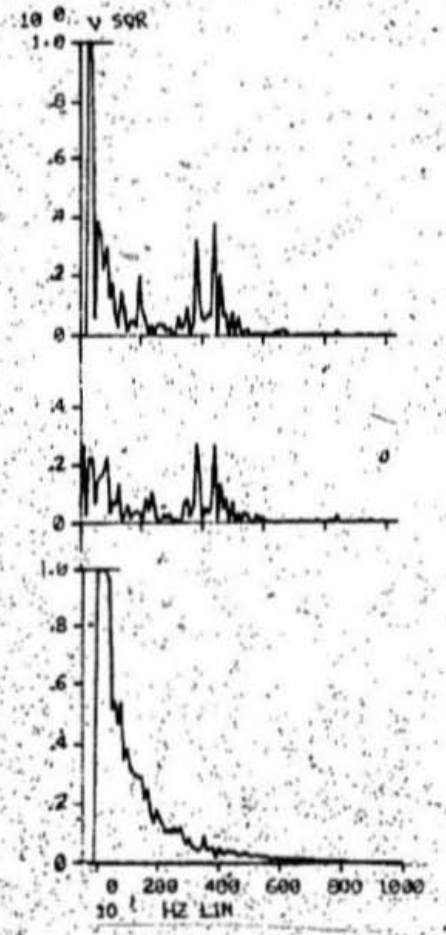


Figure 4.5.3.b

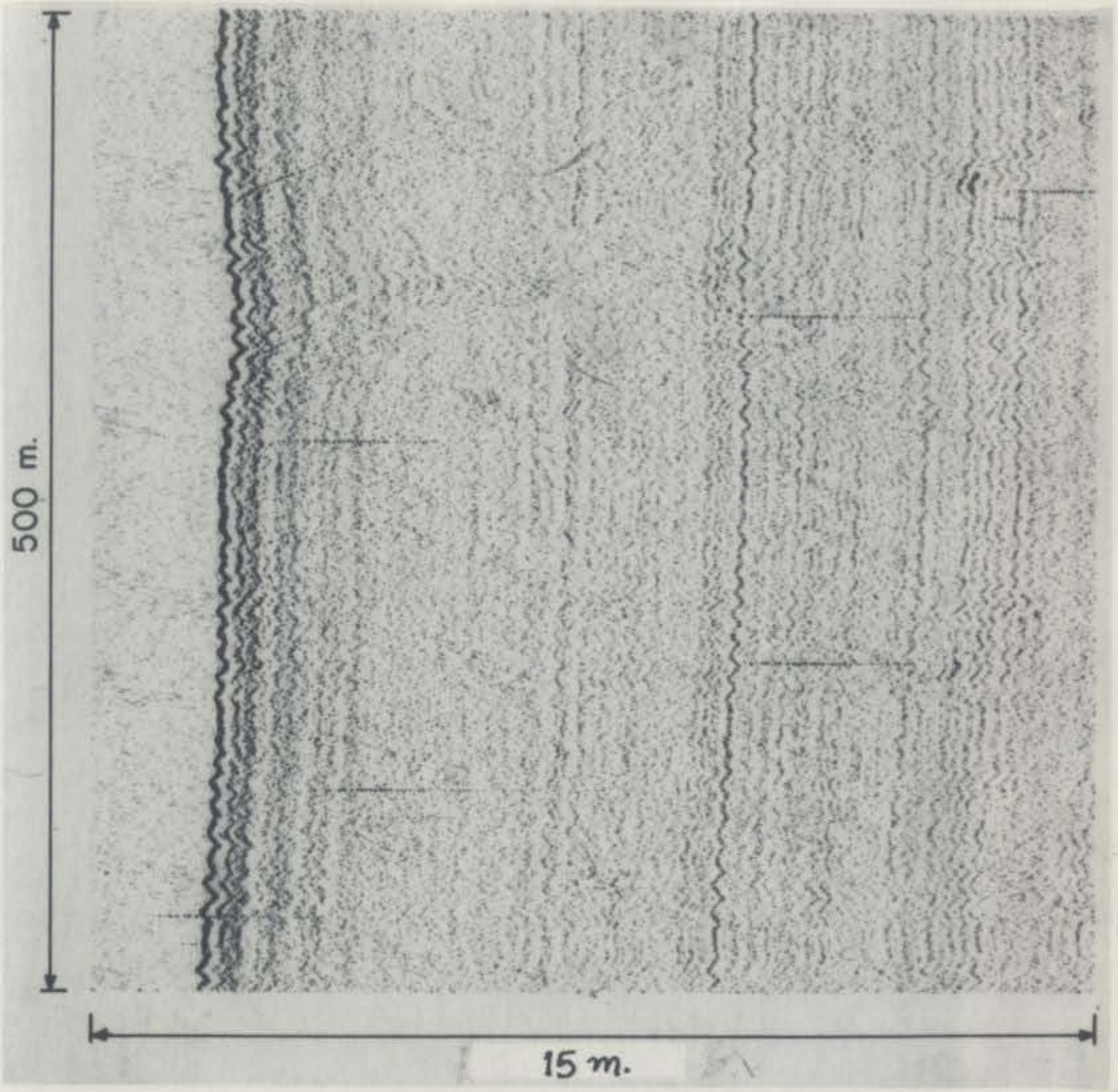


Figure 4.5.4 a. Grey scale display of uncompensated profile.

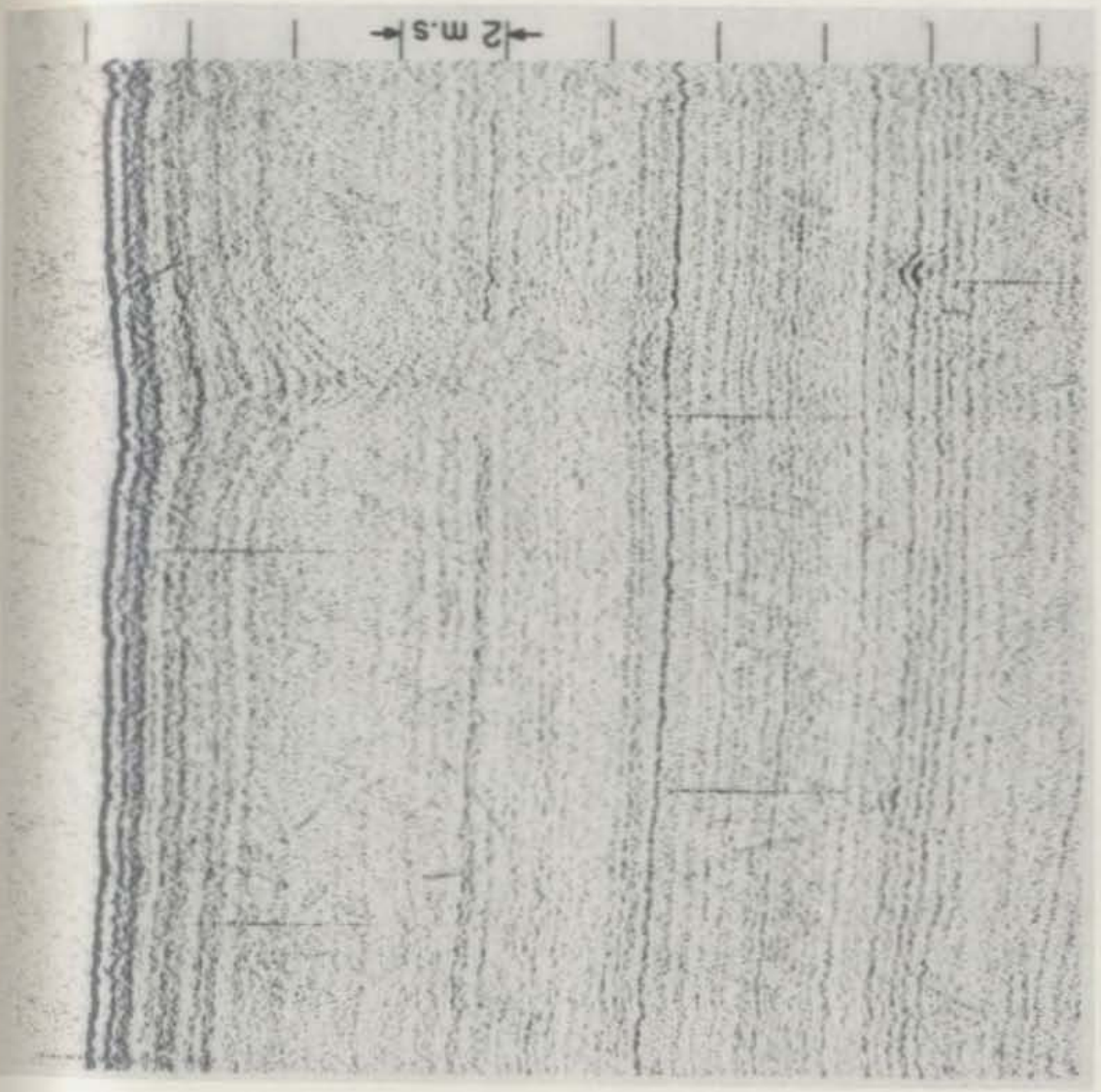


Figure 4.5.4b. Grey scale display of compensated profile.

# Chapter 5

# EXTRACTING INFORMATION FROM THE SEA-BED RESPONSE

## 5.1 Introduction

This chapter presents some newly developed procedures for processing acoustic return signals. The objective common to all procedures is to provide reliable estimates of the amplitude and delay parameters associated with source signal replicas present in the return signal. The procedures utilize some fundamental, yet powerful, tools from communications, and estimation theory.

The chapter is organized such that the different problem formulations of each of the proposed procedures are presented first. This is followed by three sections treating each procedure. In each case the outline of the procedure is given as well as results pertaining to some simulated return signals and actual field signals obtained during the sea trial. The use of simulated return signals provides a basis for performance evaluation since in this case the actual values of the parameters required are known by construction.

## 5.2 Problem formulation for estimation purposes

The input-output expression relating the signal y(t) received by the hydrophone to the source signal m(t) obtainable by either ray tracing or from the layer geometry Equation (3.2.11), is made more realistic by including the measurement noise v(t). This accounts in reality for physical effects not accommodated by the noise-free, simple reflection model as well as for sensor and instrumentation inaccuracies and acoustical disturbances, primarily scattering and reverberation. Thus the model is given by

$$y(t) = \sum_{i=1}^{n} a_i \, m(t-\tau_i) + v(t) \qquad (5.2.1)$$

where each term in the summation is a delayed and scaled replica of the source wavelet. These arise from primary, secondary and higher order reflections. Thus $a_i$ are functionally related to the reflection coefficients at the layer interface and $\tau_i$ are related to the layer travel times. Details of the development of (5.2.1) were given in Section (3.2).

In view of Equation (5.2.1), identification of sub-bottom structure and geometry reduces to a problem in parameter estimation. This is due to the functional relations between the parameters of Equation (5.2.1) and the structure and geometry of the sub-bottom. The esti-

mation task is to determine in an optimal sense, the amplitude parameters $a_i$ and the delay times $\tau_i$.

The observation Equation (5.2.1) can be expressed in a number of ways to facilitate the estimation procedure. The first formulation proceeds assuming the availability of an observation sequence $\{y(t_i), i=o,\ldots,N-1\}$. In this case a vector-matrix equation replaces (5.2.1). This is given by

$$\begin{bmatrix} y(t_o) \\ y(t_1) \\ \vdots \\ y(t_{N-1}) \end{bmatrix} = \begin{bmatrix} m(t_o-\tau_1) & m(t_o-\tau_2) & \ldots & m(t_o-\tau_n) \\ m(t_1-\tau_1) & m(t_1-\tau_2) & & m(t_1-\tau_n) \\ \vdots & \vdots & & \\ m(t_{N-1}-\tau) & m(t_{N-1}\tau_2) & & m(t_{N-1}-\tau) \end{bmatrix} \begin{bmatrix} a_1 \\ a_2 \\ \vdots \\ a_n \end{bmatrix} + \begin{bmatrix} v(t_o) \\ v(t_1) \\ \vdots \\ v(t_{N-1}) \end{bmatrix} \tag{5.2.2}$$

More compactly this is of the form

$$\underline{y} = \underline{H}\,\underline{p} + \underline{V} \tag{5.2.3}$$

The second formulation assumes that for a given time interval $[t_{q_i}, t_{q_{i+w-1}}]$, only one signal replica appears corresponding to the ith component.

$$y(t) = a_i\, m(t-\tau_i) + v(t) \qquad t_{q_i} < t < t_{q_{i+w-1}} \tag{5.2.4}$$

As a result, the vector matrix equation takes on the form

$$\begin{bmatrix} y(t_{q_i}) \\ y(t_{q_{i+1}}) \\ \vdots \\ y(t_{q_{i+w-1}}) \end{bmatrix} = \begin{bmatrix} m(t_{q_i}-\tau_i) \\ m(t_{q_{i+1}}-\tau_i) \\ \vdots \\ m(t_{q_{i+w-1}}-\tau_i) \end{bmatrix} a_i + \begin{bmatrix} v(t_{q_i}) \\ v(t_{q_{i+1}}) \\ \vdots \\ v(t_{q_{i+w-1}}) \end{bmatrix} \tag{5.2.5}$$

This can be represented by the compact form

$$\underline{y}_i = \underline{m}_i a_i + \underline{v}_i \tag{5.2.6}$$

The third alternative formulation assumes that estimates $\hat{\tau}_i$ are available for the delay parameters and that the improvements $\Delta\tau_i$ are to be obtained

$$\Delta\tau_i = \tau_i - \hat{\tau}_i \tag{5.2.7}$$

A truncated Taylor series of the following form is utilized

$$m(t-\tau_i) = m(t-\hat{\tau}_i) - (\Delta\tau_i)\dot{m}(t-\hat{\tau}_i) \tag{5.2.8}$$

where the dot denotes the time derivative $\frac{dm}{dt}$. The truncation is justified since $\Delta\tau_i$ are assumed to have

small magnitudes. As a result the observed signal is given by

$$y(t) = \sum_{i=1}^{n} a_i\, m(t-\hat{\tau}_i) + \sum_{i=1}^{n} b_i \dot{m}(t-\hat{\tau}_i) + v(t) \qquad (5.2.9)$$

In (5.2.9), the variables $b_i$ are defined by

$$\underline{b}_i = (\underline{a}_i)(\Delta\tau_i) \qquad (5.2.10)$$

In vector-matrix notation one can write

$$\underline{y}(t) = [M\ \tilde{M}] \begin{bmatrix} a \\ b \end{bmatrix} + \underline{v}(t) \qquad (5.2.11)$$

where as before the following vectors and matrices are defined:

$$\underline{y}(t) = \begin{bmatrix} y(t_o) \\ y(t_1) \\ \vdots \\ y(t_{N-1}) \end{bmatrix} \qquad (5.2.12)$$

$$\underline{a}^T = [a_1\ a_2\ \ldots\ a_n] \qquad (5.2.13)$$

$$\underline{b}^T = [b_1\ b_2\ \ldots\ b_n] \qquad (5.2.14)$$

$$\underline{v}^T = [V(t_o)\ V(t_1)\ \ldots\ V(t_{N-1})] \qquad (5.2.15)$$

$$\underline{M} = \begin{bmatrix} m(t_o-\hat{\tau}_1) & m(t_o-\hat{\tau}_2) \ldots & m(t_o-\hat{\tau}_n) \\ m(t_1-\hat{\tau}_1) & m(t_1-\hat{\tau}_2) & m(t_1-\hat{\tau}_n) \\ \vdots & & \\ m(t_{N-1}-\hat{\tau}_1) & m(t_{N-1}-\hat{\tau}_2) & m(t_{N-1}-\hat{\tau}_n) \end{bmatrix} \quad (5.2.16)$$

$$\tilde{\underline{M}} = \begin{bmatrix} \dot{m}(t_o-\hat{\tau}_1) & \dot{m}(t_o-\hat{\tau}_2) \ldots & \dot{m}(t_o-\hat{\tau}_n) \\ \dot{m}(t_1-\hat{\tau}_1) & \dot{m}(t_1-\hat{\tau}_2) & \dot{m}(t_1-\hat{\tau}_n) \\ \vdots & & \\ \dot{m}(t_{N-1}-\hat{\tau}_1) & \dot{m}(t_{N-1}-\hat{\tau}_2) & \dot{m}(t_{N-1}-\hat{\tau}_n) \end{bmatrix} \quad (5.2.17)$$

Equation (5.2.11) can be expressed as

$$\underline{y} = \underline{H}\,\underline{p} + \underline{v} \quad (5.2.18)$$

where

$$\underline{H} = [\underline{M} \;\; \tilde{\underline{M}}] \quad (5.2.19)$$

The above discussion indicates that the estimation task using any of the proposed formulations (5.2.3), and (5.2.18) corresponds to finding an estimate $\hat{p}$ of the ran-

dom parameter vector p in some optimal sense. Note that (5.2.6) is structurally of the same form as (5.2.3) and (5.2.18). The additive noise vector v is assumed to have the following statistical properties

$$E\{\underline{v}\} = \underline{o} \tag{5.2.20}$$

$$E\{\underline{v}\ \underline{v}^T\} = \underline{V} \tag{5.2.21}$$

The parameter vector's statistical properties are assumed to be

$$E\{\underline{p}\} = \bar{\underline{p}} \tag{5.2.22}$$

$$E\{(\underline{p}-\bar{\underline{p}})(\underline{p}-\bar{\underline{p}})^T\} = \underline{P} \tag{5.2.23}$$

The noise and parameter vectors are assumed to be uncorrelated.

$$E\{\underline{p}\underline{v}^T\} = \underline{o} \tag{5.2.24}$$

The following section summarizes some useful results from the theory of linear parameter estimation.

## 5.3 Relationships for parameter estimation

A basic problem in the theory of linear parameter estimation is that of finding the optimal estimate $\hat{\underline{p}}$ of a random parameter vector $\underline{p}$ from observation $\underline{y}$ related to $\underline{p}$ according to Equation (5.2.3) or (5.2.18), repeated here as

$$\underline{y} = \underline{H}\,\underline{p} + \underline{v} \qquad (5.3.1)$$

Where $\underline{H}$ is a given matrix and $\underline{v}$ is a vector of additive random noise with statistical properties as given in (5.2.20) through (5.2.24)

The estimate vector $\hat{\underline{p}}$ is assumed to be of the unbiased linear form

$$\hat{\underline{p}} = \bar{\underline{p}} + \underline{K}[\underline{y} - \underline{H}\,\bar{\underline{p}}] \qquad (5.3.2)$$

$\underline{K}$ is a gain matrix to be evaluated according to the estimation criterion. As a result the covariance of the estimation error can be shown to reduce to

$$\hat{\underline{P}} = [\underline{I}-\underline{K}\underline{H}]\,\underline{P}\,[\underline{I}-\underline{K}\underline{H}]^T + \underline{K}\,\underline{V}\,\underline{K}^T \qquad (5.3.3)$$

Consider an estimation criterion which is a compound least squares error minimization, with weighting matrices $\underline{A}$ and $\underline{B}$, given by

$$J_{WLS} = (\underline{p}-\bar{\underline{p}})^T\,\underline{A}\,(\underline{p}-\bar{\underline{p}}) + (\underline{y}-\underline{H}\underline{p})^T\,\underline{B}\,(\underline{y}-\underline{H}\underline{p}) \qquad (5.3.4)$$

This criterion penalizes both the deviations from the a-priori estimate $\bar{p}$ and the observation error. $\underline{A}$ and $\underline{B}$ are positive definite matrices such that $(\underline{A} + \underline{H}^T \underline{B} \underline{H})$ is non-singular. In this case the gain matrix $\underline{K}$ is given by

$$\underline{K}_{WLS} = [\underline{A} + \underline{H}^T \underline{B} \underline{H}]^{-1} \underline{H}^T \underline{B} \qquad (5.3.5)$$

Another estimation criterion is that of minimum variance

$$J_{MV} = \text{trace } E\{(\underline{p}-\bar{\underline{p}})(\underline{p}-\bar{\underline{p}})^T\} \qquad (5.3.6)$$

The gain matrix $\underline{K}$ in this instance is given by

$$\underline{K}_{MV} = \underline{P} \underline{H}^T[\underline{H} \underline{P} \underline{H}^T + \underline{V}]^{-1} \qquad (5.3.7)$$

Comparison of (5.3.5) and (5.3.7) shows that the particular least square weighting

$$\underline{A} = k \underline{P}^{-1}$$

$$\underline{B} = k \underline{V}^{-1}$$

for an arbitrary k leads to the minimum variance condition [Vetter, 1971]. Using the matrix inversion lemma, the gain $\hat{\underline{K}}$ is found to be

$$\hat{\underline{K}} \triangleq \underline{K}_{MV} = [\underline{P}^{-1} + \underline{H}^T \underline{V}^{-1} \underline{H}]^{-1} \underline{H}^T \underline{V}^{-1} \qquad (5.3.8)$$

The error covariance matrix is given by

$$\hat{\underline{P}} = [\underline{P}^{-1} + \underline{H}^T \underline{V}^{-1} \underline{H}]^{-1} \qquad (5.3.9)$$

Combining (5.3.1) and (5.3.8), the minimum variance estimate of $\underline{p}$ is given by

$$\hat{\underline{p}} = \bar{\underline{p}} + (\underline{P}^{-1} + \underline{H}^T \underline{V}^{-1} \underline{H})^{-1} \underline{H}^T \underline{V}^{-1} (\underline{y} - \underline{H}\bar{\underline{p}}) \qquad (5.3.10)$$

In the absence of a-priori information one would set $\bar{\underline{p}} \to o$ and $\underline{P}^{-1} \to o$ (or $\underline{P} \to \infty$), which would reflect the complete prior ignorance for estimates of the parameters. Entries for the covariance matrix of the disturbance must be chosen to reflect the disturbance activity.

## 5.4 Sequential estimation of delay and amplitude parameters

In this section a procedure for estimating the amplitude and delay parameters is proposed. The procedure is sequential in the sense that the delay parameters $\tau_i$ are estimated first using the cross-correlation of the source signal $m(t)$ and the received signal $y(t)$. The second step is to obtain the amplitude parameters estimate $\hat{a}_i$ using the minimum variance estimator results. The cross-correlation calculated in the first step is used in the second step to simplify the computational procedure.

The use of the cross-correlation function provides a simple, yet powerful means for obtaining time delays of signals [Ferrel,G. Stremler, 1977]. Assume that a signal $f(t)$ is cross-correlated with a function $g(t)$ which is a delayed replica of $f(t)$, plus a random waveform

$$g(t) = f(t-t_o) + n(t) \qquad (5.4.1)$$

The cross-correlation function $\Phi_{fg}(\tau)$ will exhibit a large peak at the value of the time delay $t_o$. This is shown in Figure (5.4.1).

The application of the above principle to estimate the delay parameters in Equation (5.2.1) is straight forward. The cross-correlation $\Phi_{my}(\tau)$ is generated, then the extrema of $\Phi_{my}(\tau)$ are detected by a direct search. The extrema times are the required estimates of the delay parameters, $\hat{\tau}_i$.

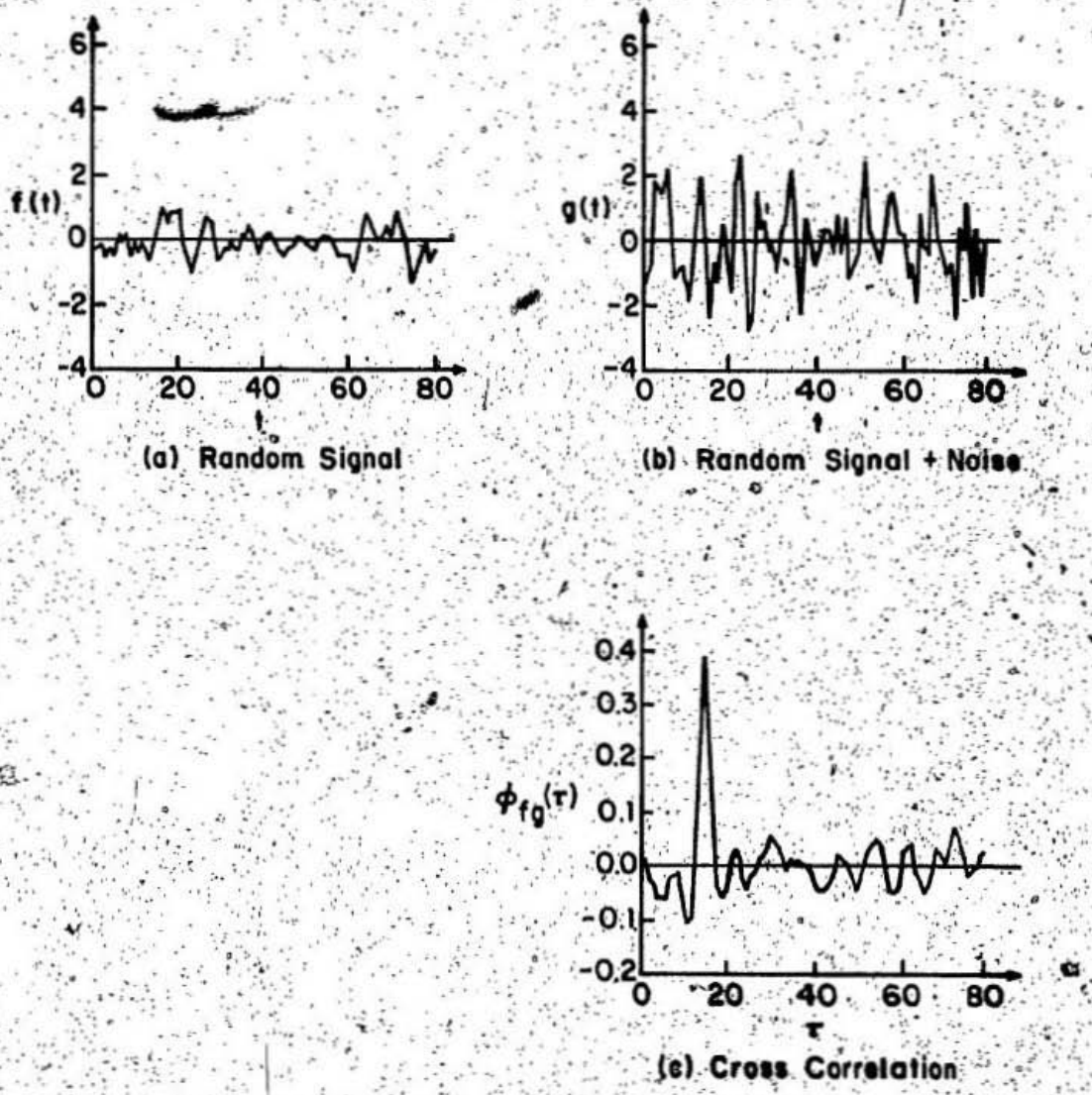


Figure 5.4.1 Cross-correlation of a signal and its delayed replica in noise.

In the practical application there is a need to establish a threshold on the magnitude of the extrema to be considered. A threshold might be chosen as a small margin on the magnitude of the extremum of the cross-correlation of signal with a return-pulse-free portion of y(t) but ex-

cluding the portion near $\tau = o$.

The second step involves the application of the minimum variance estimator results to the problem of estimating the amplitude parameter $a_i$ using the model of Equation (5.2.6). The minimum variance estimate $\hat{a}_i$ is, by Equation (5.3.10),

$$\hat{a}_i = \bar{a}_i + \frac{1}{(1/\sigma_{a_i}^2)+(m_i^T m_i/\sigma_v^2)} \left(\frac{m_i^T}{\sigma_v^2}\right)(y_i - m_i \bar{a}_i) \tag{5.4.2}$$

This reduces to

$$\hat{a}_i = \frac{(\sigma_v^2/\sigma_{a_i}^2)}{(\sigma_v^2/\sigma_{a_i}^2)+(m_i^T m_i)} \bar{a}_i + \frac{(m_i^T y_i)}{(\sigma_v^2/\sigma_{a_i}^2)+(m_i^T m_i)} \tag{5.4.3}$$

$\sigma_{a_i}^2$ and $\sigma_v^2$ are the variances of the parameter $a_i$ and the noise v respectively.

An interpretation of the above result in terms of correlation functions can be obtained by considering the following two terms

$$m_i^T y_i = \sum_{k=o}^{W-1} m(t_k - \hat{\tau}_i) y(t_k) \tag{5.4.4}$$

$$m_i^T m_i = \sum_{k=o}^{W-1} m(t_k - \hat{\tau}_i) m(t_k - \hat{\tau}_i) \tag{5.4.5}$$

The first expression can be interpreted as the cross-correlation of the signal m(t) with y(t) at correlation time $\tau = \hat{\tau}_i$. Thus using correlation notation

$$\phi_{my}(\hat{\tau}_i) = m_i^T y_i \qquad (5.4.6)$$

The second can be interpreted as the autocorrelation of m(t) at $\tau = o$. Thus

$$\phi_{mm}(o) = m_i^T m_i \qquad (5.4.7)$$

As a result the estimate $\hat{a}_i$ is given by

$$\hat{a}_i = \frac{(\sigma_v^2/\sigma_{a_i}^2)}{(\sigma_v^2/\sigma_{a_i}^2) + \phi_{mm}(o)} \bar{a}_i + \frac{\phi_{my}(\hat{\tau}_i)}{(\sigma_v^2/\sigma_{a_i}^2) + \phi_{mm}(o)} \qquad (5.4.8)$$

In the absence of a-priori information $\bar{a}_i$ and $\sigma_{a_i}^2$, $\sigma_{a_i}^2 \to \infty$, the above simplifies to

$$\hat{a}_i = \frac{\phi_{my}(\hat{\tau}_i)}{\phi_{mm}(o)} \qquad (5.4.9)$$

While the error is $\tilde{a}_i \triangleq a_i - \hat{a}_i$

With the associated (minimum variance) estimation error variance is

$$\hat{\sigma}^2_{\tilde{a}_i} = \frac{1}{(1/\sigma^2_{a_i})+(m_i^T m_i/\sigma_v^2)} = \frac{\sigma_v^2}{(\sigma^2_{v_i}/\sigma^2_{a_i}) + \Phi_{mm}(o)}$$

(5.4.10)

The simplification without a-priori information leaves us with

$$\hat{\sigma}^2_{\tilde{a}_i} = \frac{\sigma_v^2}{\Phi_{mm}(o)} \qquad (5.4.11)$$

The minimum variance estimate can be obtained from a matched-filter implementation. The matched-filter maximizes the signal-to-noise ratio at the filter output. The filter's impulse response is a reverse time replica of the known signal m(t), given by

$$h(t) = k\, m(\tau_d - t) \qquad (5.4.12)$$

The scaling parameter k is often chosen to provide a unity gain for the filter. The delay $\tau_d$ is inserted to make the filter realizable. The filter output is the convolution of h(t) with y(t) and can be shown to reduce to the cross-correlation of the signal m(t) with the received signal y(t).

The practical implementation of the above procedure and computations to detect a sequence of well separated

response pulses on a given observation record consists of the following steps

(1) Generate $\Phi_{mm}(\tau)$, the autocorrelation of the source signal (or determine $\Phi_{mm}(o) \triangleq \sigma_m^2$)

(2) Determine an estimate for $\sigma_v^2$ from a response-pulse-free portion of return signal, e.g. as $\sigma_v^2 = \Phi_{vv}(o)$.

(3) Generate the cross-correlation $\Phi_{my}(\tau)$. Detect by search the extrema of $\Phi_{my}(\tau)$ which occur at $\tau = \tau_i$ and use these correlation time values as estimates $\hat{\tau}_i$. At the respective $\hat{\tau}_i$ determine peak values $\Phi_{my}(\hat{\tau}_i)$, and use these together with $\sigma_v^2$, $\sigma_m^2$, $\sigma_{a_i}^2$, and $\bar{a}_i$ to evaluate estimate return parameter values $\hat{a}_i$ and associated error variance $\delta_{a_i}^2$.

A refinement on the above procedure can be made by considering the observation sequence $y(t)$ in the form given in Equation (5.2.2). Suppose that we have detected an amplitude parameter $\hat{a}_1$ at a delay $\hat{\tau}_1$ by the procedure given above based on Equation (5.2.5). We may then rearrange (5.2.2) to the form

$$\begin{bmatrix} y(t_o) - \hat{a}_1\, m(t_o-\tau_1) \\ y(t_1) - \hat{a}_1\, m(t_1-\hat{\tau}_1) \\ \vdots \\ y(t_N) - \hat{a}_1\, m(t_N-\hat{\tau}_1) \end{bmatrix} = \begin{bmatrix} m(t_o-\tau_2)\; m(t_o-\tau_3)\ldots \\ m(t_1-\tau_2)\; m(t_1-\tau_3)\ldots \\ \vdots \\ m(t_N-\tau_2)\; m(t_N-\tau_3)\ldots \end{bmatrix} \begin{bmatrix} a_2 \\ a_3 \\ \vdots \end{bmatrix} + \begin{bmatrix} v_1(t_o) \\ v_1(t_1) \\ \vdots \\ v_1(t_N) \end{bmatrix} \qquad (5.4.13)$$

Denoting this by

$$y^{(1)} = H^{(1)}\, p^{(1)} + v^{(1)} \qquad (5.4.14)$$

We may use (5.4.14) to repeat exactly the earlier procedure. Equations (5.4.8) and (5.4.10) are used to find estimates of $\hat{a}_i$ and $\hat{\sigma}^2_{a_i}$ with Equation (5.4.14) as the observation model. The cross-correlation $\phi_{my}(\tau_i)$ in this case is replaced by $\phi^{(1)}_{my}(\hat{\tau}_i)$. Using the defining relationships (5.4.13) and (5.4.14) this cross-correlation is given by

$$\phi^{(1)}_{my}(\tau) = \sum_{k=o}^{N-1} m(t_k+\tau)\left[y(t_k) - \hat{a}_1\, m(t_k-\hat{\tau}_1)\right] \qquad (5.4.15)$$

or

$$\phi^{(1)}_{my}(\tau) = \phi_{my}(\tau) - \hat{a}_1\, \phi_{mm}(\tau-\hat{\tau}_1) \qquad (5.4.16)$$

Equation (5.4.16) specifies that the new estimates $\hat{\tau}_i$, $\hat{a}_i$, with $\hat{\sigma}^2_{a_i}$ are to be obtained from the ith pulse of the

cross-correlation residual $\phi_{my}^{(1)}(\tau)$, i.e. from the original cross-correlation record $\phi_{my}(\tau)$ after subtracting $\hat{a}_i$ times the shifted autocorrelation $\phi_{mm}(\tau-\tau_i)$.

An obvious practical implementation is to find in sequence the dominating peaks in the respective residuals obtained by successive subtraction of $\hat{a}_i\phi_{mm}(\tau-\tau_i)$ from $\phi_{my}(\tau)$, and the $\hat{\tau}_k$, $\hat{a}_k$, and $\sigma^2_{a_k}$ associated therewith. In portions of the y(t) record where return pulse overlap occurs, one should expect to obtain estimates of the delay and return parameters $\tau_i$ and $a_i$ which are less accurate than those at well separated signals. The variance associated with $\hat{a}_i$ according to equation (5.4.8), is not affected by the presence of return pulse overlap. [El-Hawary and Vetter, 1977]. If greater accuracy than that attendant with the above procedure were required, the estimates $\hat{\tau}_i$, $\hat{a}_i$ with $\hat{\sigma}^2_{a_i}$ for a composite of return pulses might be used in a linearized form of the equation set for a window containing the composite signal.

Simulation results

The procedure outlined above was applied to a simulated return signal y(t) shown in Figure 5.4.2 detail (C). The signal is composed of a set of seven replica pulses of an actual broad-band signal source as shown in detail (A). The noise free signal is shown in detail (B). Table (5.4.1) details the actual amplitude and delay parameters for the simulated signal. The delays given in the table are delay indices for a record of 256 points which contains all positive signals.

The autocorrelations of signal $\phi_{mm}(\tau)$ and noise $\phi_{vv}(\tau)$ are shown in detail (D) while the cross-correlation function $\phi_{mv}(\tau)$ of source signal and noise for purposes of choosing a threshold for the detection scheme is shown in detail (E). The cross-correlation of source signal and return signal $\phi_{my}(\tau)$ is shown in detail (F). It is noted that four major peaks occur in this function corresponding to four delay parameters. Detail (G) shows the cross-correlation residual from $\phi_{my}(\tau)$ after subtraction of the four major peaks. This residual shows three minor peaks of value higher than the chosen threshold. The result of subtracting these minor peaks is the residual cross-correlation shown in detail (H). Finally, detail (I) shows the return pulse sequence estimate, displayed together with actual pulse leight used in simulation (horizontal marker

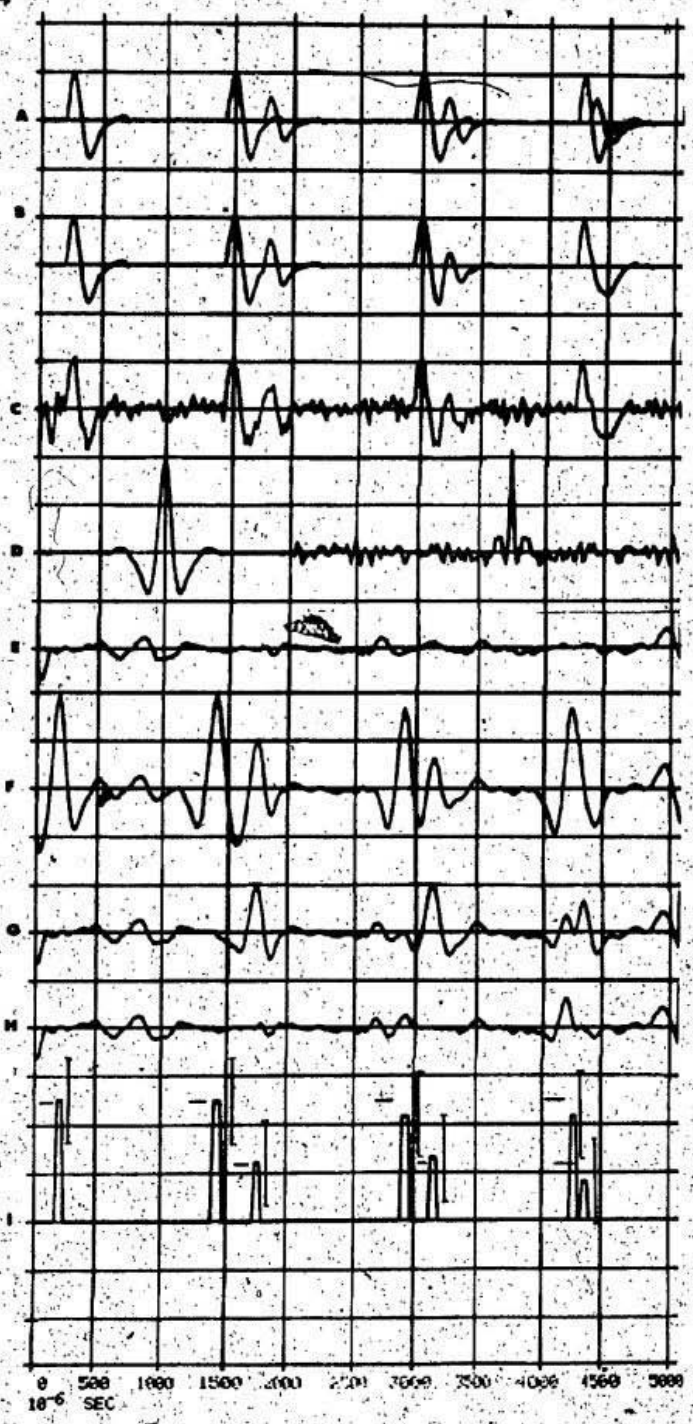


Figure 5.4.2 Simulation Record #1

to the left of pulses) and the one-sigma range associated with the estimation variance (vertical markers to the right of pulses). Table (5.4.2) summarizes the estimated parameters.

Figure 5:4.3 details the results for a second simulated record which contains positive and negative signals, with tables (5.4.3) and (5.4.4) giving the pertinent parameter values. It is evident from the above results that the estimation procedure is remarkably effective on this simulated signal, even though the simulated return pulses are closely spaced and generate in part apparently single pulse composites.

Table (5.4.1)

Actual amplitude and delay parameters for simulated signal.
(Record #1)

| i | 1 | 2 | 3 | 4 | 5 | 6 | 7 |
|---|---|---|---|---|---|---|---|
| $a_i$ | 1.0 | 1.0 | 1.0 | 1.0 | 0.5 | 0.5 | 0.5 |
| $\tau_i$ | 11 | 72 | 147 | 212 | 87 | 157 | 217 |

Table (5.4.2)

Estimated amplitude and delay parameters for simulated signal.
(Record #1)

| i | 1 | 2 | 3 | 4 | 5 | 6 | 7 |
|---|---|---|---|---|---|---|---|
| $\hat{a}_i$ | 1.011 | 1.002 | 0.863 | 0.862 | 0.488 | 0.522 | 0.328 |
| $\hat{\tau}_i$ | 10 | 71 | 146 | 212 | 86 | 156 | 217 |

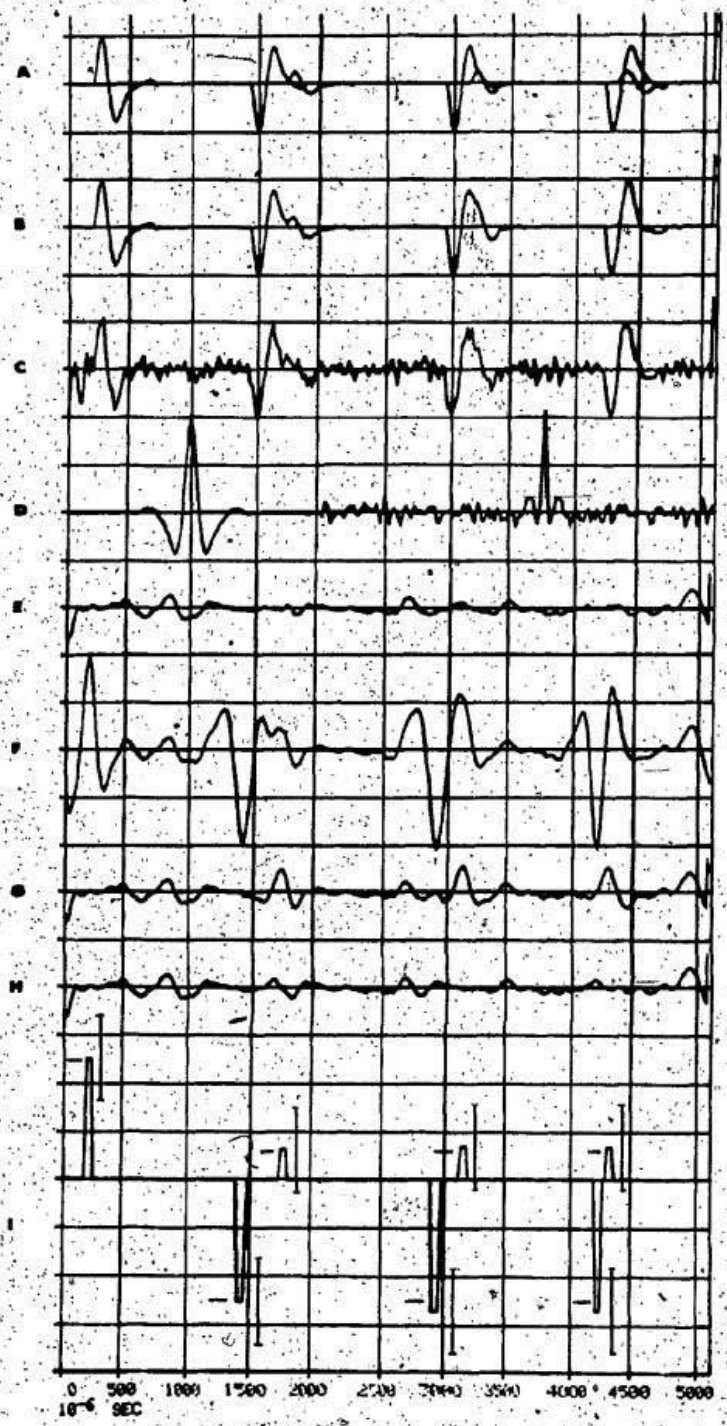


Figure 5.4.3 Simulation Record #2

Table (5.4.3)

Actual amplitude and delay parameters for simulated signal.
(Record #2)

| i | 1 | 2 | 3 | 4 | 5 | 6 | 7 |
|---|---|---|---|---|---|---|---|
| $a_i$ | 1.0 | -1.0 | -1.0 | -1.0 | 0.25 | 0.25 | 0.25 |
| $\tau_i$ | 11 | 72 | 147 | 212 | 87 | 157 | 217 |

Table (5.4.4)

Estimated amplitude and delay parameters for simulated signal.
(Record #2)

| i | 1 | 2 | 3 | 4 | 5 | 6 | 7 |
|---|---|---|---|---|---|---|---|
| $\hat{a}_i$ | 1.010 | -1.001 | -1.079 | -1.067 | 0.2570 | 0.2855 | 0.2751 |
| $\hat{\tau}_i$ | 10 | 71 | 146 | 211 | 87 | 156 | 216 |

Estimates from field data

As reported in simulation results the procedure was remarkably effective for extracting $\hat{\tau}_i$ and $\hat{a}_i$ parameters from simulated return signals in a noisy base signal. Even with replica pulse overlap, a residual adaptation of the above procedure gave quite reasonable results as shown in Figures 5.4.2 and 5.4.3.

The preceding procedure, when applied to some of the real reflection data, may not give results that are immediately useful. Figure 5.4.4 consists of data and processed data for a sequence of 10 successive pings, at 0.5 second intervals (corresponding to about one meter spatial separation between echo records at the ship speed which prevailed). In the set of records one has: a) the raw unprocessed hydrophone signals, b) the signals after band-pass filtering between 2 and 13 KHz to remove the low and high frequency noise effects, c) the filtered signal cross-correlated with the source signal from a calibration test, d) a reflection sequence from the cross-correlation record by peak detection, for an ad hoc threshold level.

The major problems are readily evident, namely:
(i) reflection pulse levels which are barely above and occasionally completely within, the noise level.
(ii) signal distortion by the medium, due to effects of frequency spreading and scattering and reflections from

bands or transitions, rather than the ideal boundaries (discernible from the broadening and overlap of cross-correlation pulses). (iii) detection of noise reflection pulses, and omission of detection of pulses due to layer presence. [El-Hawary and Vetter, 1979 and 1980]. The results suggest that one apply a record to record filtering or smoothing procedure, to eliminate all pulses which do not occur consistently from record to record, and to substitute pulses where they should occur on the basis of consistency in nearby signal records. Work along these lines, using transition models which are consistent with expected variations in layer positions (sea-floor slopes) and layer reflection effects (spatial consistency in layer properties), and using information of the type as in Figure (5.4.4)(D) as quasiobservations with estimates of attendant uncertainty treated as noise can be carried out using the procedures discussed in chapter 4.

To ease the task of processing, layer positions are first estimated from records of return signal squared and its correlation with the square of the source pulse. Either of these have superior signal to noise ratio information for thresholding purposes. The determination of reflection sequence pulse amplitudes $a_i$, will then be confined to narrow pulse occurrence windows so obtained.

Figure 5.4.5 shows, for return records as in Figure 5.4.4, a) the filtered signal squared, b) the squared signal as in a) on expanded amplitude scale and with bottom return and sea surface reflection suppressed, c) the cross-correlation of this signal squared with the square of the source signature. Also shown in Figure 5.4.5.D is the EPC chart from the commercial HUNTEC DTS system. This signal derives from the source signal after bandpass filtering, negative part clipping, and conversion of signal amplitude to a grey-scale density in the temperature sensitive display chart.

Figure 5.4.4

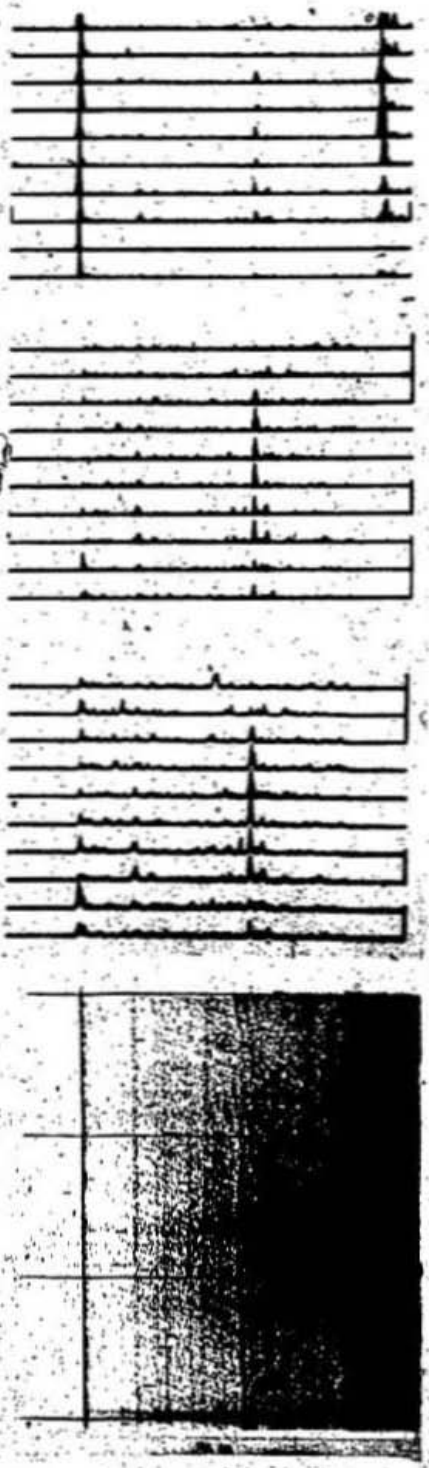

Figure 5.4.5

## 5.5 Simultaneous estimation of delay and amplitude parameters using the linearized model

In Section (5.2) a reformulation of the model Equation (5.2.1) was given leading to Equation (5.2.18). The procedure employs the truncated Taylor series given by Equation (5.2.8). It is assumed that a rough estimate of the delay parameters $\tau_i$ is available and that a refinement $\Delta\tau_i$ as defined by Equation (5.2.7) is to be estimated together with the amplitudes $a_i$. The parameter vector $\underline{p}$ is of the form

$$\underline{p}^T = [\underline{a}^T \; \underline{b}^T] \qquad (5.5.1)$$

The vectors $\underline{a}$ and $\underline{b}$ are defined by Equations (5.2.13) and (5.2.14) respectively. The model equation is given by Equation (5.2.18) which is repeated here for convenience

$$\underline{y} = \underline{H}\,\underline{p} + \underline{V}$$

The linearized model given above is in the desired form for estimation purposes. According to the results summarized in Section (5.3) and in the absence of a-priori information, the minimum variance estimates are given by Equation (5.3.2), with the gain $\hat{\underline{K}}$ given by Equation (5.3.8) as:

$$\hat{\underline{p}} = \hat{\underline{K}}\,\underline{y} \qquad (5.5.2)$$

$$\hat{\underline{K}} = [\underline{H}^T \underline{V}^{-1} \underline{H}]^{-1} \underline{H}^T \underline{V}^{-1} \qquad (5.5.3)$$

Entries for the covariance matrix of the noise vector V must be chosen to reflect the disturbance activity. For the special case

$$\underline{V} = \sigma_v^2 \underline{I} \quad , \qquad (5.5.4)$$

The optimal gain $\hat{\underline{K}}$ reduces to

$$\hat{\underline{K}} = [\underline{H}^T \underline{H}]^{-1} \underline{H}^T \qquad (5.5.5)$$

Initial estimates of the delay parameters are obtained using the procedure described in Section (5.4). As a result the elements of the matrix $\underline{H}$ as defined by Equations (5.2.16), (5.2.17) and (5.2.19) can be calculated. The gain matrix $\hat{\underline{K}}$ is therefore obtained using Equation (5.5.2), and hence the parameter estimate vector. The procedure therefore provides a measure of the possible improvement in the evaluation of the parameters over the sequential method of Section (5.4). If the initial estimates of the delay parameters are close enough to their actual value then one would expect the refinement $\Delta\tau_i$ to be of relatively small values justifying the linearization process. If on the other hand $\Delta\tau_i$ obtained using this process is of relatively large value then the results are not reliable. In this case an extension of the procedure to include second order terms in the Taylor expansion of Equation (5.2.8) may prove useful. This however will in-

volve a matrix $\underline{H}$ of a size 1.5 times the size of the matrix $\underline{H}$ associated with Equation (5.2.11)

Simulation Results

The procedure outlined above was applied first to a simulated return signal y(t) shown in Figure 5.5.1.B. The signal is made of four components of a set of replica pulses as shown in step (A). The simulated signal with the added noise component is shown in step (B). The cross-correlation $\phi_{my}(\tau)$ is shown in step (C). The return pulse sequence estimate using the procedure of Section (5.4) is shown in step (D). Results of the linearization procedure are shown in step (E).

Table (5.5.1) summarizes the actual and estimated parameter values before and after applying the linearization procedure. It is apparent from the results that the linearization process provides estimates that are much closer to the actual values than those obtained by the procedure of Section (5.5.4)

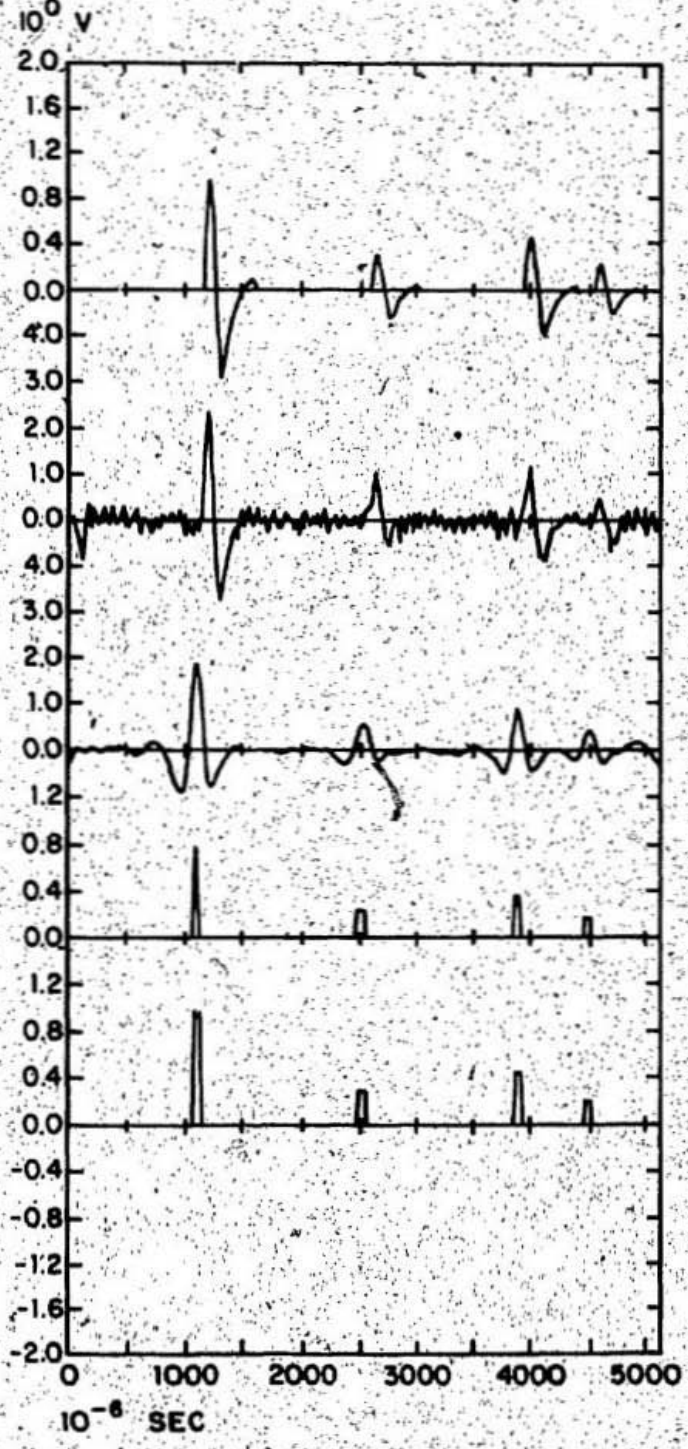
$10^0$ V
2.0
1.6
1.2
0.8
0.4
0.0
(A)
4.0
3.0
2.0
1.0
0.0
(B)
4.0
3.0
2.0
1.0
0.0
(C)
1.2
0.8
0.4
0.0
(D)
1.2
0.8
0.4
0.0
(E)
-0.4
-0.8
-1.2
-1.6
-2.0
0
1000
2000
3000
4000
5000
$10^{-6}$ SEC

Figure 5.5.1

Table 5. 5. 1

The actual and estimated parameter values before and after applying the linearization procedure for non-overlapping signals.

| Spike Nos. | Noise free signal | | Actual Signal | | Sequential estimates | | Linearization estimates | |
|---|---|---|---|---|---|---|---|---|
| | $\tau_i$ | $a_i$ | $\tau_i$ | $a_i$ | $\hat{\tau}_i$ | $\hat{a}_i$ | $\hat{\tau}_L$ | $\hat{a}_L$ |
| 1 | 59 | 0.979 | 59 | 0.954 | 54 | 0.783 | 57 | 0.9891 |
| 2 | 131 | 0.327 | 131 | 0.432 | 126 | 0.246 | 129 | 0.305641 |
| 3 | 199 | 0.490 | 200 | 0.489 | 194 | 0.378 | 197 | 0.471338 |
| 4 | 229 | 0.245 | 229 | 0.201 | 224 | 0.181 | 226 | 0.221722 |

In practice the return signal contains overlapping replicas of the source signal. One reason for the overlap is due to the presence of thin layers. In this case considering primaries only, the signal reflected from (i+1)th. interface arrives while that reflected from the ith interface is still being received. A second simulated record which exhibits the overlap phenomenon was used to evaluate the procedure. Figure 5.5.2, detail (A) shows the component replicas which are combined to produce the noise free return signal shown in detail (B). Detail (D) shows the simulated record with the added noise shown in detail (C). The cross-correlation $\phi_{my}(\tau)$ is shown in detail (E). The return pulse sequence estimate using the procedure of section (5.4) is shown in detail (F). Results of the linearization procedure are shown in detail (G).

Table(5.5.2)summarizes the actual and estimated parameter values for this case before and after applying the linearization procedure. It is again apparent from the results that the linearization process of Section (5.5) provides estimates that are much closer to the actual values than those obtained by the procedure of Section (5.4).

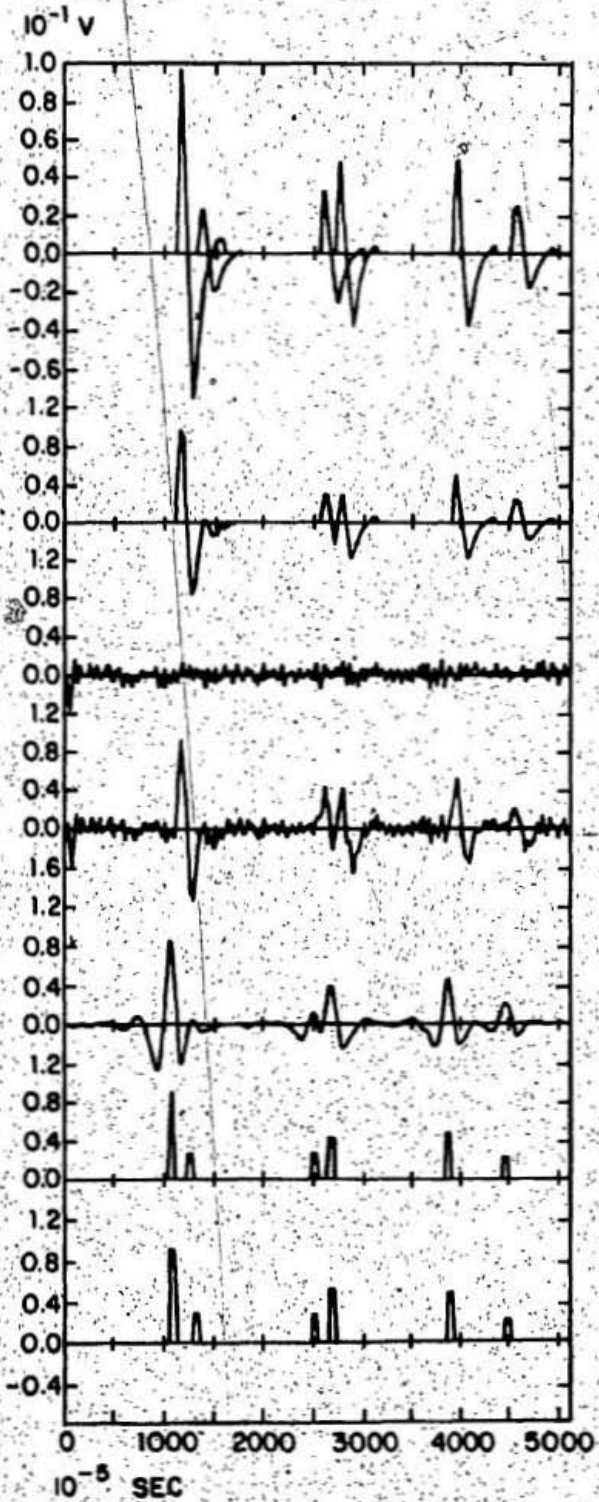
$10^{-1}$ V
1.0
0.8
0.6
0.4
0.2
0.0
-0.2
-0.4
-0.6
1.2
0.8
0.4
0.0
1.2
0.8
0.4
0.0
1.2
0.8
0.4
0.0
1.6
1.2
0.8
0.4
0.0
1.2
0.8
0.4
0.0
1.2
0.8
0.4
0.0
-0.4
(A)
(B)
(C)
(D)
(E)
(F)
(G)
0
1000
2000
3000
4000
5000
$10^{-5}$ SEC

Figure 5.5.2

Table 5.5.2

The actual and estimated parameter values before and after applying the linearization procedure for signals with overlap.

| Spike number | Noise free signal | | Actual signal | | Sequential estimates | | Linearization estimates | |
|---|---|---|---|---|---|---|---|---|
| | $\tau_i$ | $a_i$ | $\tau_i$ | $a_i$ | $\hat{\tau}_i$ | $\hat{a}_i$ | $\hat{\tau}_L$ | $\hat{a}_L$ |
| 1 | 59 | 0.979 | 59 | 0.954 | 54 | 0.783 | 56 | 0.989 |
| 2 | 70 | 0.047 | 70 | 0.041 | 64 | 0.0278 | 67 | 0.0295 |
| 3 | 131 | 0.327 | 131 | 0.432 | 126 | 0.246 | 128 | 0.305 |
| 4 | 139 | 0.316 | 140 | 0.424 | 135 | 0.434 | 136 | 0.414 |
| 5 | 199 | 0.490 | 200 | 0.489 | 194 | 0.378 | 197 | 0.472 |
| 6 | 229 | 0.245 | 229 | 0.201 | 224 | 0.181 | 226 | 0.222 |

Results from field record

Figure 5.5.3 shows the second half of a single field record. Figure 5.5.4 shows the results of estimating the locations $\hat{\tau}_i$ and magnitude of wavelets $\hat{a}_i$ using the procedure detailed in Section (5.4).

Table (5.5.3) gives a comparison of the estimated amplitude and delay parameters using the procedure described in this section (subscript L) and those estimated using the procedure of the previous section. It is observed that the delay estimates are fairly close, on the other hand the amplitude estimates are different by up to 30%.

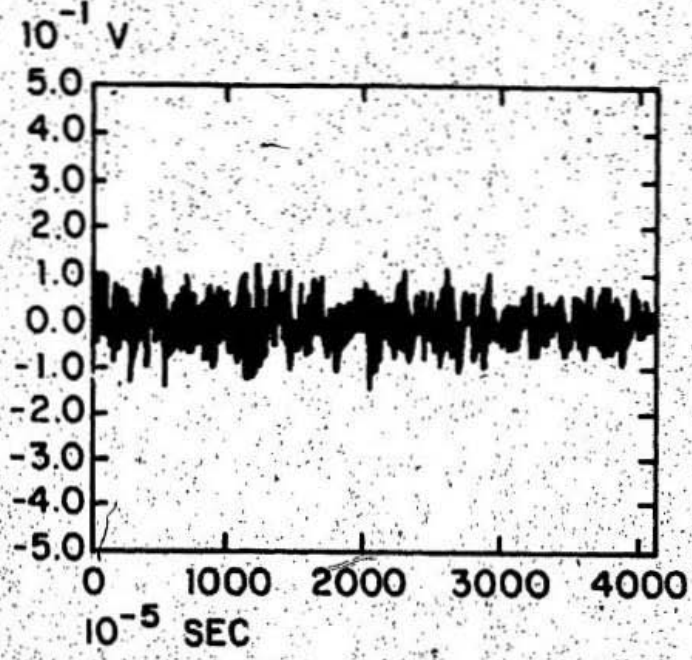


Figure 5.5.3

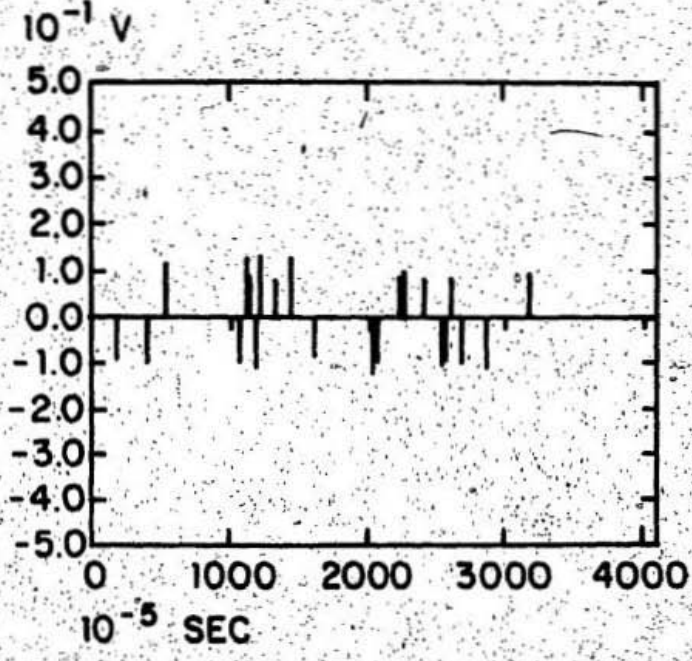


Figure 5.5.4

Table (5.5.3)

Results of estimation algorithm for improved delays and amplitude values for the record shows in Figure 5.5.2.

| Spike index | $\hat{a} \times 10^{-4}$ | $\hat{a}_L \times 10^{-4}$ | $\Delta\hat{a}(10^{-4}$ volts) $=\hat{a}-\hat{a}_L$ | $\hat{\tau}$ | $\hat{\tau}_L$ | $\Delta\hat{\tau}(10^{-6}$ sec) $=\hat{\tau}-\hat{\tau}_L$ |
|---|---|---|---|---|---|---|
| 1 | -906 | -627 | -279 | 86 | 84 | 2 |
| 2 | -980 | -801 | -179 | 203 | 202 | 1 |
| 3 | +1181 | 990 | 191 | 260 | 259 | 1 |
| 4 | -957 | -851 | -106 | 533 | 533 | 0 |
| 5 | +1294 | 1182 | 112 | 556 | 555 | 1 |
| 6 | +918 | 761 | 157 | 570 | 569 | 1 |
| 7 | -1111 | -1173 | 62 | 593 | 593 | 0 |
| 8 | +1363 | 968 | 395 | 604 | 603 | 1 |
| 9 | +866 | 772 | 94 | 663 | 662 | 1 |
| 10 | +1271 | 1152 | 119 | 715 | 715 | 0 |
| 11 | -838 | -699 | -139 | 799 | 798 | 1 |
| 12 | -1239 | -1022 | -217 | 1012 | 1011 | 1 |
| 13 | -991 | -812 | -179 | 1033 | 1032 | 1 |
| 14 | +833 | 696 | 137 | 1114 | 1113 | 1 |
| 15 | +993 | 751 | 242 | 1131 | 1130 | 1 |
| 16 | +845 | 666 | 179 | 1201 | 1200 | 1 |
| 17 | -1008 | -842 | -166 | 1267 | 1266 | 1 |
| 18 | -946 | -823 | -123 | 1282 | 1281 | 1 |
| 19 | +851 | 790 | 061 | 1302 | 1302 | 0 |
| 20 | -962 | -930 | -32 | 1341 | 1341 | 0 |
| 21 | -1109 | -1051 | -58 | 1427 | 1427 | 0 |
| 22 | +908 | 798 | 110 | 1587 | 1586 | 1 |

## 5.6 Delay estimation using balance property of source signal derivative

A consequence of the assumption of a lossless earth model is that the medium does not alter the waveform of the propagating and reflected pulses. The resulting distortionless received waveforms can thus be assumed to be scaled and shifted replicas of the source signal. The proposed procedure utilizes a property of the signal m(t) available from the broad-band boomer displacement type source. The derivative of the source signal m'(t) has been observed to display an approximate positive and negative amplitude balance over the significant signal duration [El-Hawary and Vetter, 1980 and 1981]. The signal m(t) and its derivative m'(t) are shown in Figure 5.6.1.

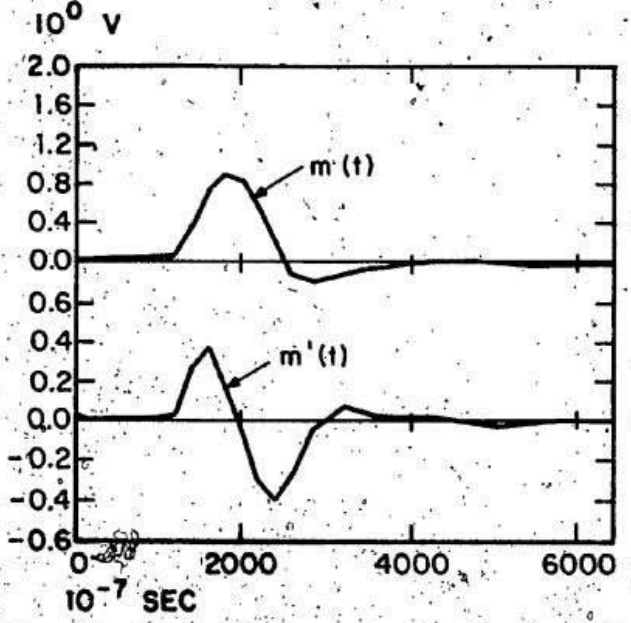


Figure 5.6.1
The signal m(t) and its derivative m'(t)

Based on this property, a procedure for signal conditioning of the response wavelets has been developed. This is detailed as follows:

A) To identify positive reflection events the following sequence of operations is performed:

1. The sign of the negative part of the derivative signal is changed.
2. The result of (1) is shifted in time to overlap the corresponding positive part giving $m'_s(t)$. This is shown in Figure 5.6.2, step (b).
3. The signal $m'(t)$ is multiplied by $m'_s(t)$ with the result shown in step (c).

The result is a spike for each positive reflection event. Figure 5.6.3 shows the application of the procedure to a negative reflection event signal which will vanish under the same operation.

B) To identify negative reflection events the reverse procedure is applied:

1. The sign of the positive part of the derivative signal is changed.
2. The result of (1) is shifted in time to overlap the corresponding negative part as shown in Figure 5.6.4, step (b).
3. The signal $m'(t)$ is multiplied by the result of (2) with the result shown in step (c).

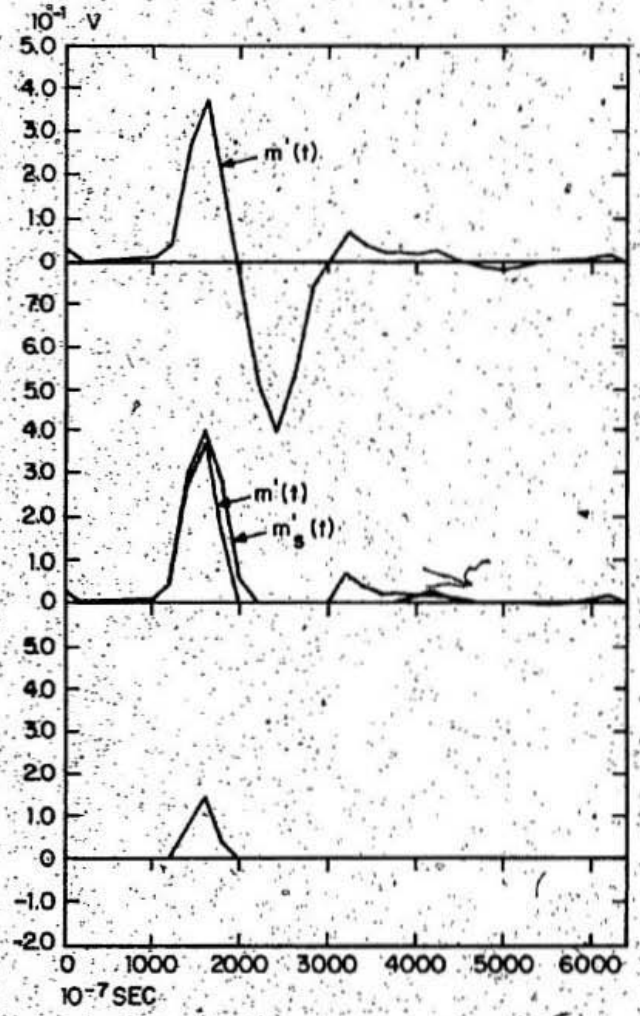


Figure 5.6.2
The steps to identify positive reflection

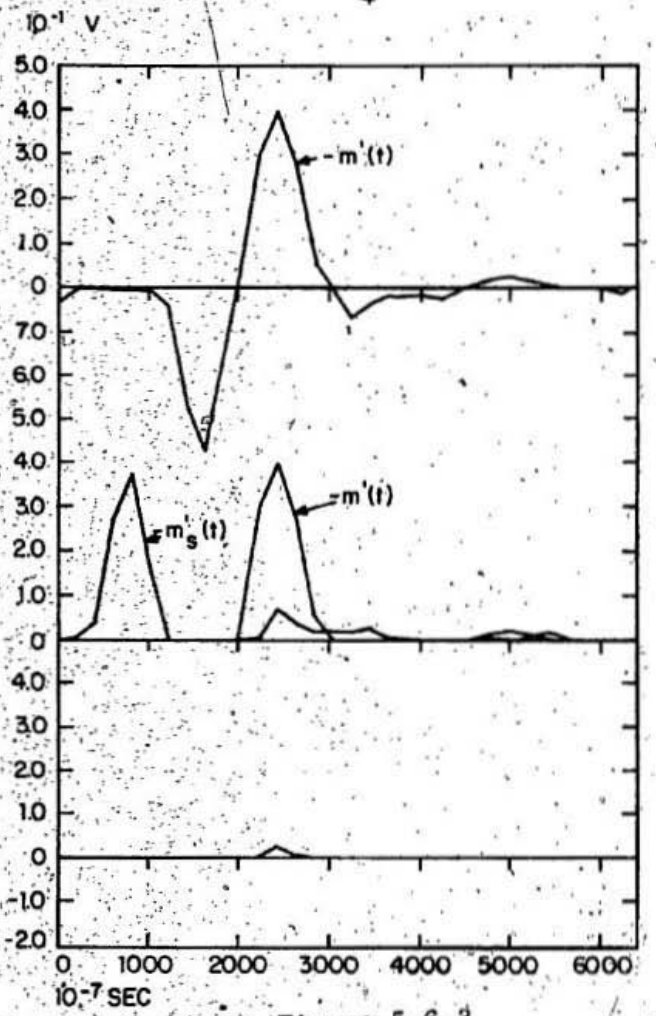


Figure 5.6.3
Same steps in Fig. 5.6.2 applied to the negative reflection

The result is a spike for each negative reflection event. For a positive reflection event the result of this procedure is a vanishing event as shown in Figure 5.6.5. A block diagram representing the procedure is shown in Figure 5.6.6.

The source signal provides information for the optimum amount of shift and the results of positive and negative reflection event signals should be consistent from record to record. On the other hand, since noise is random, the result of shifting and multiplication on random signal sections should be small and inconsistent from record to record.

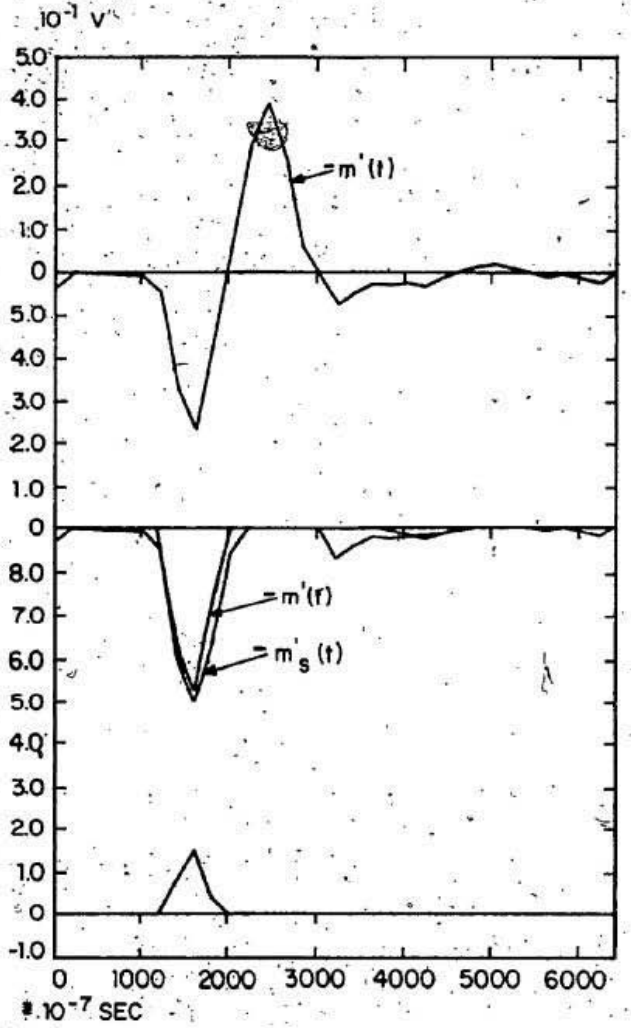


Figure 5.6.4

Steps to identify negative reflection

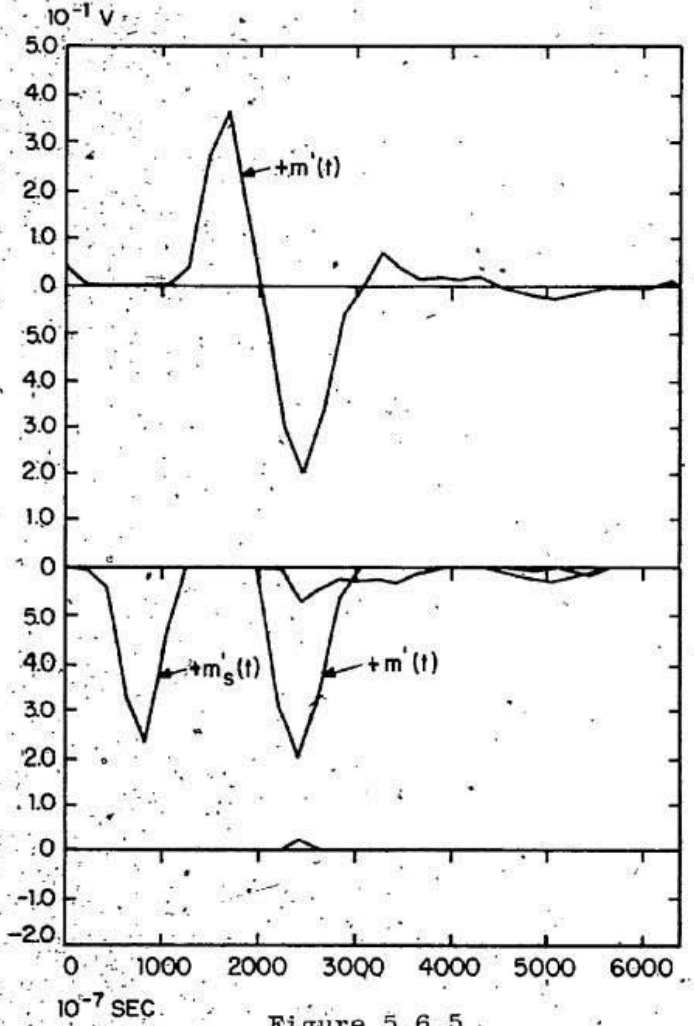


Figure 5.6.5

Same steps as in Fig. 5.6.4 applied on the positive reflection

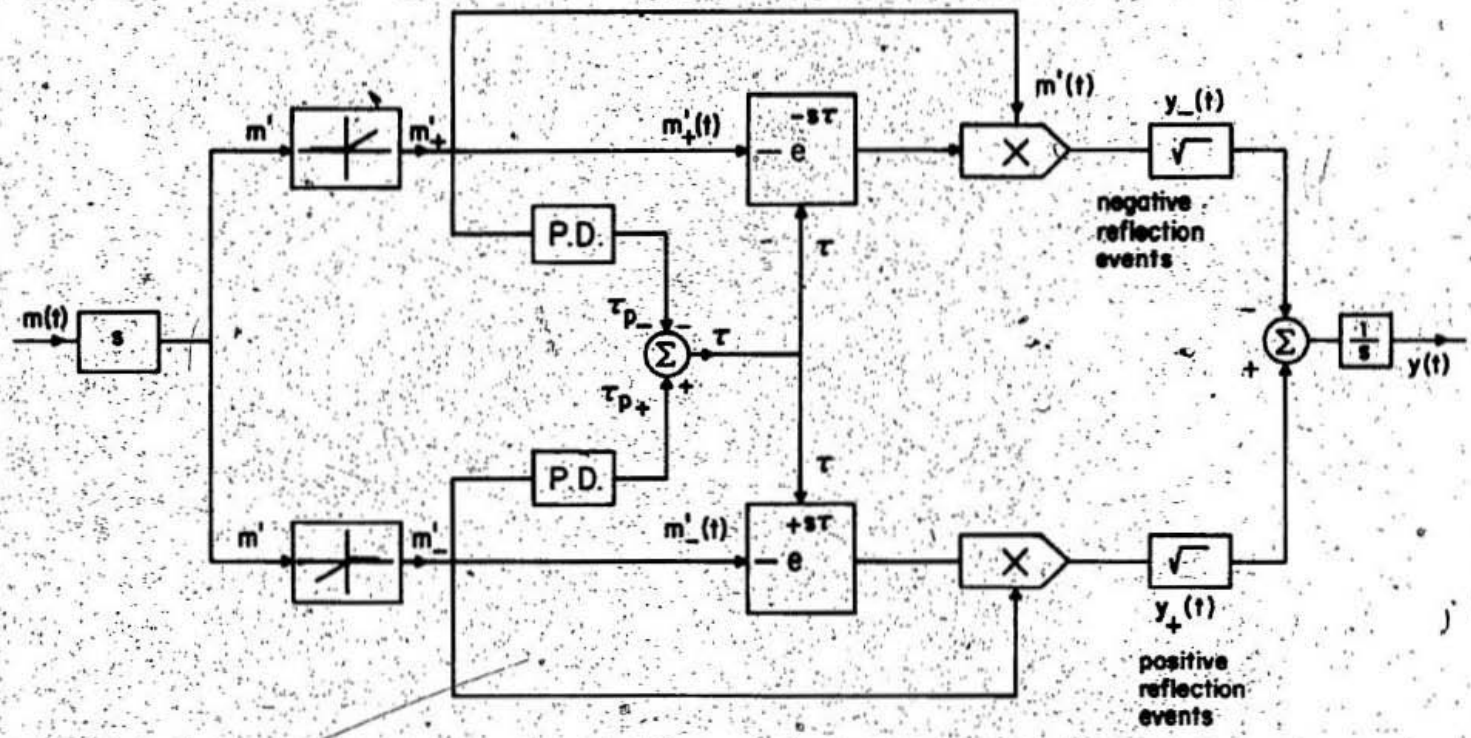


Figure 5.6.6 A block diagram representing the procedure in Section (5.6)

Results from field data

A sequence of 9 successive records obtained at 0.5 second intervals (corresponding to about one meter spatial separation) is shown in Figure 5.6.7. Part (a) of the figure shows the data after band-pass filtering from 1.5 KHz to 12.5 KHz, while part (b) shows the derivatives of the records. It is noted here that as the background noise decreases with increasing frequency, differentiation is a simple approximation to pre-whitening filtering resulting in an increase in the useful high frequency band width.

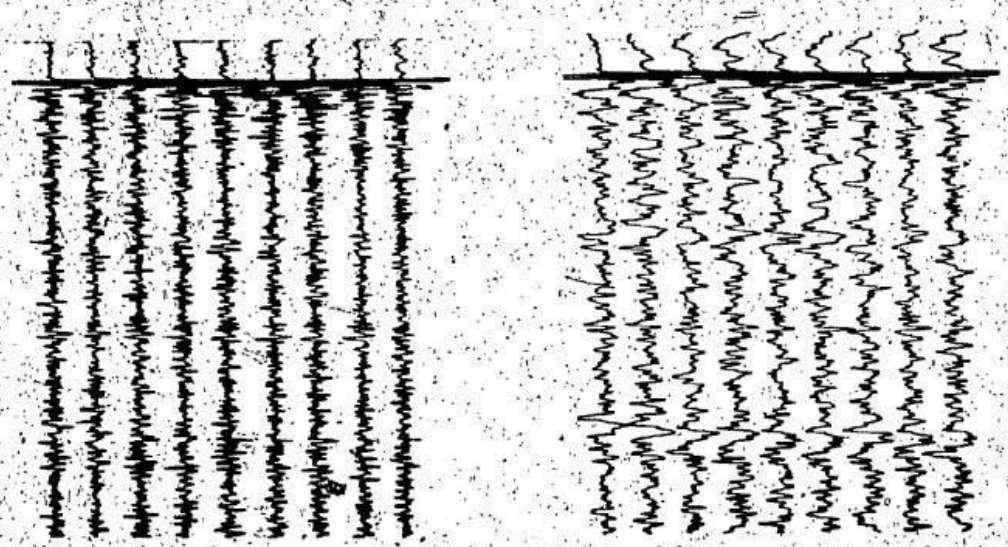

Figure 5.6.7
A sequence of individual records with its derivatives

The display in Figure 5.6.8 is the output of the ANAC digital grey scale graphic recorder on an original scale of 16.6 mm/m. Data for a region of 500 meters along the track is shown in Figure 5.6.8. Display (a) shows the positive part of the raw-pre-processed hydrophone signals, while (b) shows the corresponding negative part. In parts (c) and (d) the negative and positive parts of the band-pass filtered, differentiated signals are shown respectively.

Figure 5.6.9 shows the results of the positive reflection event signals after applying the enhancement procedure for: (a) the nine records from the area of Figure 5.6.8, and (b) to the total area of Figure 5.6.8. Figure 5.6.10 shows the corresponding results for negative reflection event signals. Both figures show better consistency than the original response records, in that the estimated delay times for each event are better aligned from record to record. This supports the proposed approach as a possibly useful complement to response signal analysis.

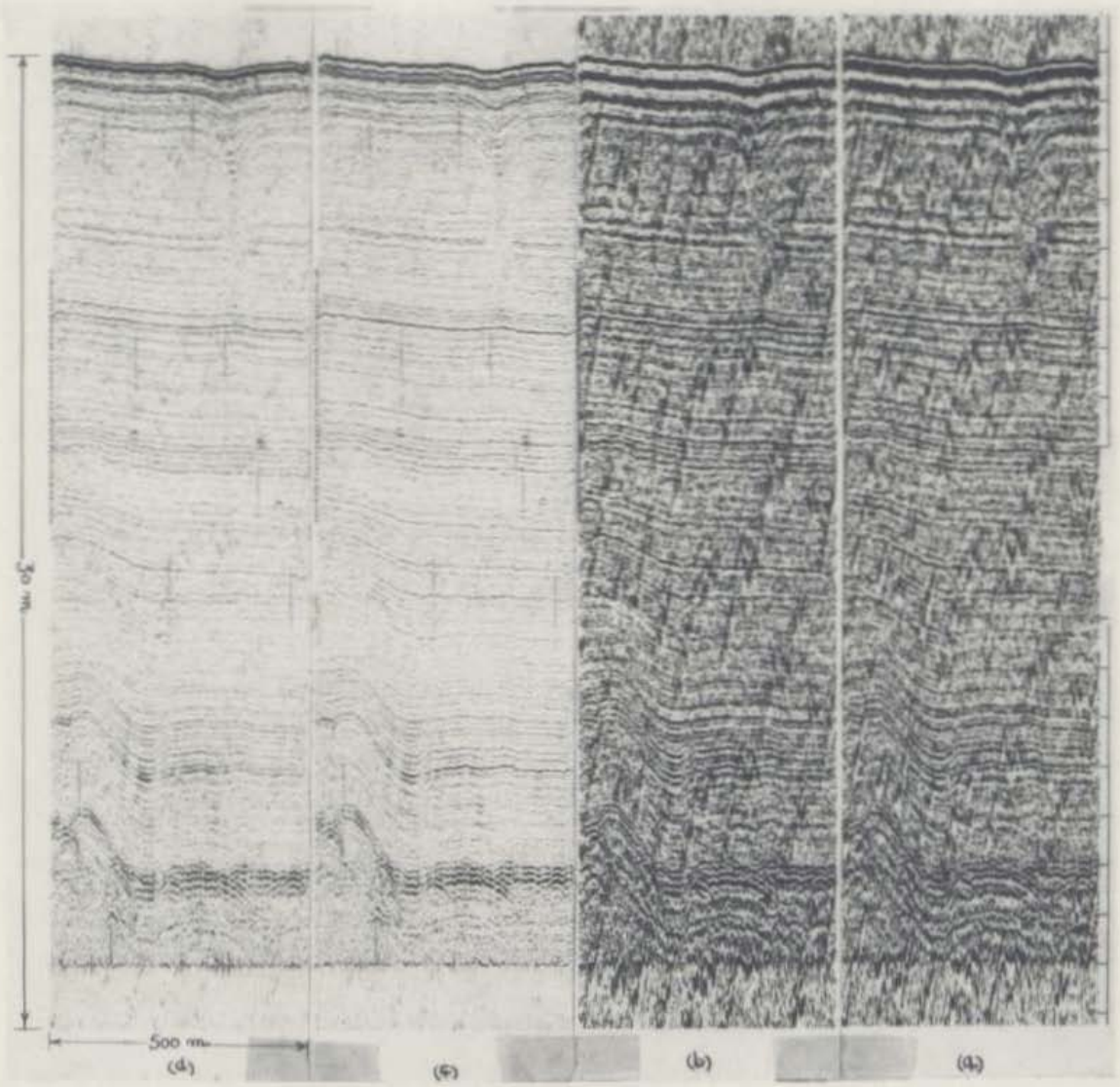


Figure 5.6.8

A graphic grey scale display for an area of 500 m. along the track and depth of 30 m. with the pre-processed positive and negative part also after processed

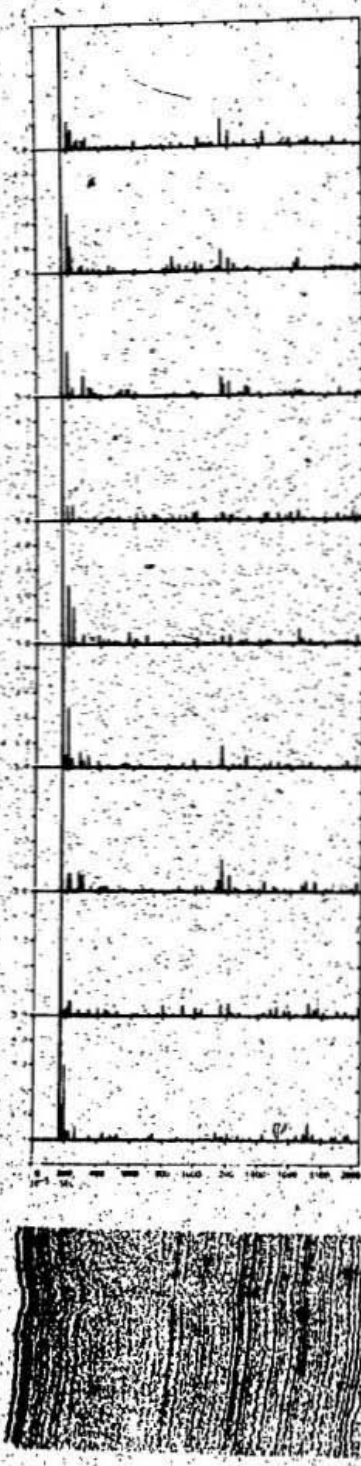

Figure 5.6.9

The results of the positive reflection event signals

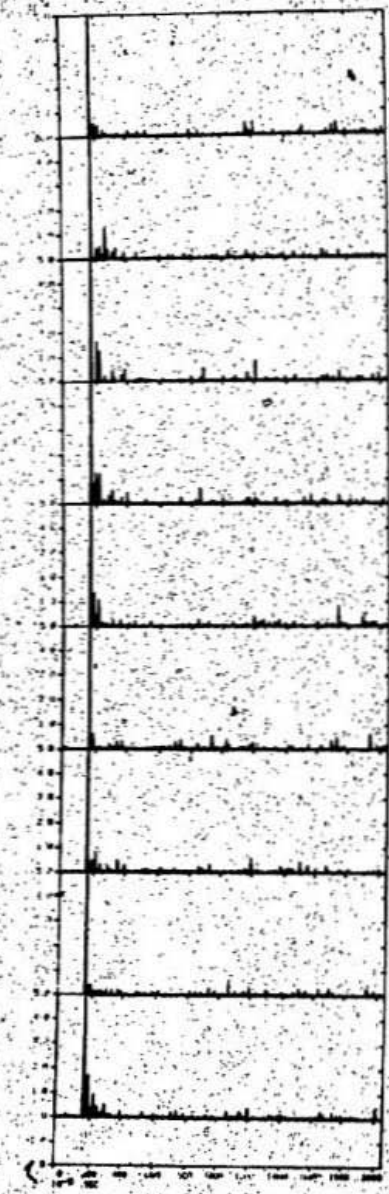

Figure 5.6.10
The results of the negative reflection event signals

# CHAPTER 6

## CONCLUDING REMARKS

### 6.1 Retrospective Overview

In this thesis the application of modeling, and signal processing for the identification of the ocean subsurface layered media have been considered. The real data used in this investigation pertain to an area from the outer Placentia Bay region on the Newfoundland Grand Banks.

In Chapter 2 a review of concepts from underwater acoustics has been given. In Chapter 3 a survey of a number of models of wave propagation in lossless layered media has been detailed. The models are classified as either non-parametric (one dimensional) or parametric (two dimensional). The models are used essentially to develop reflection seismograms. In Section (3.10) a layer indexed model of the non-parametric type has been presented. The model includes all higher order reflection effects, which is a refinement over other models reviewed in this category. The model was developed within the framework of this enquiry.

A problem encountered with data collected in marine seismic experiments is the presence of a component due to the dynamics of the towed body. The extraction of this component is referred to as source heave compensation.

Chapter 4 has been addressed to two aspects of this problem. The first involves the modeling of the source heave process. A state space model has been obtained on the basis of trial data. The second aspect is the application of Kalman filter results to obtain refined estimates of the heave component in the data.

A number of procedures to assist in extracting amplitude and delay parameters associated with the return signal have been presented in Chapter 5. These procedures constitute one main contribution of this thesis. The first procedure presented in Section (5.4) is basically a consolidation of well known results from estimation and communication theory to suit the present task. This is followed by a procedure for simultaneous estimation of the parameters of interest based on a linearization of the process model. The third procedure described in this chapter involves the utilization of the signal waveform properties to enhance the reflection events. All the procedures described have been applied to the non-parametric representation of the layered earth model. The procedures have been tested using simulated data first and then applied to real data. All operations have been programed and performed on the Hewlett-Packard Fourier Analyzer 5451 Signal Processing System of the Faculty of Engineering and Applied Science.

## 6.2 Summary of Contributions

The main contributions of this thesis in order of importance are considered to be the following:

1. Chapter 4 contains a number of contributions. A new procedure for extracting a preliminary estimate of the heave component effects of the towed body has been proposed. This is obtained as the sequence of the time-to-first peak on the sequence of return signals. An interpretation of the frequency response obtained from the heave record, leads to a newly proposed model for the heave effects as a simple narrow-band filter. It is on the basis of a state space formulation of this model that a Kalman filtering algorithm has been detailed. Although Kalman filtering has been used in many areas of applications, its adoption to source heave compensation appears to be new.

2. In Chapter 5 a number of contributions have been made. Three compact vector-matrix formulations for estimating the amplitude and delay parameters have been proposed.

   a. On the basis of the first formulation, a sequential procedure has been proposed to estimate the amplitude and delay parameters. It is believed that the proposed procedure of section 5.4 is novel in this specific application.

   b. The formulation of the problem to facilitate the simutaneous estimation of delay and amplitude parameters is based on the well-known Taylor expansion and appears to be a new application of this powerful

technique.

c. The observation of the balance property in the derivative of the source signal and its replicas provided a simple yet effective procedure for reflection event enhancement and hence delay time evaluation. The procedure and its mechanization seem to be new.

3. A unified treatment of the many approaches to modeling the earth response to acoustic excitation has been given in Chapter 3. A new model based on time domain raypath analysis accommodating multiple reflection effects has also been presented.

It is the author's experience, however, that the heave compensation according to the procedure of Chapter 4, is required as an important pre-processing step to enhance the reflection events in real data. The main advantage of that procedure is to obtain refined estimates of the heave component, thus allowing the data to be corrected in real time as well as in off-line application. The disadvantage of the procedure is that Kalman filtering requires predicting two different error covariances $\underline{Q}$ and $\underline{R}$. This has been handled for this specific experiment in an iterative manner to arrive at the appropriate error covariances.

To obtain an estimate of the delay parameters, we could use the procedure of section 5.6 (balance property) which involves less computational effort. The operation could also

be done in real time. The only disadvantage is that a precise peak position is not obtained in the case of overlapping signals and no amplitude parameter estimates are obtained. Alternatively, the approach of section 5.4 may be used with more computational effort to obtain the associated minimum variance on the amplitude parameters. We could also expect more accurate results with improved discrimination between the pulses in the case of overlapping signals as shown in the simulation and real data results in section 5.5.

## 6.3 Suggestions for further research

A number of opportunities for further research in the areas addressed in this thesis, are indicated here:

(1) The models and techniques discussed in this thesis relate to plane wave motion normal to the reflecting interfaces. Extensions of the treatment to include non-normal incidence, is an interesting problem for further area of research.

(2) The inclusion of attenuation effects due to lossy wave propagation in a parametric type model presents a natural extension to which the proposed estimation procedures may be applied.

(3) The choice of mathematical functions to approximate the variation of velocity of sound propagation and acoustic impedance with depth in models treated in Chapter 3 provides an interesting area of investigation. Functions other than those utilized (such as polynomials) may provide better approximations or more tractable solution.

(4) Heave modeling and filtering is an area of promising future research. The desirability and effectiveness of higher order models describing the heave phenomenon could be investigated. Extensions of the filtering algorithm to higher order models might be carried out. Algorithmic improvements on the filtering procedure could also be considered.

Microprocessor implementation of the modeling and estimation functions for real-time in-situ application is an exciting prospect.

(5) The area of amplitude and delay parameter estimation presents a number of possible extensions and future work. The choice of an optimum threshold in the procedure of Section (5.4) is still an open question that needs further examination. Performance evaluation of the procedure of Section (5.5) when applied to a region with thin layers might be carried out. The use of second order Taylor expansion approximations to the delayed functions could be considered. The spectral characteristics of the output of the filter representing the procedure of Section (5.5) might be considered to further verify the enhancement to reflection events.

# BIBLIOGRAPHY AND LIST OF REFERENCES


Andersen, N., Short notes on "The Calculation of Filter Coefficients for Maximum Entropy Spectral Analysis", Geophysics, Vol. 39, No. 1, February (1974).

Anstey, N.A., Volume 1, "Signal Characteristics and Instrument Specifications", Gebruder, Borntraeger, Berlin, (1970).

Anstey, N.A., "Seismic Interpretation: The Physical Aspects". International Human Resources Development Corporation. Boston, Massachusetts, 02116, U. S. A., (1977).

Backus, M.M., "Water reverberations - their nature and Elimination". Geophysics, Vol. 24, pp. 233-261, (1959).

Baranov, V., et Kunetz, G., "Film Synthetique Avec Reflexions Multiples Theorie et Calcul Practique". Geophysical Prospecting, Vol. 8. (1960).

Barnard, G. R., Bardin, J.L., and Hempkins, W.B., "Underwater Sound Reflection from Layered Media", J. Acoust. Soc. Am., 36: 2119, (1964)

Bendat, J.S., and Piersol, A.G., "Random Data Analysis and Measurement Procedures", Wiley-Interscience, New York, (1971).

Bendat, J. S., and Piersol, A.G., "Engineering Applications of Correlation and Spectral Analysis". Wiley-Interscience, N.Y., (1980).

Berryman, L.H., Goupillaud, P.L., and Waters, K.H., "Reflections from Multiple Transition Layers". Geophysics, Vol. 23, No. 2, pp. 223-243., April, (1958).

Bhattacharyya, R., "Dynamics of Marine Vehicles", Wiley-Interscience, N.Y., (1978)

Camp, Leon, "Underwater Acoustics", Wiley-Interscience, N.Y., (1970).

Clay, C.S., and Medwin, H., "Acoustical Oceanography". Principles and Applications, Wiley-Interscience, U. S. A., (1977).

Claerbout, J. F., "Fundamentals of Geophysical Data Processing". With Applications to Petroleum Prospecting, McGraw-Hill. (1976).

Chesterman, W.D., "Sediment Mapping with Isometric Side-Scan Systems", Proceedings of the Acoustical Society for Underwater Technology, (1971).

Crump, N., "A Kalman Filter Approach to the Deconvolution of Seismic Signals", Geophysics, Vol. 39, No. 1, February (1974).

Damotte, B., "Analog Filtering of Marine Seismic Records", a Chapter in "Seismic Filtering", edited by Nostrand, R.V., Society of Expl. Geophysicists, Tulsa, (1971).

Darby, E.K., and Neidell, N.S., "Application of Dynamic Programming to the Problem of Plane Wave Propagation in a Layered Medium", Geophysics, Vol. 31, December (1966).

Dash, B.P., and Obaidullah, K.A., "Determination of Signal and Noise Statistics Using Correlation Theory", Geophysics, Vol. 35, No. 1, February, (1970).

Davis, J.M., "Velocity Analysis: An Application of Deterministic Estimation to Reflection Seismology", Short Notes, IEEE Transactions on Computers, July (1972).

Disher, D.A., and Naquin, P.J., "Statistical Automatic Statics Analysis", Geophysics, Vol. 35, No. 4, August, (1970).

Dodds, D.J., "Attenuation Estimates from High Resolution Subbottom Profiler Echoes", NATO SACLANT Research Conference on Ocean Acoustics Influenced by the Sea Floor. La Spezia, Italy, Plenum Press, June, (1980).

Doherty, S.M., and Claerbout, J.F., "Structure Independent Velocity Estimation", Geophysics, Vol. 41, No. 5, October, (1976).

El-Hawary, Ferial, and Vetter, W.J., "Estimation of Subsurface Layer Parameters by Use of a Multiple-Reflection Model for Layered Media", Proceedings of the Fourth International Conference on Port and Ocean Engineering Under Arctic Conditions (POAC '77), St. John's, Newfoundland, pp.1087-1099, September, (1977).

El-Hawary, Ferial, and Vetter, W. J., "Spatial Parameter Smoothing for Ocean Subsurface Layered Media". Fourth International Symposium on Computers, Electronics and Control, Toronto, November, (1978).

El-Hawary, Ferial, and Vetter, W.J., "Subsurface Layered Media Parameter Estimation Using a Linearized Multiple Reflection Model", Proceedings of IEEE Oceans '78, Washington, D.C., pp. 713-717, September, (1978).

El-Hawary, Ferial, and Vetter, W.J., "Spatial Parameter Estimation for Ocean Subsurface Layered Media", Canadian Electrical Engineering Journal Vol. 5, No. 1, pp. 28-31, (1980).

El-Hawary, Ferial, and Vetter, W.J., "Multiple Reflections of Subsurface Layered Media". Proceedings of IEEE Oceans '80, Seattle, Washington. Submitted to IEEE Journal of Oceanic Engineering, (1980).

El-Hawary, Ferial, and Vetter, W.J., "Kalman Filtering for Heave Compensation in Marine Seismic Exploration". Proceedings of IEEE Oceans '81, Boston, Massachusetts, (1981).

Ellsworth, T.P., "Multiple Reflections", Geophysics, Vol. 13, pp. 1-18, (1948).

Ferrel, G. Stremler, "Introduction to Communication Systems". Addison-Wesley, (1977).

Ford, W., Hearne, J.H., "Least-Squares Inverse Filtering", Geophysics, Vol. 31, No. 5, October, (1966).

Fryer, G. J., Odegard, M.E., and Sutton, G.H., "Deconvolution and Spectral Estimation Using Final Prediction Error", Geophysics, Vol. 40, No. 3, June (1975).

Gelb, A., "Applied Optimal Estimation". The Analytic Sciences Corporation, U.S.A., (1974).

Goodyear, C.C., "Signals and Information", Butterworths, London, (1971).

Goupillaud, P.L., "An Approach to Inverse Filtering of Near-Surface Layer Effects from Seismic Records". Geophysics, Vol. 26, No. 6, pp. 754-760, (1961).

Grant, F.S., and West, G.F., "Interpretation Theory in Applied Geophysics", McGraw-Hill, N.Y., (1965)

Griffiths, J. W.R., Stocklin, P.L., Schoonevald, C.V., "Signal Processing". A Nato Advanced Study Institute, Academic Press, New York, (1973).

Hamilton, E.L., "Elastic Properties of Marine Sediments". Journal of Geophysical Research, Vol. 76, No. 2, January, (1971).

Hamilton, E.L., "Compressional-Wave Attenuation in Marine Sediments", Journal of Geophysics, Vol. 37, No. 4, August, (1972).

Harris, B., "Theory of Probability", Addison-Wesley, (1966).

Haykin, S., "Communication Systems". Wiley-Interscience, N.Y., (1978).

Hutchins, R.W., McKeown, D.L., and King, L.H., "A Deep Tow High Resolution System for Continental Shelf Mapping". Geoscience Canada 32 (2): pp. 95-100, (1976).

Hutchins, R.W., "Removal of Tow Fish Motion Noise from High Resolution Seismic Profiles". Presented at SEG-US Navy symposium on Acoustic Imaging Technology and on Broad Data Recording and Processing Equipment, National Space Technology Laboratories, Bay St. Louis, Mississippi, U. S. A. August, (1978).

Hron, F., "Criteria for Selection of Phases in Synthetic Seismograms for Layered Media". Bulletin of the Seismological Society of America 61, pp. 765-779. (1971).

Kanasewich, E.R., "Time Sequence Analysis in Geophysics". The University of Alberta Press, Edmonton, Canada, (1973).

Kinsler, L.E., and Frey, A.R., "Fundamentals of Acoustics", second edition, Wiley-Interscience, (1962).

Lampson, C.W., Final report on "Effects of Underground Explosions": NDRC Report No. A-479, ORSD Report No. 6645, (1945).

Lindseth, R.O., "Digital Processing of Geophysical Data". A review (continuing education program Society of Exploration Geophysicists). Teknica LTD., 339 Sixth Avenue, S.W., Calgary, Alta. T2P 0R8. Ph. (403) 269-4386, (1976)

McCormick, M.E., "Ocean Engineering Wave Mechanics". Wiley-Interscience, N.Y., (1973).

McGarthy, T.P., "Stochastic Systems and State Estimation". Wiley-Interscience, N.Y., (1974).

McKeown, D.L., "Evaluation of the Huntec ('70) Hydrosonde Deep Tow Seismic System", Report BI-R-75-4, Bedford Institute of Oceanography, Dartmouth, Nova Scotia, Canada, (1975).

McKinny, C.M., Anderson, C.D., "Measurements of Backscattering of Sound from the Ocean Bottom", J. Acoust. Soc. Am., Vol. 36, No. 1, (1964).

Meditch, J.S., "Stochastic Optimal Linear Estimation and Control", McGraw-Hill, N.Y., (1969).

Mendel, J.M., Volume 1, "Discrete Techniques of Parameter Estimation", Marcel Dekker, Inc., N.Y., (1973).

Mendel, J.M., "White Noise Estimators for Seismic Data Processing in Oil Exploration", Information Processing for Oil and Gas Exploration. Volume 1, USCEE Report: 486, Interim Technical Report, November (1975).

Mendel, J.M., "Single-Channel White Noise Estimators for Predictive Deconvolution", Information Processing for Oil and Gas Exploration, Volume 2, USCEE Report: 488, January, (1976).

Mendel, J.M., and Lee, J.S., "Reinforcement of Reflections", Presented at 47th. Annual International Meeting of the Society of Exploration Geophysicists, Calgary, Canada, September, (1977).

Mendel, J.M., and Farrokh Habibi Ashrafi, 1980, "A Survey of Approaches to Solving Inverse Problems for Lossless Layered Media Systems". IEEE transactions on Geoscience and Remote Sensing, Vol. GE-18, No. 4, October, (1980).

Mersereau, R.M., and Dudgeon, D.E., "Two-Dimensional Digital Filtering", Proceedings of IEEE, Vol. 63, No.4 April, (1975).

Myers, J.J., Holm, C.H., and, McAllister, R.F., "Handbook of Ocean and Underwater Engineering", McGraw-Hill, N.Y., (1969).

Nahi, N.E., and Assefi, T., "Bayesian Recursive Image Estimation", IEEE Transactions on Computers, July (1972).

Nahi, N.E., and Mendel, J.M., "A Time Domain Approach to Seismogram Synthesis for Layered Media", Information Processing for Oil and Gas Exploration, Volume 3, USCEE Report: 490, June, (1976).

Nahi, N.E., Mendel, J.M., and Silverman L.M., "Recursive Derivation of Reflection Coefficients from Noisy Seismic Data", Presented at IEEE Int. Conf. Acoustics, Speech, and Signal Processing, Tulsa, OK., (1978).

Officer, C.B., "The Refraction Arrival in Water Covered Areas", (1953).

Officer, C.B., "Introduction to the Theory of Sound Transmission with Application to the Ocean". McGraw-Hill, N.Y., (1958).

Ogata, K., "State Space Analysis of Control Systems". Prentice-Hall, INC., (1967).

Oppenheim, A.V., and Schafer, R.W., "Digital Signal Processing". Prentice-Hall, (1974).

Papoulis, A., "System and Transforms with Applications In Optics", McGraw-Hill, N.Y., (1968).

Peacock, K.L., and Treitel, S., "Predictive Deconvolution: Theory and Practice", Geophysics, Vol. 34, No. 2, April, (1969).

Peterson, R.A., Fillippone, W.R., and Coker, F.B., "The Synthesis of Seismograms from Well Log Data". Journal of Geophysics, Vol.XX, No. 3, pp. 516-538, July, (1955).

Plemons, T.D., Shooter, J.A., and Middleton, D., "Some Statistical Properties of Nonstationary Reverberation", In Signal Processing, A Nato Advanced Study Institute, Griffiths, Stocklin, and Van Schooneveld, Ed., Academic Press, New York, (1973).

Price, W.G., and Bishop's R.E.D., "Probabilistic Theory of Ship Dynamics". John Wiley-Interscience, N.Y. (1974).

Rabiner, L.R., and Rader, C.M., "Digital Signal Processing". IEEE Press, N.Y., (1972).

Richards, P.I., "Manual of Mathematical Physics". Pergamon Press, N.Y. (1959).

Ricker, N., "The Form and Nature of Seismic Waves and the Structure of Seismograms". Geophysics, Vol. V, pp. 348-366, (1940).

Ricker, N., "The Form and Laws of Propagation of Seismic Wavelets", Geophysics, Vol. 18, (1953).

Ricker, N.H., "Transient Waves in Visco-Elastic Media", Developments in Solid Earth Geophysics. Elsevier Scientific Publishing Company, (1977).

Robinson, E.A., "Predictive Decomposition of Seismic Traces", Geophysics, Vol. 22, No. 4, October (1957).

Robinson, E.A., "Predictive Decomposition of Time Series with Applications to Seismic Exploration". Geophysics, Vol. 32, No. 3, June, (1967).

Robinson, E.A., "Multichannel Time Series Analysis with Digital Computer Programs". Holden-Day, San Francisco, (1967).

Robinson, E.A., and Treitel, S., "Geophysical Signal Analysis". Prentice-Hall, (1980).

Schench, H., Jr., "Introduction to Ocean Engineering, McGraw-Hill, N.Y.

Schweppe, F.C., "Uncertain Dynamic Systems", Prentice-Hall, Englewood Cliffs, New Jersey, (1973).

Sengbush, R.L., Lawrence, P.L., and McDonal, F.J., "Interpretation of Synthetic Seismograms". Geophysics, Vol. XXIV, No. 2, pp. 138-157, (1961).

Shanmugam, K.S., "Digital and Analog Communication Systems". John Wiley & Sons, N.Y., (1979).

Sheriff, R.E., "Inferring Stratigraphy from Marine Seismic Data", Offshore Technology Conference, Paper Number OTC 2268, (1975).

Sherwood, J.W.C., and Trory, A.W., "Minimum Phase and Related Properties of the Response of a Horizontally Stratified Absorptive Earth to Plane Acoustic Waves", Geophysics, Vol. 30, (1965).

Silvia, M.T., "Deconvolution of Geophysical Time Series", Doctoral Dissertation, Northeastern University, (1977).

Spencer, T.W., and Bhambani, D.J., "Dip-Dependent Reverberation Operator", Geophysics, Vol. 40, No. 3, June, (1975).

Stone, D.G., "Velocity and Bandwidth", Offshore Technology Conference, Paper No. OTC 2270, (1975).

Taner, M.T., Cook, E.E., and Neidell, N.S., "Limitations of the Reflections Seismic Method", Lessons from Computer Simulations. Geophysics, Vol. 35, No. 4, August (1970).

Thomson, W.T., "Transmission of Elastic Waves through a Stratified Solid Medium". Journal of Applied Physics, Volume 21, pp. 89-93, February, (1950).

Treitel, S., and Robinson, E.A., "Seismic Wave Propagation in Layered Media in Terms of Communication Theory", Geophysics, Vol. 31, No. 1, February, (1966).

Tribolet, J.M., "Seismic Applications of Homomorphic Signal Processing", Prentice-Hall, (1979).

Trorey, A. W., "Theoretical Seismograms with Frequency and Depth Dependent Absorption", Geophysics, Vol. 27, (1962).

Tucker, M.J., and Stubbs, A. R., "Underwater Acoustics as a Tool in Oceanography", in Underwater Acoustics, V.M. Albero Ed., Plenum Press, N.Y., (1963).

Uric, R.J., "Principles of Underwater Sound for Engineers", McGraw-Hill, New York, (1967).

Vetter, W.J., and El-Hawary, Ferial, "A Layer-indexed Reflection Model for Multilayered Media", IEEE OCEANS '79, San Diego, California, pp. 21-26, (1979).

Vetter, W.J., "On Linear Estimates, Minimum Variance and Least-Squares Weighting Matrices", IEEE Trans-Automatic Control, Vol. Ac-16, No. 3, pp. 265-266, (1971).

Vetter, W. J., 1980, "On Dimensional Complexity of Reflections in Multilayered Media". Third International Symposium on Large Engineering Systems, St. John's, Newfoundland, Canada, pp. 335-342, July (1980).

Vetter, W.J., "A Forward Generated Synthetic Seismogram for Equal-Delay Layered Media Models", Geophysical Prospecting, 29,000-000, (1981).

Wadsworth, G.P., Robinson, E.A., Bryan, J.G., Hurley, P.M., "Detection of Reflections on Seismic Records by Linear Operators", Geophysics, Vol. 18, (1953).

Waters, K.H., "Reflection Seismology", A Tool for Energy Resource Exploration, Wiley-Interscience, (1978).

White, J.E., "Seismic Waves" Radiation, Transmission and Attenuation, McGraw-Hill, N.Y., (1965).

Wood, L.C., and Treitel, S., "Seismic Signal Processing". Proceedings of the IEEE, Vol. 63, No. 4, April (1975).

Wuenschel, P.C., "Seismogram Synthesis Including Multiples and Transmission Coefficients", Geophysics, Vol. XXV, No. 1, pp. 106-129, (1960).

Yacoub, N.K., Scott, J.H., and McKeown, F.A., "Computer Ray Tracing Through Complex Geological Models for Ground Motion Studies", Geophysics, Vol. 35, No. 4 August (1970).

Young, D.M., "Matrix Iterative Solution of Large Linear System", Academic Press, N.Y., (1971).